Deterministic and Stochastic Modelling of Infectious Diseases in the Early Stages

by

Manting Wang
M.Sc., Donghua University, 2020
B.Sc., Huaibei Normal University, 2017

A Dissertation Submitted in Partial Fulfillment of the
Requirements for the Degree of

DOCTOR OF PHILOSOPHY

in the Department of Mathematics and Statistics

We acknowledge and respect the Lək̓ʷəŋən (Songhees and Xʷsepsəm/Esquimalt) Peoples on whose territory the university stands, and the Lək̓ʷəŋən and W̱SÁNEĆ Peoples whose historical relationships with the land continue to this day.

Deterministic and Stochastic Modelling of Infectious Diseases in the Early Stages

by

Manting Wang
M.Sc., Donghua University, 2020
B.Sc., Huaibei Normal University, 2017

Supervisory Committee

Dr. Junling Ma, Co-supervisor
(Department of Mathematics and Statistics)

Dr. Pauline van den Driessche, Co-supervisor
(Department of Mathematics and Statistics)

Dr. Dean Karlen, Outside Member
(Department of Physics and Astronomy)

Dr. Michael Y. Li, External Examiner
(Department of Mathematical and Statistical Sciences, University of Alberta)

ABSTRACT

During the early stages of an epidemic, case counts typically grow exponentially, influenced by disease transmissibility, contact patterns, and implemented control measures. Understanding this exponential growth and disentangling the effects of various interventions are critical for public health decision-making. This dissertation investigates the dynamics of the early stages of an epidemic under control measures, addressing two key topics: evaluating the effectiveness of contact tracing and estimating the exponential growth rate of cases.

Contact tracing is a key public health measure to reduce disease transmission. However, due to limited public health capacity, it is mostly effective during the early stage when the case counts are low. In Chapter 2, I develop a novel modelling framework to track contacts in a randomly mixed population. This approach borrows the idea of edge dynamics from network models to track contacts included in a compartmental SIR model for an epidemic spreading. Using COVID-19 as a case study, I evaluate the effectiveness of contact tracing during the early stage when multiple control measures were implemented in Chapter 3. I conduct a simulation study to determine the necessary dataset for parameter estimation. I find that new case counts, cases identified through contact tracing (or voluntary testing), and symptomatic onset counts are necessary for parameter identification. Finally, I apply our models to the early stages of the COVID-19 pandemic in Ontario, Canada.

Chapters 4 and 5 focus on reliably estimating the exponential growth rate during the early stages of an outbreak, a key measure of the speed of disease spread. To establish a suitable likelihood function for accurate growth rate estimation, I derive the probability generating function for new cases using a linear stochastic SEIR model and obtain formulas for its mean and variance in Chapter 4. Numerical simulations show that the binomial or negative binomial distribution closely approximates the distribution of new cases. To determine the most appropriate method for estimating the growth rate, I compare the performance of the negative binomial regression model and the hidden Markov model (HMM) in Chapter 5. My results show that the 95% credible intervals produced by the HMM have a higher probability of covering the true growth rate.

Contents

List of Tables

List of Figures

List of Abbreviations

CTMC	Continuous Time Markov Chain
DTMC	Discrete Time Markov Chain
HMM	Hidden Markov Model
MLE	Maximum Likelihood Estimation
MCMC	Markov Chain Monte Carlo
NPI	Non-Pharmaceutical Intervention
ODE	Ordinary Differential Equation
PDF	Probability Distribution Function
PGF	Probability Generating Function
PMF	Probability Mass Function
SARS	Severe Acute Respiratory Syndrome
SDE	Stochastic Differential Equation
SEAIR	Susceptible-Exposed-Asymptomatic-Infectious-Recovered
SEIR	Susceptible-Exposed-Infectious-Recovered
SIR	Susceptible-Infectious-Recovered
SIRS	Susceptible-Infectious-Recovered-Susceptible
SIS	Susceptible-Infectious-Susceptible

ACKNOWLEDGEMENTS

I would like to thank:

My supervisors for their mentoring, support, encouragement, and patience. I am incredibly lucky to have met you. I hope you will always be healthy and happy!

My family for always supporting me and allowing me to freely choose the direction of my life.

My friends for your encouragement and companionship, making the supposedly terrible and boring life of a PhD full of laughter, sparkle, and unforgettable memories.

Victoria for your beautiful flowers and sunshine, which always make me feel the beauty of life.

Life is like a long river, and the storms we encounter are just part of its natural course. Look! The leaves are smiling, the sakura is blooming. Rub your tired eyes and take in the beauty of life. The spring rain falls, the summer cicadas sing, tomorrow will be a good day!

Chapter 1

Introduction

Infectious diseases have profoundly impacted human health, society, and the global economy throughout history. In recent decades, multiple major outbreaks have highlighted the persistent threat posed by emerging and re-emerging infectious diseases. The 2002–2003 SARS outbreak spread to over 30 countries and regions, causing significant morbidity and mortality [1]. The 2009 influenza A (H1N1) pandemic spread globally, leading to widespread infections and straining healthcare systems [2]. The COVID-19 pandemic drastically altered people's lifestyles, disrupted economies, and challenged public health systems worldwide.

In early 2025, health authorities observed an unusually severe and early onset of the influenza season. Reports indicate that this year's strain has led to higher hospitalization rates and more severe symptoms compared to previous years [3]. These epidemics underscore the need for a deeper understanding of disease transmission and the development of effective outbreak control strategies.

With advancements in science, technology, and global connectivity, individual behavior has become an increasingly influential factor in disease transmission. People modify their behavior in response to disease outbreaks, which, in turn, affects epidemic dynamics. For example, during the H1N1 and COVID-19 outbreaks, individuals chose to stay home, wear masks, and limit social interactions to reduce exposure. In addition to voluntary behavioral changes, public health interventions such as non-pharmaceutical interventions (NPIs), contact tracing, and vaccination play a crucial role in curbing disease spread.

Contact tracing is an important control measure during the early stages of an epidemic. Early detection through contact tracing reduces severe cases and prevents hospital strain. When combined with other measures like vaccination and social distancing, it strengthens outbreak control [4]. However, its success depends on adequate resources and careful planning. While it can effectively reduce transmission, it also imposes economic and social costs. Therefore, evaluating different control strategies is critical to identifying the most effective and feasible intervention policies.

During the early stages of an epidemic, case counts typically grow exponentially within a population and its subpopulations, influenced by factors such as age, sex, gender, and other demographics. A key characteristic of epidemic curves in this phase is the exponential growth rate, which is determined by disease transmissibility, contact patterns, and control measures. For instance, during the COVID-19 pandemic, interventions such as travel restrictions, social distancing, school and workplace closures, and contact tracing were implemented almost simultaneously. Disentangling the effects of these control measures from observed changes in the growth rate remains a crucial challenge for public health policymakers.

Mathematical models are powerful tools for exploring disease dynamics and assessing intervention strategies. Unlike controlled experiments, which are often infeasible during epidemics, models provide a theoretical framework for understanding disease spread and interpreting outbreak data. Their ability to approximate real-world epidemics depends on how well they capture key transmission mechanisms and explain data. By calibrating models to disease data, key parameters can be estimated to ensure that the model results reflect the patterns of real epidemic data. Through a combination of mathematical analysis and numerical simulations, these models help researchers and policymakers predict epidemic trajectories, optimize control measures, and assess the impact of interventions. The accuracy of model predictions is inherently limited by model assumptions. In some cases, simplifying assumptions such as homogeneously mixed populations are made for mathematical tractability at the cost of accuracy. Nonetheless, these models provide valuable theoretical insights, helping to explain observed patterns and inform public health decision making.

In this dissertation, I aim to develop a mathematical model to evaluate the effectiveness of contact tracing during the early stages of an epidemic when multiple control measures are in place. The exponential growth rate at this stage serves as a key indicator of disease spread, providing insights into the effectiveness of these measures. Statistical methods such as Maximum Likelihood Estimation (MLE) and Bayesian Markov Chain Monte Carlo (MCMC) are commonly used to estimate this growth rate [5–7]. Accurately estimating the initial growth rate using these methods requires a thorough understanding of how the case count distribution evolves over time and the establishment of the corresponding likelihood function. While this distribution has been analyzed for stochastic Susceptible-Infectious-Recovered (SIR) models [8], it remains mathematically intractable for Susceptible-Exposed-Infectious-Recovered (SEIR) models, leaving the impact of the latent stage on case distribution unclear. However, SEIR models are essential for diseases like COVID-19, which have long incubation periods. Therefore, I aim to study the probability distribution of daily new cases in the SEIR model and establish a more appropriate likelihood function to estimate the initial exponential growth rate.

1.1 Compartmental Model

1.1.1 Classic Compartmental Model

The traditional compartmental model is widely used in theoretical research on disease control and epidemic prediction. It simplifies disease dynamics by dividing a population into distinct compartments based on infection status, so it is easy to analyze theoretically and calibrate to data.

Kermack and McKendrick [9] proposed the first compartmental modeling framework in 1927. This model divides a population into three compartments: Susceptible (S), Infectious (I), and Recovered (R). The model assumes a constant population size N by ignoring births and deaths. Contact patterns within the population are assumed to be homogeneous (i.e., every individual has the same probability of contact). Figure 1.1 illustrates the population dynamics of the classic SIR compartmental model. Here, β is the transmission rate, and γ is the recovery rate.

Figure 1.1: The dynamics of the SIR model.

The disease dynamics are governed by the following system of ordinary differential equations (ODEs):

$$\begin{aligned} S' &= -\beta\frac{SI}{N}, \\ I' &= \beta\frac{SI}{N} - \gamma I, \\ R' &= \gamma I. \end{aligned}$$

To account for the possibility of reinfection and waning immunity, the SIS and SIRS models were later developed based on this framework [10,11]. Based on data fitting and theoretical research by Anderson and May [12,13], many studies on infectious diseases have ignored the incubation period of a disease in their analyses.

However, some diseases, such as measles, influenza, and HIV/AIDS, involve a latent period during which infected individuals are not yet infectious. To address this, the SEIR model was developed [14, 15]. The system is given by:

$$\begin{aligned} S' &= -\beta\frac{SI}{N}, \\ E' &= \beta\frac{SI}{N} - \sigma E, \\ I' &= \sigma E - \gamma I, \\ R' &= \gamma I. \end{aligned}$$

Here, exposed individuals experience a latent period of duration $1/\sigma$.

To better reflect real-world epidemiological scenarios, classic compartmental models such as SIR and SEIR are often extended to include additional factors such as control measures, age structure, spatial immigration, and viral evolution [16–20].

1.1.2 Compartmental Models for Contact Tracing

The purpose of contact tracing is to identify and notify individuals who may have been exposed to an infected person. By isolating cases and quarantining contacts, it helps slow the spread of the disease. Many contact tracing models extend traditional compartmental models to include quarantined compartments [21, 22]. Since contact tracing relies on timely intervention by public health professionals, its effectiveness is constrained by limited resources. As the number of infections increases, delays in contact tracing become more likely, and not all contacts can be successfully traced. Therefore, when constructing models, the contact tracing rate is typically considered.

Lipsitch et al. [23] proposed a model incorporating contact tracing to estimate the transmission of SARS. In their model, diagnosed patients trigger contact tracing, leading to the identification and quarantine of their contacts. The classic SEIR model is extended to include three quarantined compartments: quarantined susceptible individuals (S_Q), quarantined exposed individuals (E_Q), and quarantined infectious individuals (I_Q). The unquarantined infectious compartment is further divided into two groups: undiagnosed infectious individuals (I_U) and diagnosed infectious individuals (I_D). The full model is described by the following system of equations:

$$\begin{aligned}
S' &= -[kb + k(1-b)q]I_U\frac{S}{N} + r_Q S_Q,\\
S_Q' &= k(1-b)qI_U\frac{S}{N} - r_Q S_Q,\\
E' &= kb(1-q)I_U\frac{S}{N} - \sigma E,\\
E_Q' &= kbqI_U\frac{S}{N} - \sigma E_Q,\\
I_U' &= \sigma E - (\gamma + d + w)I_U,\\
I_Q' &= \sigma E_Q - (\gamma + d + w)I_Q,\\
I_D' &= w(I_U + I_Q) - (\gamma + d)I_D,\\
R' &= \gamma(I_U + I_D + I_Q),
\end{aligned}$$

where k is the contact rate, and b is the probability of transmission per contact between an infectious case and a susceptible individual, giving a transmission rate of $\beta = kb$. Here, q represents the quarantine rate, r_Q is the rate at which quarantined uninfected contacts are released, d is the disease-induced death rate, and w is the rate at which diagnosed infectious individuals transition to the isolated infectious class.

In this model, susceptible individuals become infected through contact with undiagnosed infectious individuals and progress to the infectious stage after a latent period. Infectious individuals lose infectiousness through recovery, isolation, or death. The model does not account for births or non-SARS-related deaths. It assumes that when quarantine is implemented, a fixed proportion q of new infections are quarantined before they become infectious.

With the emergence of asymptomatic patients in some diseases, such as COVID-19, the spread caused by asymptomatic individuals cannot be ignored in the process of disease transmission. Therefore, the compartmental model is extended to include additional compartments, such as asymptomatic (A) or pre-symptomatic (P) individuals, to better capture disease dynamics [24,25]. These extensions provide a more comprehensive framework for studying transmission patterns and assessing the effectiveness of control measures.

1.2 Network Model

In reality, the rapid development of information and technology has highlighted the heterogeneity of contact patterns. To account for this, contact network models based on graph theory have been proposed to study the structure of population contacts, and many studies on infectious disease dynamics now rely on network-based approaches [26–28].

In network models, individuals are represented as nodes, and their interactions or contacts are depicted as edges. The number of edges connected to a node is referred to as its degree. In recent years, numerous theoretical studies have explored the infectious dynamics of complex networks, utilizing concepts such as average degree, degree distribution , and clustering coefficient to characterize network structures [29]. Different types of networks can be established based on their structural properties. Commonly used network models include:

- Erdos-Rényi networks: the degree distribution follows a binomial distribution;
- Small-world networks: characterized by high clustering and short path lengths, meaning that each node is “close” to almost every other node;
- Scale-free networks: the degree distribution follows a power-law;
- Configuration network model: nodes are assigned degrees independently according to a given degree distribution, and edges are formed by randomly pairing node stubs.

Some studies use graph theory to identify key nodes that influence disease transmission in networks, aiming to develop targeted control strategies. Two well-established approaches for studying disease transmission on random networks are (1) analyzing the transmission threshold, such as the basic reproduction number ($\mathcal{R}_0$), which represents the average number of secondary infections generated by a single infected individual in a fully susceptible population, and the final outbreak size using percolation theory, and (2) constructing infectious disease models based on the infection status of nodes within the network.

In 2000, Moore and Newman [30] studied the SIR model in small-world networks. In 2001, Pastor-Satorras and Vespignani [31] studied the SIS model in Scale-free networks. Newman [32] studied the SIR disease model on random networks in 2002, and analyzed the epidemic threshold and outbreak size of SIR model on random networks by using the percolation theory. In 2003, Boguná, Pastor-Satorras and Vespignani [33] proposed an epidemic model with degree correlation in Scale-free random network.

1.2.1 Pair Approximation Model

In 1999, Keeling [34] described the dynamic behaviour of node states through the dynamics of edge states and proposed the pair approximation model. He considered an SIR model in a homogeneous network with n nodes, where each node has the same degree n. The total number of nodes in state A is denoted as $[A]$. The interactions between two nodes form pairs AB, and interactions involving three nodes form triples ABC, where $A, B, C \in \{S, I, R\}$.

In this model, a susceptible node can be infected by its infectious neighbors. For example, in pairs SI, the susceptible node S can be infected by the infectious node in the pair with rate β. It can also be infected by other infectious neighbors, such as in the case of ISI. Figure 1.2 illustrates the pair dynamics.

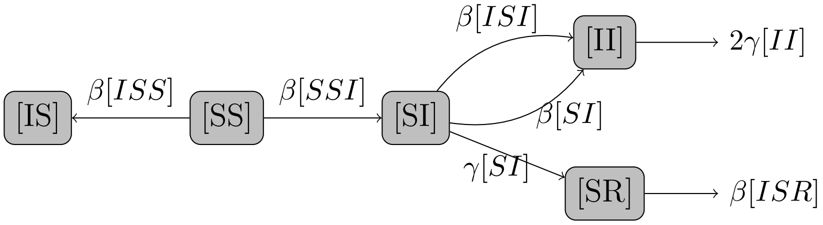

Figure 1.2: The pair dynamics of the SIR model.

The pairs (or triples) are assumed to be symmetric: $[AB] = [BA]$ (or $[ABC] = [CBA]$), so each pair in $[AA]$ is counted twice. Hence, the dynamics of the pairs are modelled as follows:

$$\begin{aligned}
[SS]' &= -2\beta[SSI]\,, \\
[SI]' &= \beta([SSI] - [ISI] - [SI]) - \gamma[SI]\,, \\
[SR]' &= -\beta[RSI] + \gamma[SI]\,, \\
[II]' &= 2\beta([ISI] + [SI]) - 2\gamma[II]\,.
\end{aligned}$$

In this system, the pair dynamics depend on the dynamics of the triples. Similarly, the dynamics of the triple are influenced by higher-order connections. To close the system, triples are approximated as

$$[ABC] = \left(\frac{n-1}{n}\right)\frac{[AB][BC]}{[B]}.$$

Here, the total number of edges starting from nodes in state B is $n[B]$. A proportion $\frac{[AB]}{n[B]}$ of these edges lead to A, while a proportion $\frac{[BC]}{n[B]}$ lead to C nodes. Thus, if we choose a node in state B along with two neighbours in states A and C, the probability of forming a triple is $\frac{[AB][BC]}{n^2[B]^2}$. Since there are $n(n-1)$ ways to choose A and B, the expection of $[ABC]$ is

$$[B]n(n-1)\frac{[AB][BC]}{n^2[B]^2} = \frac{n-1}{n}\frac{[AB][BC]}{[B]}.$$

In 2008, Volz [35] perfected Keeling's epidemic model based on edge state and established an SIR dynamic model with heterogeneous connection on random networks. Miller [36] further simplified the Volz model in 2011 and revealed the spreading process of SIR epidemics on random networks.

1.2.2 Network Models for Contact tracing

The pair approximation framework can be extended to study contact tracing by introducing additional states for traced individuals. In traditional network-based epidemic models, nodes are classified into compartments based on infection status, such as susceptible, infectious, or recovered. However, contact tracing alters the transmission dynamics by identifying and isolating potentially exposed individuals, leading to new node states and interactions.

In 2002, Hurta et al. [4] proposed deterministic mean-field equations (assuming a homogeneous network) to study the effectiveness of contact tracing. They extended the SIR model to include a new state, T, representing traced individuals who are identified through their contact with diagnosed cases. The transitions between states are influenced not only by infection and recovery processes but also by tracing efforts. When an infectious individual is diagnosed, their recent contacts can be traced at a rate τ. They assume that there is a random checking probability v for individuals who do not have diagnosed contacts.

Figure 1.3 illustrates the pair dynamics of this model. When an infectious node in the pair SI is detected randomly or through its confirmed contacts, SI will become

ST. When the susceptible node in this pair is infected by other infectious neighbors, it will become IT. Similarly, when the infectious node in the pair II is detected randomly or through contact tracing, the state of the pair II will also become IT.

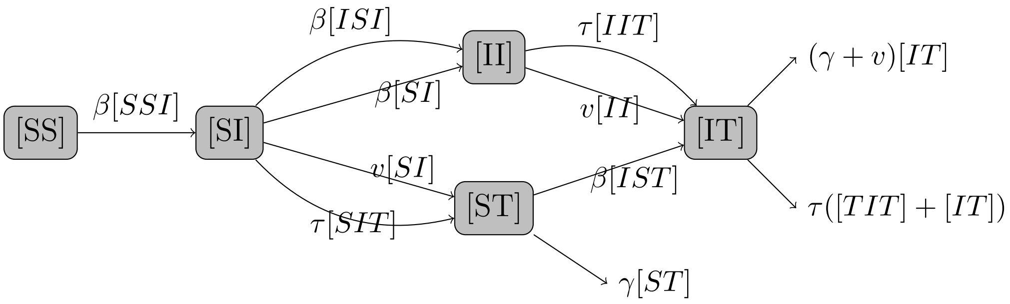

Figure 1.3: The pair dynamics of the contact tracing network model.

The pair dynamics is described by the following equations:

$$\begin{aligned}
[SS]' &= -2\beta[SSI],\\
[SI]' &= \beta([SSI]-[ISI]-[SI]) - v[SI] - \tau[SIT],\\
[II]' &= 2\beta([ISI]+[SI]) - 2(v+\gamma)[II] - 2\tau[IIT],\\
[ST]' &= -\beta[IST] + v[SI] + \tau[SIT] - \gamma[ST],\\
[IT]' &= \beta[IST] + v[II] - \gamma[IT] - v[IT] + \tau([IIT]-[TIT]-[IT]).
\end{aligned}$$

Here, they use a triple closure scheme in [37]

$$[ABC] \approx \frac{[AB][BC]}{[B]}.$$

For example,

$$[IIT] \approx \frac{[II][IT]}{[I]}, [TIT] \approx \frac{[TI][IT]}{[I]}.$$

The network approach can also be extended to incorporate asymptomatic infections, which play a crucial role in disease transmission. In such an extension, additional compartments can be introduced to distinguish between symptomatic and asymptomatic infectious individuals, as well as traced asymptomatic cases. However, implementing network-based models requires detailed knowledge of the underlying contact structure, including degree distributions, clustering, and correlations between connected nodes. In real-world applications, obtaining such data is challenging, particularly for large-scale populations.

1.3 Stochastic Epidemic Model

A stochastic epidemic model is a mathematical framework used to simulate and analyze the spread of infectious diseases where randomness plays a significant role. Unlike deterministic models, which predict outcomes based on fixed parameters and initial conditions, stochastic models incorporate randomness to reflect the unpredictable nature of disease transmission, recovery rates, or the introduction of new cases.

There are different types of stochastic epidemic models, including discrete time Markov chain (DTMC) models, continuous time Markov chain (CTMC) models, stochastic differential equation (SDE) models, and branching processes. These stochastic processes differ in the underlying assumptions regarding the time and the state variables.

1.3.1 Stochastic SIS and SIR Model

The SIS model describes infectious diseases where individuals can recover but do not develop immunity, meaning they return to the susceptible state. The stochastic SIS model extends the deterministic SIS model by treating transitions between compartments as probabilistic events. Instead of using differential equations to describe average changes, the number of susceptible and infectious individuals evolves according to random processes.

Let $S(t)$ and $I(t)$ represent the number of susceptible and infectious individuals at time t, respectively. The population size is N. There are two types of events:

- Infection event: A susceptible individual becomes infectious at rate $\beta I/N$, where β is the transmission rate.
- Recovery event: An infectious individual recovers and returns to the susceptible state at rate γ.

Assume that both processes are CTMC, where the state of the system at time t is described by $(S, I)(t)$, representing the number of susceptible and infectious individuals, respectively. The model assumes that infections and recoveries occur as Poisson processes, the transitions are give by:

$$\begin{aligned}(S, I) &\xrightarrow{\beta I \frac{S}{N}} (S-1, I+1),\\ (S, I) &\xrightarrow{\gamma I} (S+1, I-1).\end{aligned}$$

Let

$$P_j(t) = P[I(t) = j]$$

represents the probability of the number of infectious individuals is j at time t, where $j \in 0, 1, \ldots, N$. At the same time, $S(t) = N - j$. The master equation for this process can be written as below:

$$\dot{P}_j(t) = (j-1)\frac{\beta(N-j+1)}{N}P_{j-1} - j\frac{\beta(N-j)+\gamma}{N}P_j + \gamma(j+1)P_{j+1}.$$

For the SIR model, the state of the system is described by $(S, I, R)(t)$, representing the number of susceptible, infectious, and recovered individuals at time t, respectively. Similarly, there are two possible transitions:

$$\begin{aligned}(S, I, R) &\xrightarrow{\beta I \frac{S}{N}} (S-1, I+1, R),\\ (S, I, R)) &\xrightarrow{\gamma I} (S, I-1, R+1).\end{aligned}$$

Let

$$P_{ij}(t) = P[S(t) = i, I(t) = j]$$

represent the probability that the number of susceptible individuals is i and infectious individuals is j at time t, where $i, j \in 0, 1, \ldots, N$. For this process, the master equation is given by

$$\dot{P}_{i,j}(t) = (j-1)\frac{\beta(i+1)}{N}P_{i+1,j-1} - j\frac{\beta i+\gamma}{N}P_{i,j} + \gamma(j+1)P_{i,j+1}.$$

1.3.2 Branching Process Model for Contact Tracing

In the early stages of an outbreak, when the number of infectious individuals is small, disease transmission can be approximated as a branching process. This approach assumes that each infectious individual generates new infections independently, making it particularly useful for studying stochastic extinction and the effects of contact tracing.

Hellwell et al. [38] implemented a stochastic branching process model to simulate the spread of an infectious disease and assessed the effectiveness of isolation and contact tracing during the outbreak of COVID-19. They assume that the number of secondary infections generated by each infectious individual follows a negative binomial distribution. Each potential secondary case is assigned an infection time based on the serial interval distribution. A key feature of the model is case isolation, which prevents further transmission once an individual is identified. If an infectious individual is isolated before transmitting to all their potential secondary cases, the number of actual infections is lower than their initial transmission potential. The model accounts for delays from symptom onset to isolation, it assumes that symptomatic individuals are isolated based on a delay distribution, with isolation being fully effective in preventing further spread.

A simplified contact tracing process from [38] is shown in Figure 1.4. In this figure, nodes B and C are infected by node A. When diagnosed cases trigger contact tracing, the infectious nodes A and B are traced, preventing them from infecting other susceptible individuals. However, node C is not traced, allowing it to infect nodes D and E. While the branching process easily incorporates realistic distributions for the latent period and the delay in contact tracing, it becomes difficult to study the disease dynamics.

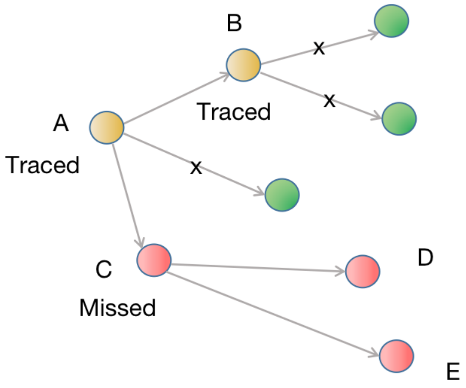

Figure 1.4: Example of the contact tracing process. The red nodes represent infectious individuals who have not been traced, the yellow nodes represent traced patients, and the green nodes represent susceptible individuals.

1.4 Parameter Estimation

Mathematical models are widely used to study infectious disease dynamics, evaluate control strategies, and predict future outbreaks. We need to know model parameter values to do model predictions. Some parameters, such as the mean incubation period and mean infectious period, can be estimated directly from case data, while others, such as the transmission rate, must be inferred from model calibration. Parameter estimation is crucial for calibrating models to real-world outbreaks, improving the reliability of predictions, and informing public health decision-making.

Several statistical methods have been developed to estimate parameters from epidemiological data. Among them, Maximum Likelihood Estimation (MLE) and Bayesian inference using Markov Chain Monte Carlo (MCMC) are two widely used approaches.

1.4.1 Maximum Likelihood Estimation

Maximum Likelihood Estimation (MLE) is a fundamental statistical method used to estimate the parameters of a mathematical model from observed data [39]. In epidemiology, MLE is commonly used to estimate the initial exponential growth rate of an epidemic [6]. The core idea behind MLE is to determine the parameter values that maximize the probability of the observed data given the assumed model.

Definition 1.4.1. *Likelihood Function: Let* $\boldsymbol{\theta} = (\theta_1, \theta_2, \ldots, \theta_k)$ *be a set of unknown parameters, and let* $\mathbf{X} = (X_1, X_2, \ldots, X_n)$ *be a random sample from a distribution with parameter* $\boldsymbol{\theta}$*. Given a dataset* $\mathbf{x} = (x_1, x_2, ..., x_n)$ *representing observed values of* $\mathbf{X}$*, the probability density function (PDF) or probability mass function (PMF) of the data given* $\boldsymbol{\theta}$ *is denoted as* $f(x_i|\boldsymbol{\theta})$ *for each observation* x_i*. The likelihood function, which represents the probability of observing the dataset as a function of* $\boldsymbol{\theta}$*, is defined as:*

$$L(\mathbf{x}|\boldsymbol{\theta}) = \prod_{i=1}^{n} f(x_i|\boldsymbol{\theta}).$$

The maximum likelihood estimate of $\boldsymbol{\theta}$, denoted by $\hat{\boldsymbol{\theta}}$, is obtained by maximizing the likelihood function:

$$\hat{\boldsymbol{\theta}} = \arg\max_{\boldsymbol{\theta}} L(\mathbf{x}|\boldsymbol{\theta}).$$

Since the likelihood function is a product of probabilities, it is often more convenient to work with the log-likelihood function, given by:

$$\ell(\boldsymbol{\theta}) = \log L(\mathbf{x}|\boldsymbol{\theta}) = \sum_{i=1}^{n} \log f(x_i|\boldsymbol{\theta}).$$

Since the logarithm is a monotonic function, maximizing $\ell(\boldsymbol{\theta})$ is equivalent to maximizing $L(\mathbf{x}|\boldsymbol{\theta})$. The MLE estimate $\hat{\boldsymbol{\theta}}$ is obtained by solving:

$$\frac{d\ell(\boldsymbol{\theta})}{d\boldsymbol{\theta}} = 0.$$

Example 1.4.1. *Suppose* $X_1, X_2, \ldots, X_n$ *are independent and identically distributed (i.i.d.) random variables following a Poisson distribution with an unknown rate parameter* $\lambda > 0$, *i.e.,*

$$X_i \sim \mathit{Poisson}(\lambda).$$

The probability mass function (PMF) of a Poisson-distributed random variable is given by:

$$P(X_i = x_i|\lambda) = \frac{\lambda^{x_i} e^{-\lambda}}{x_i!}, \quad x_i = 0, 1, 2, \ldots$$

The likelihood function for the given dataset $\mathbf{x} = (x_1, x_2, \ldots, x_n)$ *is:*

$$L(\lambda) = \prod_{i=1}^{n} \frac{\lambda^{x_i} e^{-\lambda}}{x_i!}.$$

Taking the natural logarithm, we obtain the log-likelihood function:

$$\ell(\lambda) = \sum_{i=1}^{n} \left(x_i \ln \lambda - \lambda - \ln x_i! \right).$$

To find the MLE of λ, *we differentiate* $\ell(\lambda)$ *with respect to* λ *and set it to zero:*

$$\frac{d\ell(\lambda)}{d\lambda} = \sum_{i=1}^{n} \left(\frac{x_i}{\lambda} - 1 \right) = 0.$$

Solving for λ, *we obtain the MLE estimate:*

$$\hat{\lambda} = \frac{1}{n} \sum_{i=1}^{n} x_i.$$

Thus, the MLE of λ *is simply the sample mean.*

Example 1.4.2. *Suppose* $X_1, X_2, \ldots, X_n$ *are i.i.d. random variables following a Negative Binomial distribution with parameters* $r > 0$ *and* $p \in (0, 1)$, *i.e.,*

$$X_i \sim \mathit{NB}(r, p).$$

The PMF of a Negative Binomial distributed random variable is:

$$P(X_i = x_i | r, p) = \binom{x_i + r - 1}{x_i} p^r (1-p)^{x_i}, \quad x_i = 0, 1, 2, \ldots$$

The likelihood function is:

$$L(r, p) = \prod_{i=1}^{n} \binom{x_i + r - 1}{x_i} p^r (1-p)^{x_i}.$$

Taking the natural logarithm, the log-likelihood function is:

$$\ell(r, p) = \sum_{i=1}^{n} \left[\ln \binom{x_i + r - 1}{x_i} + r \ln p + x_i \ln(1-p) \right].$$

To estimate p*, we take the derivative with respect to* p *and set it to zero:*

$$\frac{d\ell}{dp} = \sum_{i=1}^{n} \left(\frac{r}{p} - \frac{x_i}{1-p} \right) = 0.$$

Solving for p*, we get:*

$$\hat{p} = \frac{nr}{\sum_{i=1}^{n} (x_i + r)}.$$

1.4.2 Bayesian Markov Chain Monte Carlo Method

Markov Chain Monte Carlo (MCMC) methods are a class of algorithms used for sampling from probability distributions when direct sampling is difficult. In Bayesian inference, MCMC is essential for estimating posterior distributions of model parameters when the posterior is complex and cannot be computed analytically [40].

Bayes' theorem [41] provides a framework for updating knowledge about parameters based on observed data. Given a set of observed data $\mathbf{x}$ and unknown parameters $\boldsymbol{\theta}$, we define:

- The posterior distribution, $p(\boldsymbol{\theta}|\mathbf{x})$, which represents the updated probability of the parameters $\boldsymbol{\theta}$ after observing the data $\mathbf{x}$.
- The likelihood function, $p(\mathbf{x}|\boldsymbol{\theta})$, which describes the probability of the observed data given the parameters.
- The prior distribution, $p(\boldsymbol{\theta})$, which reflects prior knowledge or beliefs about the

parameters before observing the data.

- The marginal likelihood, $p(\mathbf{x})$, which represents the total probability of the observed data, integrating over all possible parameter values.

Applying Bayes' theorem, we obtain:

$$p(\boldsymbol{\theta}|\mathbf{x}) = \frac{p(\mathbf{x}|\boldsymbol{\theta})p(\boldsymbol{\theta})}{p(\mathbf{x})}.$$

Definition 1.4.2. *Markov Chain: The process generates a sequence of random variables* $\{\boldsymbol{\theta}^{(t)}\}$ *where the next state depends only on the current state:*

$$p[\boldsymbol{\theta}^{(t+1)}|\boldsymbol{\theta}^{(t)}, \boldsymbol{\theta}^{(t-1)}, \ldots] = p[\boldsymbol{\theta}^{(t+1)}|\boldsymbol{\theta}^{(t)}].$$

Over time, the Markov chain converges to the target posterior distribution $p(\boldsymbol{\theta}|\mathbf{x})$*.*

Definition 1.4.3. *Monte Carlo Sampling: After the Markov chain has converged, we draw samples* $\{\boldsymbol{\theta}^{(t)}\}$ *to approximate expectations:*

$$\mathbb{E}[g(\boldsymbol{\theta})] \approx \frac{1}{N}\sum_{t=1}^{N} g(\boldsymbol{\theta}^{(t)}),$$

where $g(\boldsymbol{\theta})$ *is the function of the parameter vector* $\boldsymbol{\theta}$ *that you wish to evaluate or estimate from the posterior distribution.*

The central idea behind MCMC method is to define a convergent Markov Chain over the sampling process, which in the limit guarantees to draw from a true stationary (possibly high dimensional) statistical distribution [40].

Example 1.4.3. ***Metropolis-Hastings Algorithm:***

The Metropolis-Hastings algorithm generates a sequence of samples by evaluating the posterior probabilities of a new sample $\boldsymbol{\theta}^{t+1}$ *and the current sample* $\boldsymbol{\theta}^{t}$*. The acceptance probability is given by:*

$$A = \min\left(1, \frac{P(\boldsymbol{\theta}^{t+1}|\mathbf{x})q(\boldsymbol{\theta}^{t}|\boldsymbol{\theta}^{t+1})}{P(\boldsymbol{\theta}^{t}|\mathbf{x})q(\boldsymbol{\theta}^{t+1}|\boldsymbol{\theta}^{t})}\right),$$

where $q(\boldsymbol{\theta}^{t+1}|\boldsymbol{\theta}^{t})$ *is the proposal distribution.*

- *If* $A \geq 1$*, the new sample* $\boldsymbol{\theta}^{t+1}$ *is accepted.*

- *If* $A < 1$*, the new sample is accepted with probability* A*; otherwise, the algorithm retains* $\boldsymbol{\theta}^t$*.*

The process continues iteratively until the Markov chain converges to the target posterior distribution. The final sample in the chain represents the Maximum A Posteriori (MAP) estimate, which is the set of parameters that maximizes the posterior probability:

$$\hat{\boldsymbol{\theta}}_{MAP} = \arg\max_{\boldsymbol{\theta}} P(\boldsymbol{\theta}|\mathbf{x}).$$

The Posterior Mean Estimate is given by:

$$\hat{\boldsymbol{\theta}}_{mean} = \frac{1}{N}\sum_{t=1}^{N} \boldsymbol{\theta}^t.$$

The posterior mean estimate provides a more stable estimate by averaging over multiple samples.

Example 1.4.4. ***Metropolis Algorithm:***

The Metropolis algorithm is a special case of the Metropolis-Hastings algorithm, where the proposal distribution $q(\boldsymbol{\theta}^{t+1}|\boldsymbol{\theta}^t)$ *is symmetric, meaning:*

$$q(\boldsymbol{\theta}^{t+1}|\boldsymbol{\theta}^t) = q(\boldsymbol{\theta}^t|\boldsymbol{\theta}^{t+1}).$$

For example, this could be a normal distribution centered at the current state with a fixed variance.

This symmetry cancels out the proposal terms in the acceptance ratio, simplifying it to:

$$A = \min\left(1, \frac{P(\boldsymbol{\theta}^{t+1}|\mathbf{x})}{P(\boldsymbol{\theta}^t|\mathbf{x})}\right).$$

1.5 Motivation of the Dissertation

Contact tracing is an essential public health measure to reduce disease transmission. However, due to limited public health capacity, it is most effective during the early stages of an outbreak when the number of cases is relatively low. A key challenge in modelling contact tracing within compartmental models stems from their assumption of randomly mixed populations, which do not track individual contacts. Although contact network models explicitly track interactions between individuals, they require detailed network data that is often unavailable. This raises the question: can the network approach be used to model a randomly mixed population?

Methods such as Poisson regression and negative binomial regression have been proposed to estimate the exponential growth rate of an outbreak. The distribution of case counts plays a crucial role in establishing a suitable likelihood function for estimating this growth rate. For a stochastic SEIR model, analyzing its distribution through the master equation could provide new insights. Furthermore, since the exponential growth phase is short, the available data are limited. How can we construct a likelihood function that accurately estimates the exponential growth rate when data are scarce?

1.6 Structure of Dissertation

In Chapter 2, a novel modeling framework is developed to track contacts in a randomly mixed population. This approach incorporates edge dynamics from network models to track contacts within a compartmental SIR model of epidemic spread. In Chapter 3, the SIR contact tracing model is extended to include the latent period and asymptomatic transmission, allowing for a more comprehensive study of contact tracing effectiveness. We study the datasets needed for identifying model parameters and apply our contact tracing models to the Ontario COVID-19 outbreak. In Chapter 4, the approximate case count distribution is derived for a linear stochastic SEIR model using a probability-generating function. Chapter 5 compares the negative binomial regression model and the hidden Markov model (HMM) for estimating the exponential growth rate during the early stage of an epidemic. Finally, the findings and discussions are presented in Chapter 6. Additional detailed calculations are provided in the Appendix.

Chapter 2

A Contact Tracing SIR Model for Randomly Mixed Populations

This chapter is published in the *Journal of Biological Dynamics* [42]. [1]

2.1 Introduction

The introduction of a novel or rare transmissible pathogen into a susceptible population requires strong measures to control or prevent ongoing transmission. Recent examples include Ebola virus, the novel coronavirus causing severe acute respiratory syndrome (SARS), and the novel coronavirus SARS-CoV-2 causing coronavirus disease (COVID-19). Depending on the pathogen, these measures include pharmaceutical interventions (e.g., vaccination and antivirals) or non-pharmaceutical interventions (e.g., social distancing, mask-wearing, ventilation, business and school closures, and contact tracing). Specifically, contact tracing is a crucial public health intervention strategy for emerging and re-emerging infectious diseases to contain and prevent further spread of the disease [43, 44]. Following the testing and isolation of a positively diagnosed infectious case, contact tracing is initiated: contacts of the diagnosed case are identified for quarantine and subsequent testing and isolation is undertaken as required. The isolation of infectious individuals during their infectious period is crucial for inhibiting further transmission. Studies have shown that contact tracing can be effective in reducing the control reproduction number $\mathcal{R}_c$ of SARS-CoV-2, delaying the epidemic peak, and decreasing the epidemic growth rate, particularly in

---

[1] The authors in this paper are alphabetically listed. My contributions include: writing-original draft, methodology, investigation, formal analysis and conceptualization.

the presence of other non-pharmaceutical interventions; however, contact tracing on its own may not be able to adequately control an epidemic [4, 38, 45–48].

There are challenges and limitations that can impact the effectiveness of contact tracing measures. In the initial stages of an emerging outbreak, proper laboratory diagnostics may not be readily available and must be developed before being able to correctly diagnose infected patients [49, 50]. As well, case definitions, testing criteria, isolation procedures, and other public health interventions may vary over time in terms of their implementation [49, 51].

The effectiveness of contact tracing can be quantified as the reduction in cases caused by contact tracing. This reduction can be reflected in key epidemic measures such as the reproduction number (the number of secondary infectious of a patient during their infectious period), the reported cases or hospitalization. Contact tracing effectiveness depends on the proportion of transmission occurring from individuals in a pre-symptomatic or asymptomatic stage of disease as well as the number of secondary infections resulting from one infectious individual [38, 46]. For example, if a pathogen such as SARS-CoV-2 can be transmitted during a pre-symptomatic stage or from a fully asymptomatic infected individual [52] but guidelines for testing and isolation of infectious cases are based on symptomatic criteria alone, subsequent contact tracing activities may not capture a large fraction of infectious individuals that are contributing to the growing number of community-based infections in the population; thus, the epidemic may not be contained in this scenario [47]. Additionally, the evolution of pathogen characteristics over time can lead to changes in transmission capabilities and disease presentation. For example, the transmissibility and infectiousness of SARS-CoV-2 variants over the course of the COVID-19 pandemic have varied greatly [53, 54]. As infections increase, there may also be challenges in maintaining appropriate and sustainable resources and capacity levels. Laboratories may be hindered in their ability to undertake timely and accurate testing and contact tracers may become overwhelmed in attempting to identify contacts in a timely fashion [55].

Mathematical models can be used to examine the impact of contact tracing and testing on disease dynamics in terms of the magnitude and duration of transmission of an infectious pathogen in a population [48, 56, 57]. One approach is the use of compartmental models. Those that assume a random mixing population, such as the Kermack-McKendrick susceptible-infected-removed (SIR) model and their extensions, have been widely used to study disease dynamics [24, 58–60]. However, while some of these models incorporate contact tracing they are not precise because they do not track the contacts of patients, which is crucial in understanding contact tracing [23,24,61]. In fact, these models assume that a constant fraction of new infections will be traced; however, realistically this fraction increases with the number of traced patients. Other powerful approaches that mathematically model contact tracing are stochastic models, e.g., [45,62,63]. These models have been used to study the effect of contact tracing on the reduction of secondary infections (the reproduction number). However, it can be difficult to use stochastic models to study the dynamics of epidemics. Similarly, contact networks are used to study contact tracing because they keep track of neighbours [4,34,64,65]. However, applying contact networks to disease dynamics requires a detailed understanding of the underlying network structure, such as the degree distribution (the distribution of the number of neighbours of a random node) [66,67], clustering (the fraction of edges in a triangle) [34,64,65], degree correlation (whether nodes with many neighbours are likely to connect to each other) [34,68], and other information on network topology [69,70]. This network information is not usually easily available. Additionally, while agent-based models can be useful, they require the utilization of many parameters and computational capacity [60].

Instead, we borrow the idea of tracing the states of nodes and their contacts from contact network models to develop a new compartmental model for contact tracing. In this model, we keep track of the states of the patient and the infector together in a pair. This novel approach allows us to determine the rate that patients are contact traced. Our new model is introduced in Section 2.2. For validation, in Section 2.3, we introduce an agent-based model for contact tracing of an SIR epidemic, which is used to compare the simulations with the solutions of our model. In Section 2.4, the control reproduction number is calculated, and the model dependence on the contact tracing parameters is discussed. The effect of tracing capacity is considered in Section 2.5, with concluding remarks given in Section 2.6.

2.2 The Compartmental SIR Contact Tracing Model

We consider susceptible-infected-recovered (SIR) epidemic spread in a randomly mixed population that is subject to testing and contact tracing. The population is divided into the susceptible (S), infectious (I), diagnosed (T for tested positive), contact tracing initiated (X), and recovered and not diagnosed (R) classes. We assume that voluntary testing is initiated by infectious symptomatic individuals and thus we ignore asymptomatic and pre-symptomatic disease states. In addition, we assume that the diagnosed patients (T) and contact traced individuals (X) are fully isolated, and do not transmit disease. We assume that disease deaths are negligible, and are thus not considered here. We also ignore the population dynamics, so that the population size N remains constant. Assuming a randomly mixed population, T is typically a small fraction of the total population, and the number of contact traced (and quarantined) susceptible individuals is also a small fraction of the population. Therefore, these quarantined susceptible individuals have negligible effect on disease dynamics. Thus, we ignore the contact tracing and quarantining of susceptible individuals. We also assume that contact tracing has no effect on a T, X or R contact.

2.2.1 Tree of Transmission

We consider disease transmission in a randomly mixed population; specifically, the tree of transmission in such a population. Figure 2.1 provides a visualization of the chain of infections occurring from the introduction of an infectious individual (or node) in a population of susceptible individuals (or nodes). The direction of the arrows in Fig 2.1a shows the direction of transmission, or, who-infected-who. The purple nodes reflect those who have been infected and positively diagnosed. We can ignore the remaining susceptible nodes and examine the remaining tree of transmission and apply contact tracing (Fig 2.1b). Notice that each individual node that has been infected is part of a pair of nodes. Here, the orange arrows reflect the direction of contact tracing that has been initiated from the positively diagnosed node. We now want to study this tree of transmission when diagnosis and contact tracing occur.

2.2.2 Model Development

To model contact tracing, we keep track of contacts that caused infections. These contacts form a tree of infections, where the nodes are the patients, and arcs represent who-infected-who. The infection process generates this tree dynamically, while the contact tracing operates on the tree. An edge on the tree is labeled as $[A \leftarrow B]$, representing a node of class A that was infected by a node currently in class B where $A, B \in \{I, T, X, R\}$, e.g., $[I \leftarrow I]$, $[I \leftarrow T]$, $[T \leftarrow I]$, etc. Here, the direction of the arrow denotes the direction of transmission. A diagnosed patient (T) initiates contact tracing (and becomes X) at a rate θ, and their I contacts are traced with probability p and

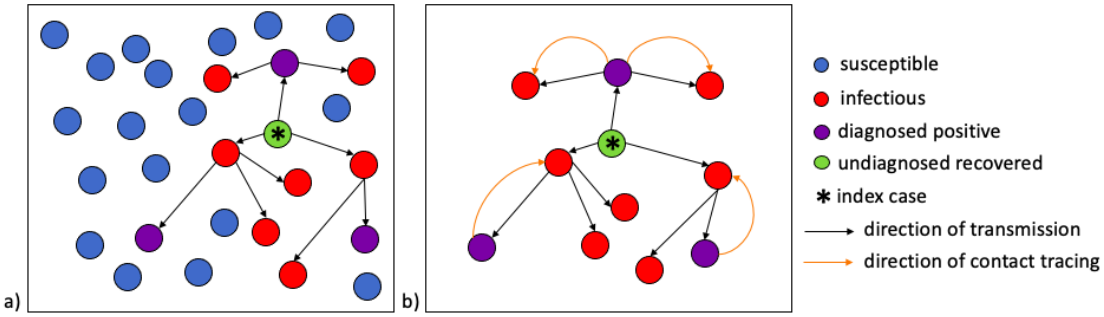

Figure 2.1: (a): A population of randomly mixed nodes. The arrows between the nodes denote the chain of transmission within the population following introduction of an initial infectious node (*). Purple nodes represent infectious nodes that have been tested and diagnosed positive. The red nodes are infectious but undiagnosed. The green node represents recovery of an infectious node that has not been diagnosed. (b): A tree of transmission resulting from interactions between infectious and susceptible nodes. The orange arcs represent the direction of contact tracing triggered from a positively diagnosed node.

becomes diagnosed (T). Thus, the $[I{\leftarrow}T]$ and $[T{\leftarrow}I]$ pairs become $[T{\leftarrow}X]$ and $[X{\leftarrow}T]$, respectively, at a rate θp. This process then propagates to all I neighbours of the newly diagnosed node.

Figure 2.2 shows the flowchart of the population dynamics. As in a standard SIR model, the susceptible individuals (S) are infected and become infectious patients according to

$$S' = -\beta \frac{SI}{N} \,,$$

where β is the transmission rate, and N is the total population size. A patient (I) may:

- recover and become R at a rate γ; or,
- be diagnosed positive and become T at a rate τ; or,
- be traced and also become T either in:
  - an $[I{\leftarrow}T]$ pair if their infector is diagnosed (T); or,
  - in a $[T{\leftarrow}I]$ pair if one of the contacts they infected is T.

We assume that a T individual triggers contact tracing at a rate θ and becomes X. We also assume that a fraction p of the contacts (independent of their state) of a T individual is captured by contact tracing. This fraction p is called the coverage probability. Then,

$$\begin{aligned}
I' &= \beta\frac{SI}{N} - \gamma I - \tau I - \theta p([I\leftarrow T] + [T\leftarrow I])\,,\\
T' &= \tau I + \theta p([I\leftarrow T] + [T\leftarrow I]) - \theta T\,,\\
X' &= \theta T\,,\\
R' &= \gamma I\,.
\end{aligned}$$

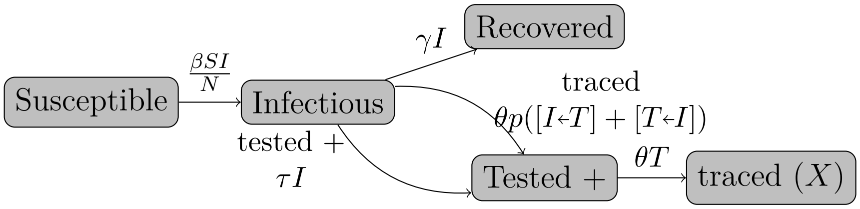

Figure 2.2: Flowchart of SIR model with testing and tracing (Population Dynamics).

To model the dynamics of the pairs $[I\leftarrow T]$ and $[T\leftarrow I]$ (Figure 2.3), we start with the dynamics of an $[I\leftarrow I]$ pair that is formed when a susceptible individual is infected. Both $[I\leftarrow T]$ and $[T\leftarrow I]$ pairs come from an $[I\leftarrow I]$ pair. In an $[I\leftarrow I]$ pair, the first I is the new patient and the second is the infector. There are several possibilities for how the state of an $[I\leftarrow I]$ pair changes:

- the patient recovers at a rate γ and enters R; or,
- the infector recovers at a rate γ and the pair becomes $[I\leftarrow R]$; or,
- the patient is voluntarily tested and diagnosed at a rate τ and the pair becomes $[T\leftarrow I]$ (while the patient enters T); or,
- the infector is tested at a rate τ and the pair becomes $[I\leftarrow T]$; or,
- the patient or the infector is contact traced (described below).

The infectee in an $[I\leftarrow I]$ pair may be contact traced from one of their secondary infections, which happens in a triple interaction $[T\leftarrow \underline{I\leftarrow I}]$ (the underline represents the original $[I\leftarrow I]$ pair). Similarly, the infector may be traced from their infector in triples $[\underline{I\leftarrow I}\leftarrow T]$, or from another of their secondary infections in $[\underline{I\leftarrow I}\rightarrow T]$. Each of these triple interactions occurs at a rate θp (because the patient is captured by contact tracing with a probability p).

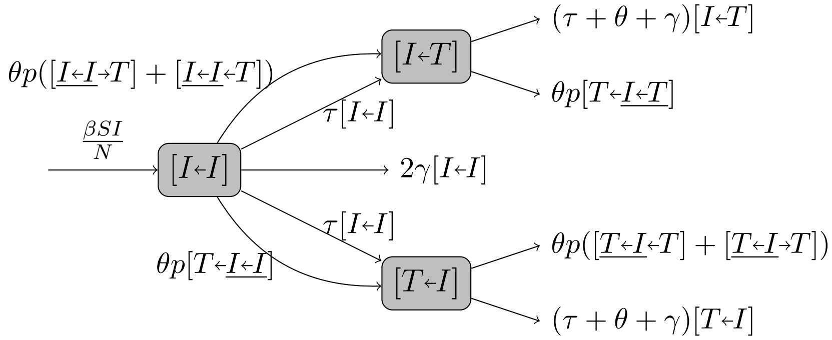

Figure 2.3: Flowchart of Pair Dynamics.

Thus,

$$[I\leftarrow I]' = \beta\frac{SI}{N} - (2\gamma+2\tau)[I\leftarrow I] - \theta p([T\leftarrow\underline{I\leftarrow I}] + [\underline{I\leftarrow I}\leftarrow T] + [\underline{I\leftarrow I}\rightarrow T])\,.$$

We also track the dynamics of the triple interactions $[T\leftarrow\underline{I\leftarrow I}]$, $[\underline{I\leftarrow I}\leftarrow T]$ and $[\underline{I\leftarrow I}\rightarrow T]$. Their dynamics further depend on the interactions of four individuals. Eventually, the full interaction dynamics give an infinite-dimensional system. Instead, we use a closure method that has commonly been used in network models [35]. For example, a $[T\leftarrow\underline{I\leftarrow I}]$ triple is a $[T\leftarrow I]$ pair followed by an $[I\leftarrow I]$ pair. Thus the number of $[T\leftarrow\underline{I\leftarrow I}]$ triples is the product of the number of $[T\leftarrow I]$ pairs and the average number of $[I\leftarrow I]$ pairs where the infector of the $[T\leftarrow I]$ pair is a patient. From the random mixing assumption, the average number of $[I\leftarrow I]$ pairs following an I can be approximated as $[I\leftarrow I]/I$. Thus,

$$[T\leftarrow\underline{I\leftarrow I}] \approx [T\leftarrow I]\frac{[I\leftarrow I]}{I}\,.$$

Similarly,

$$[\underline{I\leftarrow I}\leftarrow T] \approx [I\leftarrow I]\frac{[I\leftarrow T]}{I}\,.$$

The number of $[\underline{I\leftarrow I}\rightarrow T]$ triples is the product of the number of $[I\leftarrow I]$ pairs and the average number of $[T\leftarrow I]$ pairs when the infector of the $[I\leftarrow I]$ pair has infected the T in the $[T\leftarrow I]$ pair. That is,

$$[\underline{I\leftarrow I}\rightarrow T] \approx [I\leftarrow I]\frac{[T\leftarrow I]}{I}\,.$$

For the dynamics of the $[I\leftarrow T]$ pair, they come from $[I\leftarrow I]$ pairs as stated above. The patient may recover and become R at a rate γ, or may become $[T\leftarrow T]$ if the patient is either tested and diagnosed with a rate τ or contact traced. In the last case, the contact tracing may be initiated by the infector (and then the pair becomes either $[T\leftarrow X]$ with a probability p if the patient is successfully traced, or $[I\leftarrow X]$ otherwise), or initiated by another T infected by the patient in a $[T\leftarrow\underline{I\leftarrow T}]$ triple interaction. And thus,

$$[I\leftarrow T]' = \tau[I\leftarrow I] + \theta p([\underline{I\leftarrow I}\rightarrow T] + [\underline{I\leftarrow I}\leftarrow T]) - (\gamma+\tau+\theta)[I\leftarrow I] - \theta p[T\leftarrow\underline{I\leftarrow T}]\,,$$

where

$$[T\leftarrow\underline{I\leftarrow T}] = [T\leftarrow I]\frac{[I\leftarrow T]}{I}\,.$$

Finally, a $[T\leftarrow I]$ pair also comes from an $[I\leftarrow I]$ pair, and may become $[T\leftarrow R]$ if the infector recovers, or $[T\leftarrow T]$ if the infector either tests positive or is traced (from either the T patient in the pair, or a T infector in a $[\underline{T\leftarrow I}\leftarrow T]$ triple, or another T contact in a $[\underline{T\leftarrow I}\rightarrow T]$ triple. Thus,

$$[T\leftarrow I]' = \tau[I\leftarrow I] + \theta p[T\leftarrow\underline{I\leftarrow I}] - (\gamma+\tau+\theta)[T\leftarrow I] - \theta p([\underline{T\leftarrow I}\leftarrow T] + [\underline{T\leftarrow I}\rightarrow T])\,,$$

where

$$[\underline{T\leftarrow I}\leftarrow T] = [T\leftarrow I]\frac{[I\leftarrow T]}{I} = [T\leftarrow\underline{I\leftarrow T}]\,,\ [\underline{T\leftarrow I}\rightarrow T] = [T\leftarrow I]\frac{[T\leftarrow I]}{I}\,.$$

Therefore, the system can be written as below:

$$\begin{align}
S' &= -\beta S\frac{I}{N}\,, \tag{2.1a}\\
I' &= \beta S\frac{I}{N} - (\gamma+\tau)I - \theta p([I\leftarrow T] + [T\leftarrow I])\,, \tag{2.1b}\\
[I\leftarrow I]' &= \beta S\frac{I}{N} - 2(\gamma+\tau)[I\leftarrow I] - \theta p\frac{2[T\leftarrow I] + [I\leftarrow T]}{I}[I\leftarrow I]\,, \tag{2.1c}\\
[I\leftarrow T]' &= \tau[I\leftarrow I] + \theta p\frac{[I\leftarrow T] + [T\leftarrow I]}{I}[I\leftarrow I] - (\gamma+\tau+\theta)[I\leftarrow T] \notag\\
&\quad -\theta p\frac{[T\leftarrow I][I\leftarrow T]}{I}\,, \tag{2.1d}\\
[T\leftarrow I]' &= \tau[I\leftarrow I] + \theta p\frac{[T\leftarrow I][I\leftarrow I]}{I} - (\gamma+\tau+\theta)[T\leftarrow I] \notag\\
&\quad -\theta p\frac{[T\leftarrow I] + [I\leftarrow T]}{I}[T\leftarrow I]\,, \tag{2.1e}\\
T' &= \tau I + \theta p([I\leftarrow T] + [T\leftarrow I]) - \theta T\,, \tag{2.1f}\\
X' &= \theta T\,, \tag{2.1g}\\
R' &= \gamma I\,. \tag{2.1h}
\end{align}$$

Figure A.1 in Appendix A gives the flowchart of the model tracking all pairs for which the patient is an I or T. The I and T populations are $I = [I{\leftarrow}I] + [I{\leftarrow}T] + [I{\leftarrow}X] + [I{\leftarrow}R]$ and $T = [T{\leftarrow}I] + [T{\leftarrow}T] + [T{\leftarrow}X] + [T{\leftarrow}R]$.

2.3 Model Verification

To verify that the model is a good description of the contact tracing process we constructed an agent-based simulation model for a contact tracing process in a randomly mixed population, and showed that the ensemble average of the agent-based simulation agrees with the solutions of model (2.1).

Consider a population with N individuals. Initially, I_0 individuals are randomly selected and labeled infectious (I), while others are labeled susceptible (S). Each infectious individual maintains a list of contacts (that is initially empty). Upon becoming infectious, the individual is assigned four events. The event times are calculated as the current time (of becoming infectious) plus a waiting time. The events are

- a transmission event with a waiting time randomly drawn from an exponential distribution with a rate β;
- a recovery event with a waiting time (i.e., the infectious period) randomly drawn from a probability distribution with a density $f_I(t)$;
- a test event with a waiting time randomly drawn from a probability distribution with a density $f_T(t)$.
- a contact tracing event with waiting time randomly drawn from a probability distribution with a density $f_X(t)$.

Note that only infectious individuals have events attached. The earliest event of all individuals is determined and the corresponding infectious individual is noted. The current time is then set to the next event time. The states are adjusted according to the following algorithm:

- If it is a transmission event, then a contact is randomly chosen assuming individuals are uniformly distributed in the population. If the contact is susceptible, then the contact becomes infectious. To implement contact tracing, the contact is added to the list of contacts of the infectious individual. The infectious individual is also added to the contact list of the contact. A new contact event with an i.i.d. waiting time is assigned to the infectious individual.

- If it is a recovery event (at the end of the infectious period), the individual is labeled recovered, and the contact list and all remaining events attached to this individual are cleared. A recovered individual obtains lifetime immunity and will not be infected again.

- If it is a test event, then the infectious individual is relabeled diagnosed (T). A contact tracing event with a waiting time drawn from the distribution $f_X(t)$ is assigned to the diagnosed individual.

- If it is a contact tracing event, each contact in their contact list is traced. If the contact is infectious, then the contact becomes diagnosed with a probability p (i.e., the contact tracing coverage probability). Otherwise the contact remains intact. The contact tracing process is recursively applied to the contacts. After all the contacts are traced, the contact list and all remaining events attached to this individual are cleared. Thus, we do not keep track of recovery of diagnosed individuals in this process, and diagnosed individuals are fully isolated and do not further infect others.

The earliest event has now been handled. We then inspect the next event. This process is repeated until no event remains, or a designated time is reached in the simulation.

To compare with our compartmental SIR contact tracing model, the infectious period density $f_I(t)$ is assumed exponential with rate γ, the test waiting time density $f_T(t)$ is assumed exponential with rate τ, and the contact tracing waiting time density $f_X(t)$ is assumed exponential with rate θ.

Although our model is motivated by the COVID-19 pandemic, it is an oversimplification, and the parameter values are chosen only as a reasonable illustration of results. Time is a continuous variable. The number of infectious individuals is counted at the end of each time step in the simulation.

Figure 2.4 shows the comparison of $I(t)$ numerically solved from the compartmental SIR contact tracing model (equation (2.1)) with the ensemble average of 100 runs of agent-based simulations with identical parameter values and initial conditions. The numerical solutions of our model agree well with the agent-based simulations, especially in the initial exponential growth phase.

Although the agent-based model is relatively simple and neglects details such as heterogeneous contacts, it provides a reasonable description of the contact tracing process under the same assumptions of the ODE model. The agreement between these two models suggests that the ODE framework offers a solid theoretical understanding of contact tracing dynamics under these assumptions. Although our over-simplified assumptions such as exponentially distributed waiting times and randomly mixed population may limit the accuracy of our ODE model to capture the real contact tracing process, it is a good starting point to build more realistic models to describe real-world outbreaks, as is done in Chapter 3.

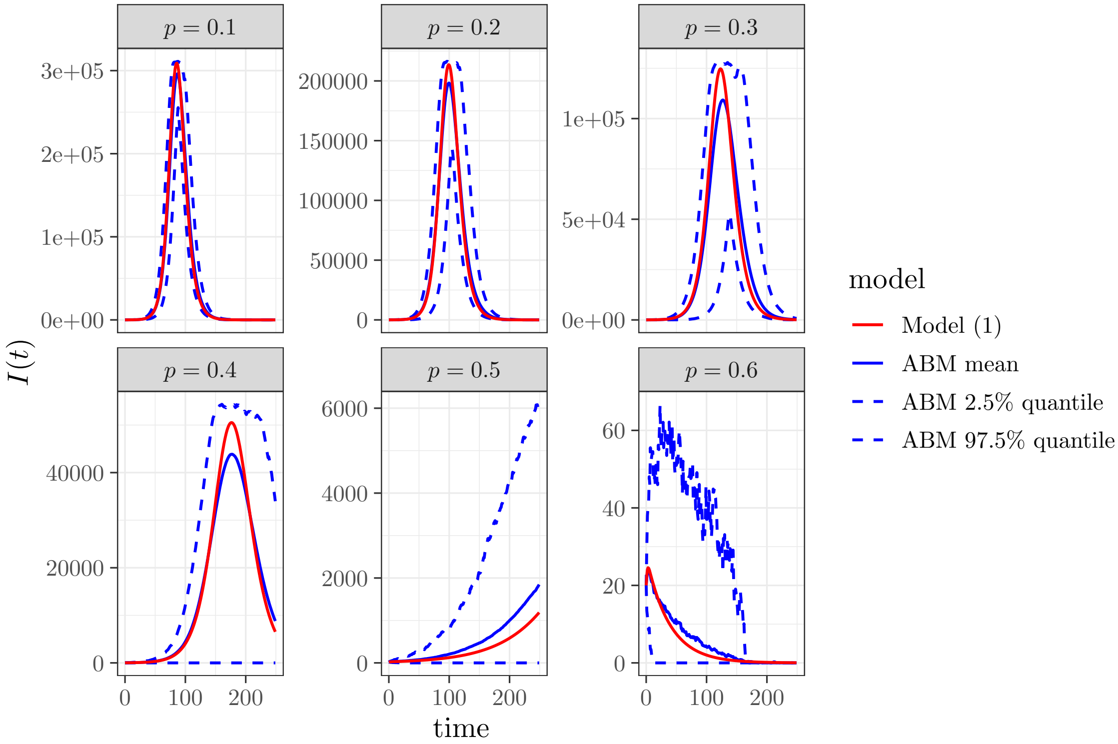

Figure 2.4: The comparison of $I(t)$ numerically solved from our contact tracing model (2.1) with the ensemble average of 100 runs of agent-based simulations with identical parameter values and initial conditions. The parameter values are $N = 5 \times 10^6$, $\beta = 0.4$, $\gamma = 0.1$, $\tau = 0.15$, $\theta = 10$, $I(0) = 20$, and the coverage tracing probability (or probability of diagnosis) was $p = 0.1, 0.2, \cdots 0.6$.

2.4 Model Analysis

In this section, we calculate the control reproduction number $\mathcal{R}_c$ for the compartmental SIR contact tracing model, and analyze how it depends on the contact tracing parameters.

2.4.1 Disease-free State and Control Reproduction Number

Without disease (i.e., $I = 0$), the fractions $[T{\leftarrow}I]/I$ and $[I{\leftarrow}T]/I$ are not defined. We change the variables to avoid this problem. Let

$$u = \frac{[I{\leftarrow}I]}{I}, \quad v = \frac{[I{\leftarrow}T]}{I}, \quad w = \frac{[T{\leftarrow}I]}{I}.$$

At the disease free equilibrium, u, v and w are defined as the limits when $I \to 0^+$. System (2.1) can be rewritten as

$$\begin{aligned}
S' &= \beta S \frac{I}{N} \qquad &(2.2a)\\
I' &= \beta S \frac{I}{N} - (\gamma + \tau)I - \theta p(v + w)I\,, \qquad &(2.2b)\\
u' &= \beta \frac{S}{N}(1 - u) - (\tau + \gamma)u - \theta p u w\,, \qquad &(2.2c)\\
v' &= \tau u + \theta p u(v + w) - (\beta + \theta)v + \theta p v^2\,, \qquad &(2.2d)\\
w' &= \tau u - (\beta + \theta)w + \theta p u w\,. \qquad &(2.2e)
\end{aligned}$$

For this system, the set $\{S = N, I = 0\}$ is invariant. In addition,

$$\mathcal{H} = \{(N, 0, u, v, w) \in \mathbb{R}^5_+, u + v \leq 1\}$$

is also invariant, because $[I{\leftarrow}I] + [I{\leftarrow}T] \leq I$. To analyse the system at the disease-free state, we restrict the system to the invariant set $\mathcal{H}$.

A disease-free equilibrium $(N, 0, u^*, v^*, w^*)$ must satisfy the following conditions. From (2.2c),

$$u^* = \frac{\beta}{\beta + \tau + \gamma + \theta p w^*}, \tag{2.3}$$

Substituting this into (2.2e) gives

$$G(w^*) := (\beta + \theta)\theta p w^{*2} + [(\beta + \theta)(\beta + \tau + \gamma) - \beta\theta p]w^* - \beta\tau = 0. \tag{2.4}$$

From (2.2d),

$$F(v^*) := \theta p v^{*2} + (\theta p u^* - \beta - \theta) v^* + \theta p u^* w^* + \tau u^* = 0. \tag{2.5}$$

We show in Appendix B that this system has a unique biologically meaningful disease-free equilibrium (DFE) that is globally asymptotically stable in the disease-free invariant set $\mathcal{H}$. Hence, we can calculate the control reproduction number by linearizing at this DFE. Note that the u, v and w equations decouple from the linearization, the behaviour of the linearized system only depends on

$$I' = [\beta - \gamma - \tau - \theta p (v^* + w^*)] I \,.$$

Thus, the control reproduction number is

$$\mathcal{R}_c = \frac{\beta}{\gamma + \tau + \theta p (v^* + w^*)} \,. \tag{2.6}$$

Here the denominator is the rate that an infectious individual leaves class I by recovery, testing, or contact tracing. Thus, $\mathcal{R}_c$ is the number of secondary infections caused by a typical infectious individual in a population where contact tracing and isolation of infectious individuals are implemented. Note that, at the beginning of the epidemic, no one is diagnosed yet, i.e., $T = 0$, and thus $v = w = 0$. Therefore, before any patient is diagnosed and the contact tracing starts, the basic reproduction number is

$$\mathcal{R}_0 = \frac{\beta}{\gamma + \tau} \,. \tag{2.7}$$

However, $v(t)$ and $w(t)$ quickly approach v^* and w^*, respectively, while $\mathcal{R}_c$ becomes the value defined in (2.6).

2.4.2 Dependency of $\mathcal{R}_c$ on Model Parameters

Because v^* and w^* depend on all of the model parameters, the control reproduction number $\mathcal{R}_c$ also depends on all model parameters.

We prove in Appendix C that v^* and w^* are increasing functions of the contact tracing coverage probability p and the testing rate τ for $\mathcal{R}_c > 1$. That is, the control reproduction number $\mathcal{R}_c$ is a decreasing function of p and τ. This is because testing and tracing increase the number of tested contacts with an infectious individual (i.e., the number of $[I \leftarrow T]$ and $[T \leftarrow I]$ pairs), and thus v^* and w^* increase with p and τ.

To investigate the sensitivity of $\mathcal{R}_c$ to coverage tracing probability p and the testing probability τ, we plot the control reproduction number as a function of p and τ in Figure 2.5. This contour plot shows that $\mathcal{R}_c$ decreases with both p and τ. In this figure, the level curves have a negative slope with a magnitude less than 1. This means that a small increase in τ has the same effect on $\mathcal{R}_c$ as a large increase in p. Thus, $\mathcal{R}_c$ is more sensitive to τ than to p. In addition, the magnitude of the slope increases as τ increases for each fixed p; thus, the sensitivity to p increases with τ. This is because more tests trigger more contact tracing, and thus makes tracing more effective.

The dependence of $\mathcal{R}_c$ on the tracing rate θ and the transmission rate β is difficult to study analytically. We illustrate these dependencies using numerical simulations. Figure 2.6 illustrates that $\mathcal{R}_c$ is a decreasing function of θ, because θv^* and θw^* are increasing functions of θ. This is because increasing θ speeds up contact tracing, and thus more contacts are traced. Note that, as θ approaches ∞, θv^*, θw^* and $\mathcal{R}_c$ have limits. Figure 2.7 shows that $\mathcal{R}_c$ is an increasing function of β. Interestingly, the average number of diagnosed infectors v^* and the average number of diagnosed secondary infections w^* are unimodal functions of β. The reason for this is not intuitive. We suspect that a moderate increase in β leads to more secondary infections, thus, increasing the average number of infectors and infectees that are diagnosed; while this increase also speeds up contact tracing and thus removes more infectors than infectees for very large β. Note that here, we use $p = 1$ to show that even if the contact tracing coverage is 1, $\mathcal{R}_c$ may still be above 1 when θ is small or when β is large.

2.5 The Effect of Tracing Capacity on $\mathcal{R}_c$

In the compartmental SIR contact tracing model, the total contact tracing rate in the population is θT. When the diagnosed population T is large, the contact tracing capacity becomes a limiting factor. To understand the effect of contact tracing capacity on the effectiveness of contact tracing, we model the per capita contact tracing rate θ as a decreasing function of T, so that θT is a saturating function of T. Specifically,

$$\theta = \frac{\theta_0}{1 + \frac{\theta_0}{\theta_\infty} T}\,, \tag{2.8}$$

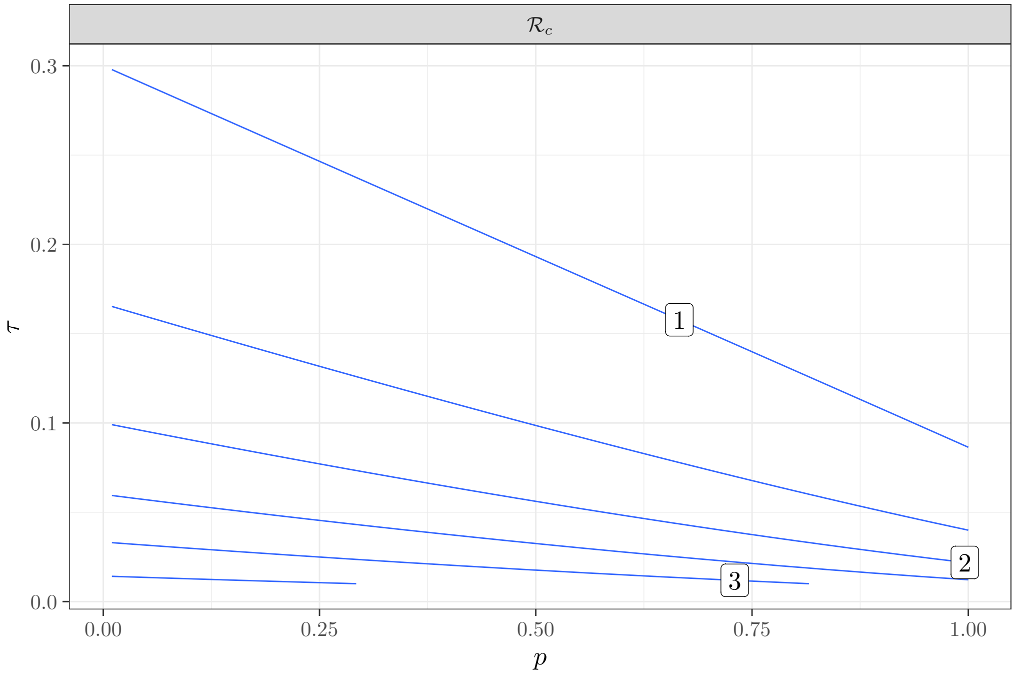

Figure 2.5: The contour plot of $\mathcal{R}_c$ as a function of the contact tracing coverage probability p and the testing rate τ. Here $\beta = 0.4$, $\gamma = 0.1$, $\theta = 1$.

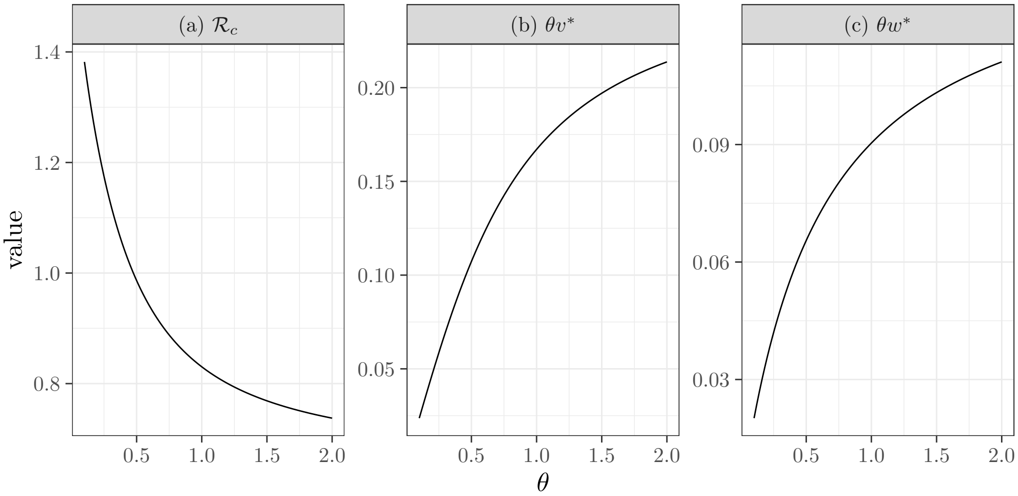

Figure 2.6: The dependence of the control reproduction number $\mathcal{R}_c$, θv^*, and θw^* on the tracing rate θ. Here $\gamma = 0.1$, $\tau = 0.15$, $p = 1$, $\beta = 0.4$. Specifically, (b) reflects the contact tracing rate initiated from the infector and (c) reflects the rate initiated from an infectee. This figure also shows that contact tracing is more likely to originate from an infector as $\theta v^* > \theta w^*$.

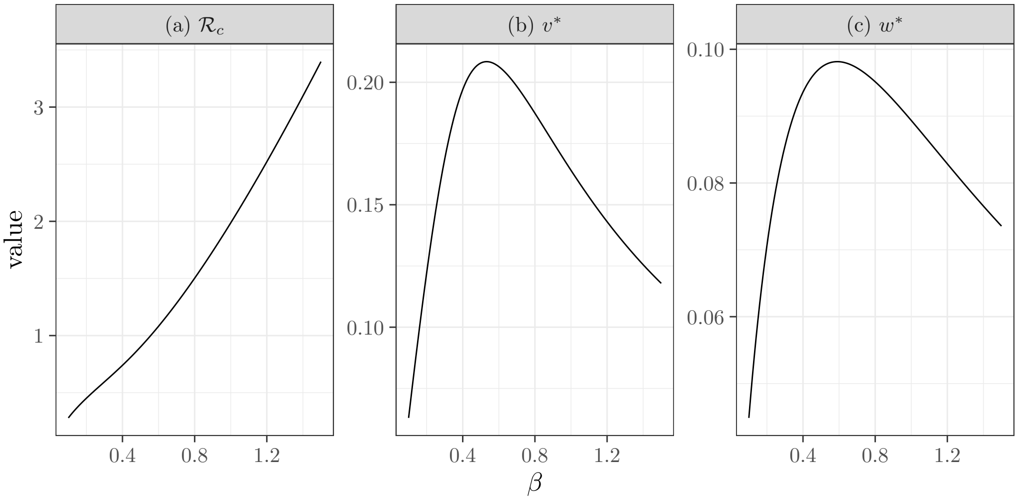

Figure 2.7: The dependence of the control reproduction number $\mathcal{R}_c$, the fraction of diagnosed infectors (v^*), and the average number of diagnosed secondary infections (w^*) on the transmission rate β. Here $\gamma = 0.1$, $\tau = 0.15$, $p = 1$, $\theta = 1$.

where θ_0 is the per capita tracing rate with units 1/time when T is small, and $\theta_\infty = \lim_{T\to\infty} \theta T$ is the tracing capacity with units person/time.

At the disease-free equilibrium, $T = 0$ and $\theta = \theta_0$, the control reproduction number defined in (2.6) becomes

$$\mathcal{R}_c = \frac{\beta}{\gamma + \tau + \theta_0 p(v^* + w^*)} .$$

On the other hand, as $T \to \infty$, $\theta \to 0$, and $\mathcal{R}_c$ becomes $\mathcal{R}_0$ in (2.7). Thus, when the number of diagnosed patients T is large so that the tracing reaches capacity, $\mathcal{R}_c$ becomes the same as without contact tracing. Figure 2.8 illustrates this effect. Note that the $\mathcal{R}_c$ starts as the basic reproduction number $\mathcal{R}_0$ because no patient has been diagnosed. Then $\mathcal{R}_c$ quickly reduces to the value given in equation (2.6), and if contact tracing reaches capacity $\mathcal{R}_c$ increases and may approach $\mathcal{R}_0$ again. This may happen long before the epidemic reaches its peak. As well, we can see that the implementation of contact tracing delays the peak of the epidemic as shown in the comparison between the curves in both panels of Figure 2.8 where $p = 0$ (no contact tracing) and the tracing capacity $\theta_\infty = 100$. The most significant impact, however, is the inhibition of the growth of $\mathcal{R}_c$ and the associated delay and restriction of the epidemic peak when the tracing capacity $\theta_\infty \to \infty$.

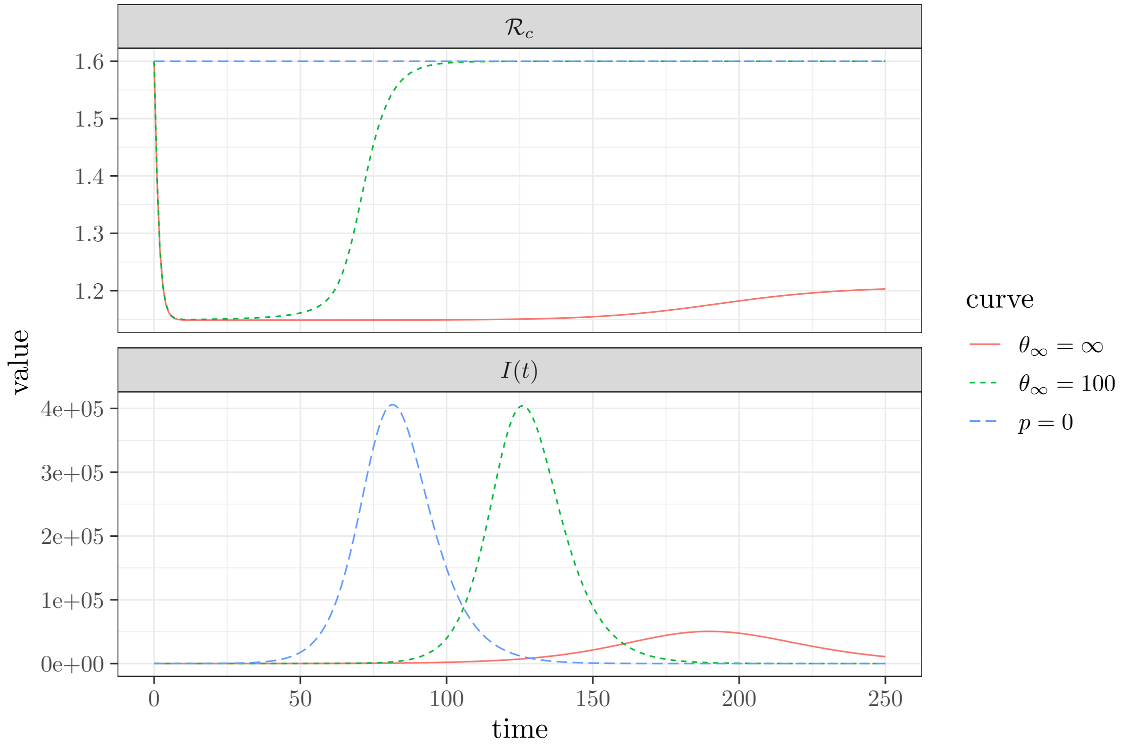

Figure 2.8: The change in the control reproduction number ($\mathcal{R}_c$, shown in the top panel), and the number of infectious individuals (I, shown in the bottom panel) as a function of time. Note that $\mathcal{R}_c$ is a function of time through θ, v and w. The blue dashed curve with $p = 0$ reflects the case where contact tracing does not occur. Comparatively, the green dashed curve shows the case where: $p = 0.4$ and $\theta_\infty = 100$. Finally, the red curve shows the case where $p = 0.3$ and $\theta_\infty = \infty$. Here, the remaining fixed values and parameters are: $N = 5 \times 10^6$, $\beta = 0.4$, $\tau = 0.15$, $\gamma = 0.1$, $\theta_0 = 10$.

2.6 Concluding Remarks

Our novel approach for modelling contact tracing of an infectious disease (Section 2.2) combines the convenience of a randomly mixed population with the precise tracking of the contacts in a network model. Thus to apply this model, detailed population contact information is not required.

Our analysis shows that the reproduction number $\mathcal{R}_c$ decreases as the contact tracing coverage probability p increases (Appendix C). This is to be expected because as the fraction of individuals identified for testing and isolation increases, the remaining unidentified fraction of individuals that contribute to transmission decreases. We also find that when there is a large transmission rate β, contact tracing alone may not control the disease (Figure 2.7); thus, additional public health measures to decrease the transmission rate will need to be implemented in order for contact tracing to be effective. These findings are in alignment with other study results mentioned previously [24,38,45–48]. We also find that $\mathcal{R}_c$ is more sensitive to the testing rate τ than to coverage probability p (Figure 2.5). Specifically, when testing rate is increased, $\mathcal{R}_c$ becomes more sensitive to the coverage probability. Thus, increasing testing coverage allows the effectiveness of contact tracing to also increase.

While this model only considers symptomatic infections and symptomatic testing, we can assess the impact of transmission from asymptomatic and pre-symptomatic infected individuals on the ability of contact tracing to effectively control the disease. When symptomatic testing is the primary method for identifying positive cases, this ultimately reduces the fraction of all infectious individuals (pre-symptomatic, asymptomatic, and symptomatic) who are tested, diagnosed, and isolated. This is represented by a reduced testing rate τ and reduced contact tracing coverage p. Thus, the reduction of the fraction of individuals tested reduces the effectiveness of contact tracing. This finding was also reported in [47].

We also show that at the initial phase of the epidemic and thus when T is small, contact tracing can reduce $\mathcal{R}_c$, and this also agrees with [47]. However, as T increases and becomes large, contact tracing becomes saturated due to limited resources to effectively trace all contacts following positive diagnosis (keeping all other parameters fixed). Thus, $\mathcal{R}_c$ quickly increases back to $\mathcal{R}_0$ (Figure 2.8). Note that this only occurs when tracing capacity $\theta_\infty \ll \infty$, and this reversal may occur much earlier than the actual epidemic peak. Overall, contact tracing is most effective during the initial exponential growth phase of the epidemic in all scenarios. We show that when all other parameters remained fixed, (i.e., no additional interventions applied to reduce the transmission rate β) and $\theta_\infty \ll \infty$, contact tracing reaches capacity and has limited effectiveness prior to the main peak of the epidemic. However, when the tracing capacity θ_∞ approaches ∞, the epidemic peak is not only delayed, but significantly suppressed. Note that these results implicitly assume a positive diagnosis rate, i.e., $\tau > 0$.

As this is a simple SIR model that has been extended to include both testing and contact tracing, it does not accurately reflect the reality of many infectious diseases that do have pre-symptomatic or asymptomatic transmission. However, this model can be extended to incorporate exposed, asymptomatic, and pre-symptomatic compartments as well as differing testing and isolation policies. With these extensions, this model may be fit to case count data to estimate the contact tracing coverage p and other parameters, and these parameter values used to evaluate the effect of contact tracing on the control reproduction number and epidemic final size. Further, the implementation of non-pharmaceutical interventions, vaccination, and treatment measures can also be included in the model. It is not clear how these extensions would affect our conclusions if incorporated; this is left for future work. In the case of SARS-CoV-2, the differences in variant transmissibility and detection should also be considered with regard to contact tracing effectiveness. Because saturation of contact tracing and testing capacity and resources have been shown to impact the effectiveness of contact tracing activities, it would be useful to incorporate cost-benefit and cost-effectiveness analyses to this model to help further inform public health interventions and policies in responding to current and future epidemics of concern. It may be that if resources for contact tracing become scarce, public health should shift to more effective mitigation strategies.

Chapter 3

Estimating the Effect of Contact Tracing During the Early Stage of an Epidemic

This chapter is published in *Infectious Disease Modelling* [71].[1]

3.1 Introduction

In recent years, there have been multiple major infectious disease outbreaks that have had a severe impact on population health. The SARS virus spread to more than 30 countries and regions in 2002-2003 [1]. In 2009, influenza A (H1N1) also spread worldwide [2], and the recent COVID-19 pandemic has significantly affected people's lives. In the early stage of an outbreak of a new infectious disease, due to a lack of understanding of the disease's characteristics, governments usually implement a series of non-pharmaceutical public health interventions (NPIs). These interventions include maintaining social distancing, wearing masks or respirators, prohibiting large gatherings, closing schools and restaurants, and contact tracing.

Contact tracing is an effective strategy for controlling certain epidemics, such as SARS [72], and has also been implemented during the COVID-19 pandemic. This strategy involves identifying and isolating individuals at high risk of infection by tracking the contacts of diagnosed patients. As a result, it reduces disease transmis-

---

[1] I am the first and corresponding author of this paper. My contributions include: writing–original draft, visualization, software, methodology, investigation, formal analysis and conceptualization.

sion among the traced contacts and helps prevent further spread of the disease [43]. Kretzschmar et al. [45] showed that in combination with social distancing, contact tracing can reduce the basic reproduction number of COVID-19 and control disease spread. However, it is important to note that the implementation of contact tracing is a time-consuming process and is limited by available resources and capabilities. As the number of cases increases, limited capacity results in only a small fraction of contacts being tracked, reducing the effectiveness of contact tracing [42,73,74]. Thus, contact tracing is most effective in the early (exponentially growing) stage of a disease outbreak when the case count is small. However, in this exponential growth stage, it is a challenge to estimate model parameters for models with many parameters [75], which hinders the assessment of the effectiveness of contact tracing.

Asymptomatic transmission poses another challenge for contact tracing, as identifying asymptomatic patients is difficult. Tupper et al. [76] showed that without additional measures in place, relying solely on contact tracing is insufficient to prevent exponential growth. Therefore, evaluating the effectiveness of contact tracing measures in the early stage of a pandemic is a topic worthy of study. In this paper, we want to address the question how to decouple the effect of contact tracing from other NPIs and assess its effectiveness.

A naive method to estimate the effect of contact tracing is to obtain data on the fraction of cases detected through contact tracing. However, this fraction does not accurately represent the effectiveness of contact tracing. First, these data may not include asymptomatic patients. During the early stage of the COVID-19 pandemic in Canada, the testing policy excluded asymptomatic patients, so these patients were not identifiable even though they may be quarantined by contact tracing. Second, this fraction is dynamic, not a constant [42]. Specifically, the effectiveness of contact tracing can be influenced by other control measures and hindered by limited resources [42].

We use mathematical models to evaluate the effectiveness of contact tracing in the early stage of an epidemic. Mathematical models are important tools for studying the dynamics of infectious diseases and evaluating control measures. Ordinary differential equation compartmental models are frequently used in the study of epidemic dynamics [24,59,60]. Based on a compartmental model of COVID-19, Wu et al. [24] confirmed that public health interventions implemented in Ontario, Canada, can slow the spread of the disease. However, classical compartmental models assume that the population's contacts on a large scale are uniform and homogeneous [9, 15], implying that each individual has the same probability of contacting every other individual. As a result, they do not track who infected whom. To better describe the actual contacts within a population, there is a growing trend in analyzing and studying the spread of epidemics from the perspective of contact networks [35, 36]. Huerta et al. [4] proposed the deterministic mean field equations in random networks to analyze the effect of contact tracing on epidemic control. However, network models require extensive information about the network structure, including degree distribution [66, 67], degree correlation [34, 68] and clustering [34, 64, 65].

We have proposed a novel method to model contact tracing in [42]. We developed an SIR model in a randomly mixed population, assuming that contacts leading to infection form a transmission tree, and then we incorporated the concept of tracing node status from network models to monitor these infection-causing contacts. However, this model is a simple SIR model that ignores the latent period and asymptomatic infections, which are important features for certain diseases. Therefore, this model cannot be used to evaluate the effectiveness of contact tracing during the COVID-19 pandemic. A more realistic disease model is needed. In subsections 3.2.1 and 3.2.2, we extend the SIR contact tracing model to include exposed and asymptomatic compartments, respectively. We consider the impact of NPIs and add the quarantined compartment, establishing SEIR and SEAIR models in a randomly mixed population. Since in the early stage of a disease outbreak, we do not know whether there are asymptomatic infections or whether asymptomatic patients are infectious, we may use the SEIR model to analyze the dynamics of the disease. Therefore, we establish these two models to study whether there is a significant difference in the analysis results. We calculate the control reproduction number for the SEIR and SEAIR models in subsection 3.2.3. In subsection 3.2.4, we compare the simulation results of our SEAIR model with those of an agent-based model to validate our model.

The case count data during the exponential growth stage of an epidemic are insufficient to estimate important parameter values such as the transmission rate and the contact tracing parameters. This is because the key quantity determined by such data is the exponential growth rate, which is jointly influenced by all disease and intervention parameters. We need to identify datasets that can be used alongside case counts to estimate parameter values of our models. To do so, we conduct a simulation study: as reported in Section 3.3. The goals of this simulation study are to determine the data needed to identify model parameters, and to compare the effectiveness of contact tracing between using the SEIR model and the SEAIR model.

In Section 3.4, we apply our contact tracing models to the early outbreak of COVID-19 in Ontario in 2020, and assess the effectiveness of contact tracing. Concluding remarks are provided in Section 3.5.

3.2 Compartmental Contact Tracing Models

In this section, we extend the SIR contact tracing model for a homogeneously mixed population [42] to incorporate exposed and asymptomatic compartments.

Classical compartmental epidemic models for homogeneously mixed populations do not track contacts, but contacts are crucial for describing contact tracing. As in [42], we track contacts using the network modelling idea of tracking edge changes. Specifically, an infection-causing contact between an infectious individual and a susceptible individual can be labelled by an arc pointing from the infectious individual to the susceptible one. The state of the arc is labeled by the state of the two individuals, as $[S \leftarrow I]$ in this case. The state of the arc changes as the infection state of either individual changes. For example, as the susceptible individual becomes infected and enters the exposed (E, i.e., latent) compartment, the state of the arc becomes $[E \leftarrow I]$. In general, an arc is labelled as $[B \leftarrow A]$, where A is the state of the infector, and B is the state of the infectee.

Contact tracing occurs with a probability p if either individual of an arc has been diagnosed (in the compartment T for tested positive). Each diagnosed individual initiates contact tracing at a rate θ, i.e., the mean delay from being diagnosed (and entering T) and triggering contact tracing (and entering the compartment X) is $1/\theta$. Here, we use the compartment X to denote diagnosed patients who have triggered contact tracing, ensuring that contact tracing can only be triggered once for each individual in T. We assume that diagnosed individuals are fully isolated. Thus individuals in T and X do not infect others. We assume that disease-related deaths are negligible and that population dynamics are ignored, maintaining a constant population size N. Using these ideas, we develop the SEIR contact tracing model in subsection 3.2.1 and the SEAIR model in subsection 3.2.2.

3.2.1 SEIR Contact Tracing Model

To establish an SEIR contact tracing model in a randomly mixed population, we divide the population into the following compartments: the susceptible individuals

S, the latent patients E, the symptomatic infectious patients I, the quarantined individuals Q (due to contact tracing initiated by their contacts), and the recovered individuals R, in addition to the T and X compartments defined above.

Since the quarantined susceptible individuals are generally a very small fraction of the total susceptible population, they have little effect on the disease dynamics. Thus, they are not followed in this model, and the only quarantined individuals counted here are latent patients who are traced from their infectors. We assume that the latent patients are not infectious, and therefore, the quarantined individuals in compartment Q cannot infect others. We do not track the recovered R, T, and X individuals, as they do not affect disease dynamics.

Figure 3.1 shows the flowchart of disease dynamics, where β_I is the transmission rate, γ_I is the recovery rate, $1/\theta$ is the mean delay from diagnosis to contact tracing, p is the probability of an infectious contact being traced (tracing coverage), $1/\sigma$ is the mean latent period, and τ_I is the voluntary testing rate after showing symptoms.

In addition to the flows of a standard SEIR model, the exposed individuals in the pairs $[E{\leftarrow}T]$ are traced at a rate θp and are quarantined (entering Q). When the quarantined individuals in Q show symptoms (at rate σ), they are diagnosed and enter T. The infectious individuals may test positive through two different pathways: voluntarily tested at a rate τ_I; or contact traced at a rate of θp.

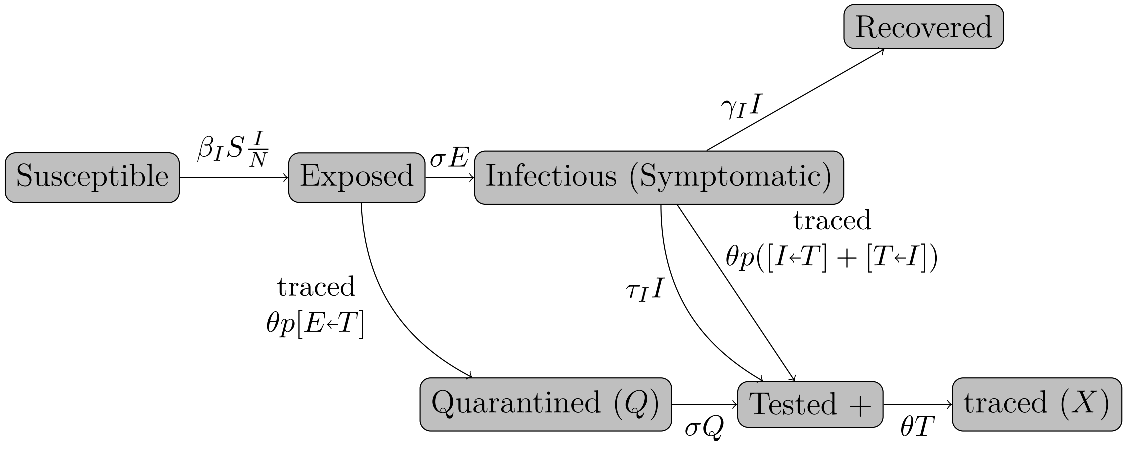

Figure 3.1: The dynamics of the SEIR model with testing and tracing.

The disease dynamics are governed by the following system

$$S' = -\beta_I S \frac{I}{N},$$

$$\begin{aligned}
E' &= \beta_I S \frac{I}{N} - \sigma E - \theta p [E{\leftarrow}T]\,, \\
I' &= \sigma E - (\gamma_I + \tau_I) I - \theta p ([I{\leftarrow}T] + [T{\leftarrow}I])\,, \\
Q' &= \theta p [E{\leftarrow}T] - \sigma Q, \\
T' &= \sigma Q + \tau_I I + \theta p ([I{\leftarrow}T] + [T{\leftarrow}I]) - \theta T\,, \\
X' &= \theta T\,, \\
R' &= \gamma_I I\,.
\end{aligned}$$

To close the model, we need to describe the dynamics of the pairs $[E{\leftarrow}T]$, $[I{\leftarrow}T]$ and $[T{\leftarrow}I]$ (Figure 3.2). Each infected individual initially forms an $[E{\leftarrow}I]$ pair with their infector. If the infector of an $[E{\leftarrow}I]$ pair is voluntarily tested and diagnosed at a rate τ_I, this pair becomes $[E{\leftarrow}T]$. If the infector is contact traced from its diagnosed infector or another infectee, this pair also becomes $[E{\leftarrow}T]$. So we need to consider the interactions of the pairs and the neighbors of the infector or infectee in the pair. These three-node interactions are called triples. Specifically, to study $[E{\leftarrow}I]$ pairs, we need to study the triples $[\underline{E{\leftarrow}I}{\rightarrow}T]$ and $[\underline{E{\leftarrow}I}{\leftarrow}T]$, where the underline represents the original $[E{\leftarrow}I]$ pair. For $[\underline{E{\leftarrow}I}{\rightarrow}T]$, the infector I has infected both contacts E and T. In $[\underline{E{\leftarrow}I}{\leftarrow}T]$, E is infected by I who has been infected by T. The $[E{\leftarrow}I]$ pairs become $[I{\leftarrow}I]$ if the latent patients show symptoms. When the infectious patient of a pair $[E{\leftarrow}I]$ recovers at rate γ_I, the state of pair $[E{\leftarrow}I]$ also changes.

When the latent patient in pair $[E{\leftarrow}T]$ shows symptoms, $[E{\leftarrow}T]$ becomes $[I{\leftarrow}T]$. When the infector in pair $[I{\leftarrow}I]$ tests positive through voluntary testing at a rate γ_I, or is traced through its diagnosed contacts in triples $[\underline{I{\leftarrow}I}{\rightarrow}T]$ and $[\underline{I{\leftarrow}I}{\leftarrow}T]$, the pair $[I{\leftarrow}I]$ becomes $[I{\leftarrow}T]$. In $[\underline{I{\leftarrow}I}{\rightarrow}T]$, T represents the infectee, whereas in $[\underline{I{\leftarrow}I}{\leftarrow}T]$, T represents the infector. If the infectee in pair $[I{\leftarrow}I]$ is diagnosed through voluntary testing or traced from its diagnosed contacts in the triple $[T{\leftarrow}\underline{I{\leftarrow}I}]$ (where T is the infectee), the pair $[I{\leftarrow}I]$ becomes $[T{\leftarrow}I]$. When the infectious individual in pair $[I{\leftarrow}I]$ recovers, the pair changes its state. Similarly, the states of pairs $[I{\leftarrow}T]$ and $[T{\leftarrow}I]$ also change due to voluntary testing, contact tracing, or disease progression.

Thus, we can write down the equations for $[E{\leftarrow}I]$, $[E{\leftarrow}T]$, $[I{\leftarrow}I]$, $[I{\leftarrow}T]$ and $[T{\leftarrow}I]$:

$$\begin{aligned}
[E{\leftarrow}I]' &= \beta_I S \frac{I}{N} - (\tau_I + \gamma_I)[E{\leftarrow}I] - \theta p ([\underline{E{\leftarrow}I}{\rightarrow}T] + [\underline{E{\leftarrow}I}{\leftarrow}T]) - \sigma [E{\leftarrow}I], \\
[E{\leftarrow}T]' &= \tau_I [E{\leftarrow}I] + \theta p ([\underline{E{\leftarrow}I}{\rightarrow}T] + [\underline{E{\leftarrow}I}{\leftarrow}T]) - \sigma [E{\leftarrow}T] - \theta [E{\leftarrow}T], \\
[I{\leftarrow}I]' &= \sigma [E{\leftarrow}I] - 2(\gamma_I + \tau_I)[I{\leftarrow}I] - \theta p ([\underline{I{\leftarrow}I}{\leftarrow}T] + [\underline{I{\leftarrow}I}{\rightarrow}T] + [T{\leftarrow}\underline{I{\leftarrow}I}]),
\end{aligned}$$

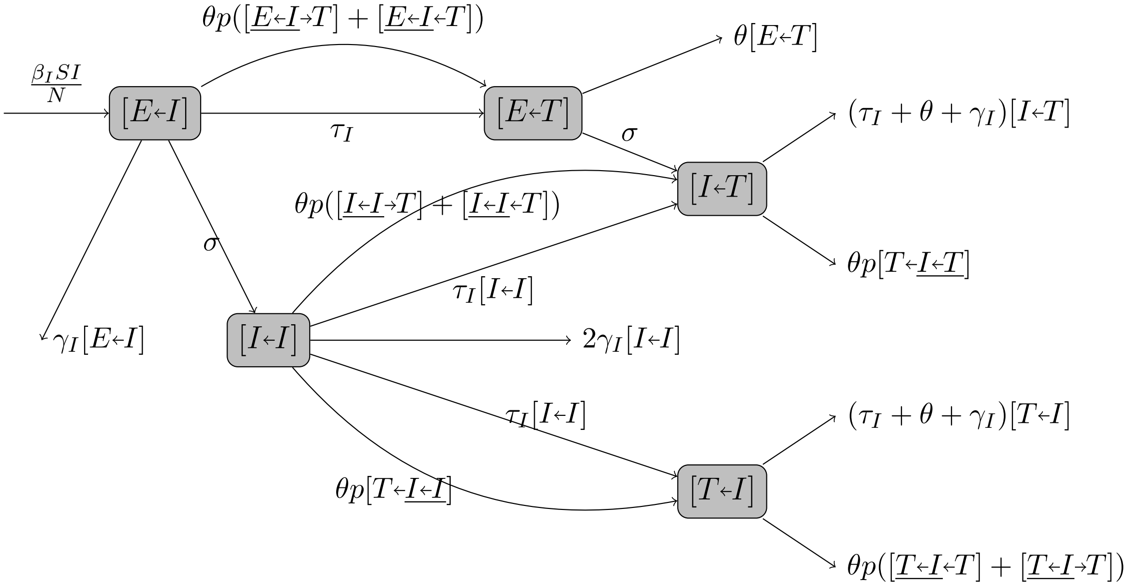

Figure 3.2: Pair dynamics of the SEIR model.

$$
\begin{aligned}
[I \leftarrow T]' &= \sigma [E \leftarrow T] + \tau_I [I \leftarrow I] + \theta p([\underline{I \leftarrow I} \leftarrow T] + [\underline{I \leftarrow I} \rightarrow T] - [T \leftarrow \underline{I \leftarrow T}]) - (\tau_I + \theta + \gamma_I)[I \leftarrow T],\\
[T \leftarrow I]' &= \tau_I [I \leftarrow I] + \theta p([T \leftarrow \underline{I \leftarrow I}] - [\underline{T \leftarrow I} \leftarrow T] - [\underline{T \leftarrow I} \rightarrow T]) - (\tau_I + \theta + \gamma_I)[T \leftarrow I],
\end{aligned}
$$

The dynamics of the triples such as $[\underline{E \leftarrow I} \rightarrow T]$ and $[\underline{E \leftarrow I} \leftarrow T]$ depend on four-node interactions, and thus the full model is infinite-dimensional. To simplify, as in [42], we use a triple closure method that is commonly used in network models [29, 34]. The number of triples $[\underline{A \leftarrow B} \leftarrow C]$ can be approximated by the number of $[A \leftarrow B]$ pairs multiplied by the average number of $[B \leftarrow C]$ pairs where the infector B in $[A \leftarrow B]$ is infected by C nodes. In a randomly mixed population, this average number can be approximated by the fraction $\frac{[B \leftarrow C]}{B}$. Thus,

$$[\underline{A \leftarrow B} \leftarrow C] \approx [A \leftarrow B] \frac{[B \leftarrow C]}{B},$$

where $A, B, C \in \{E, I, T\}$. This approximation of the triples provides a method to “close” the system using pairs, allowing the model to remain computationally manageable while still capturing essential network effects.

Similarly, the number of triples $[A \leftarrow \underline{B \leftarrow C}]$ can be approximated by the number of $[B \leftarrow C]$ pairs multiplied by the average number of $[A \leftarrow B]$ pairs following a given B node:

$$[A \leftarrow \underline{B \leftarrow C}] \approx [B \leftarrow C] \frac{[A \leftarrow B]}{B}.$$

The number of triples $[\underline{A{\leftarrow}B}{\rightarrow}C]$ can be approximated by the product of $[A{\leftarrow}B]$ pairs and the fraction of B nodes which caused infection of C nodes :

$$[\underline{A{\leftarrow}B}{\rightarrow}C] \approx [A{\leftarrow}B]\frac{[C{\leftarrow}B]}{B}.$$

Therefore, we have

$$[\underline{E{\leftarrow}I}{\leftarrow}T] = [E{\leftarrow}I]\frac{[I{\leftarrow}T]}{I},\quad [\underline{E{\leftarrow}I}{\rightarrow}T] = [E{\leftarrow}I]\frac{[T{\leftarrow}I]}{I},$$

$$[\underline{I{\leftarrow}I}{\leftarrow}T] = [I{\leftarrow}I]\frac{[I{\leftarrow}T]}{I},\quad [\underline{I{\leftarrow}I}{\rightarrow}T] = [I{\leftarrow}I]\frac{[T{\leftarrow}I]}{I},$$

$$[\underline{T{\leftarrow}A}{\rightarrow}T] = [T{\leftarrow}A]\frac{[T{\leftarrow}A]}{I},\quad [\underline{T{\leftarrow}I}{\rightarrow}T] = [T{\leftarrow}I]\frac{[T{\leftarrow}I]}{I},$$

and

$$[\underline{T{\leftarrow}I}{\leftarrow}T] = [T{\leftarrow}I]\frac{[I{\leftarrow}T]}{I} = [T{\leftarrow}\underline{I{\leftarrow}T}].$$

Then, this system is closed, and can be written as

$$S' = -\beta_I S\frac{I}{N}\,, \tag{3.3a}$$

$$E' = \beta_I S\frac{I}{N} - \sigma E - \theta p[E{\leftarrow}T]\,, \tag{3.3b}$$

$$I' = \sigma E - (\gamma_I + \tau_I)I - \theta p([I{\leftarrow}T] + [T{\leftarrow}I])\,, \tag{3.3c}$$

$$[E{\leftarrow}I]' = \beta_I S\frac{I}{N} - (\tau_I + \sigma + \gamma_I)[E{\leftarrow}I] - \theta p([E{\leftarrow}I]\frac{[T{\leftarrow}I]}{I} + [E{\leftarrow}I]\frac{[I{\leftarrow}T]}{I}), \tag{3.3d}$$

$$[E{\leftarrow}T]' = \tau_I[E{\leftarrow}I] + \theta p([E{\leftarrow}I]\frac{[T{\leftarrow}I]}{I} + [E{\leftarrow}I]\frac{[I{\leftarrow}T]}{I}) - \sigma[E{\leftarrow}T] - \theta[E{\leftarrow}T], \tag{3.3e}$$

$$\begin{aligned}[I{\leftarrow}I]' &= \sigma[E{\leftarrow}I] - 2(\gamma_I + \tau_I)[I{\leftarrow}I] - \theta p([I{\leftarrow}I]\frac{[I{\leftarrow}T]}{I} + [I{\leftarrow}I]\frac{[T{\leftarrow}I]}{I}\\ &\quad +[T{\leftarrow}I]\frac{[I{\leftarrow}I]}{I}),\end{aligned} \tag{3.3f}$$

$$\begin{aligned}[I{\leftarrow}T]' &= \sigma[E{\leftarrow}T] + \tau_I[I{\leftarrow}I] + \theta p([I{\leftarrow}I]\frac{[I{\leftarrow}T]}{I} + [I{\leftarrow}I]\frac{[T{\leftarrow}I]}{I} - [T{\leftarrow}I]\frac{[I{\leftarrow}T]}{I})\\ &\quad -(\tau_I + \theta + \gamma_I)[I{\leftarrow}T],\end{aligned} \tag{3.3g}$$

$$\begin{aligned}[T{\leftarrow}I]' &= \tau_I[I{\leftarrow}I] + \theta p([T{\leftarrow}I]\frac{[I{\leftarrow}I]}{I} - [T{\leftarrow}I]\frac{[I{\leftarrow}T]}{I} - [T{\leftarrow}I]\frac{[T{\leftarrow}I]}{I})\\ &\quad -(\tau_I + \theta + \gamma_I)[T{\leftarrow}I],\end{aligned} \tag{3.3h}$$

$$Q' = \theta p[E{\leftarrow}T] - \sigma Q, \tag{3.3i}$$

$$T' = \sigma Q + \tau_I I + \theta p([I{\leftarrow}T] + [T{\leftarrow}I]) - \theta T\,, \tag{3.3j}$$

$$X' = \theta T\,, \tag{3.3k}$$

$$R' \; = \; \gamma_I I \,. \tag{3.3l}$$

3.2.2 SEAIR Contact Tracing Model

Patients with diseases such as COVID-19 may be asymptomatic while infectious. We extend our contact tracing model to incorporate these patients by including an asymptomatic compartment. We assume that the asymptomatic individuals are infectious. These asymptomatic patients may be contact traced from their diagnosed contacts, and become quarantined because they do not show symptoms. We also assume that these quarantined asymptomatic patients do not infect others.

Figure 3.3 shows the population dynamics of the SEAIR model. This model includes a new asymptomatic compartment A. The quarantined compartment Q in the SEIR model becomes two compartments: Q_A for asymptomatic patients and Q_E for latent patients. Let q represent the fraction of infectious patients who are asymptomatic. Asymptomatic and symptomatic patients have different transmission rates (β_A and β_I) and recovery rates (γ_A and γ_I). The definitions of these parameters are shown in Table 3.1. Public health policies in Ontario initially recommended that only symptomatic patients be tested [77]. Thus, we assume that Q_A individuals are not tested and as such are not diagnosed. Ideally, these patients would be tested, and our model can be modified to incorporate their testing.

The latent patients become infectious at a rate σ, a fraction q of them are asymptomatic and enter compartment A, while a fraction $1-q$ are symptomatic and enter compartment I. They may also be contact traced and enter Q_E. The quarantined individuals in Q_E become infectious at a rate σ, and a fraction q of them enter Q_A, while the other fraction $1-q$ enter T. The individuals in I are diagnosed and enter compartment T, or they recover and enter compartment R. The individuals in A become quarantined and enter Q_A upon being contact traced, or recover at a rate γ_A. Therefore, the confirmed cases in T come from the following three pathways:

- quarantine patients in Q_E showing symptoms during quarantine; or,
- voluntary testing of symptomatic patients; or,
- symptomatic patients traced through contacts.

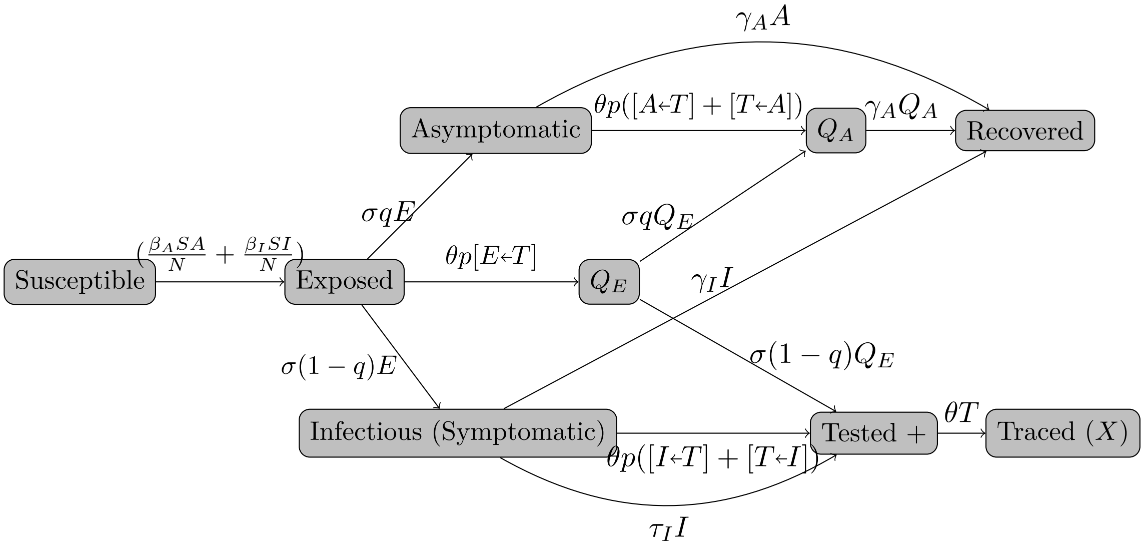

Figure 3.3: The dynamics of the SEAIR model with testing and tracing.

The population dynamics are governed by the following system:

$$
\begin{array}{rcl}
S' &=& -\beta_I S\dfrac{I}{N}-\beta_A S\dfrac{A}{N}\,,\\
E' &=& \beta_A S\dfrac{A}{N}+\beta_I S\dfrac{I}{N}-\sigma E-\theta p[E{\leftarrow}T]\,,\\
A' &=& \sigma q E-\theta p([A{\leftarrow}T]+[T{\leftarrow}A])-\gamma_A A\,,\\
I' &=& \sigma(1-q)E-(\gamma_I+\tau_I)I-\theta p([I{\leftarrow}T]+[T{\leftarrow}I])\,,\\
Q_E' &=& \theta p[E{\leftarrow}T]-\sigma q Q_E-\sigma(1-q)Q_E\,,\\
Q_A' &=& \theta p([A{\leftarrow}T]+[T{\leftarrow}A])+\sigma q Q_E-\gamma_A Q_A\,,\\
T' &=& \tau_I I+\theta p([I{\leftarrow}T]+[T{\leftarrow}I])+\sigma(1-q)Q_E-\theta T\,,\\
X' &=& \theta T\,,\\
R' &=& \gamma_A(A+Q_A)+\gamma_I I\,.
\end{array}
$$

The flowcharts of the pair dynamics of $[E{\leftarrow}T]$, $[A{\leftarrow}T]$, $[T{\leftarrow}A]$, $[I{\leftarrow}T]$ and $[T{\leftarrow}I]$ are shown in Figures 3.4 and 3.5. Figure 3.4 shows that each individual infected by an asymptomatic patient initially forms an $[E{\leftarrow}A]$ pair with the patient. If the individual E shows symptoms, which occurs with a probability $\sigma(1-q)$, the pair $[E{\leftarrow}A]$ becomes $[I{\leftarrow}A]$. If E becomes asymptomatic at a rate σq, the pair becomes $[A{\leftarrow}A]$. However, since asymptomatic individuals are not diagnosed, contact tracing cannot happen along this pair later on, and so this pair is not traced in this model. It can also leave

$[E\leftarrow A]$ if the infector A is quarantined or recovers, and becomes $[E\leftarrow Q_A]$ or $[E\leftarrow R]$, at a rate $\theta p([\underline{E\leftarrow A}\leftarrow T] + [\underline{E\leftarrow A}\rightarrow T])$ or $\gamma_A[E\leftarrow A]$, respectively. But, these pairs are not traced in this model for the same reason as $[A\leftarrow A]$ is not traced. If the symptomatic patient in pair $[I\leftarrow A]$ tests positive (through voluntary testing or contact tracing), pair $[I\leftarrow A]$ will becomes $[T\leftarrow A]$. Similarly, any individual in a pair may change its state, possibly through voluntary testing, contact tracing, or disease dynamics.

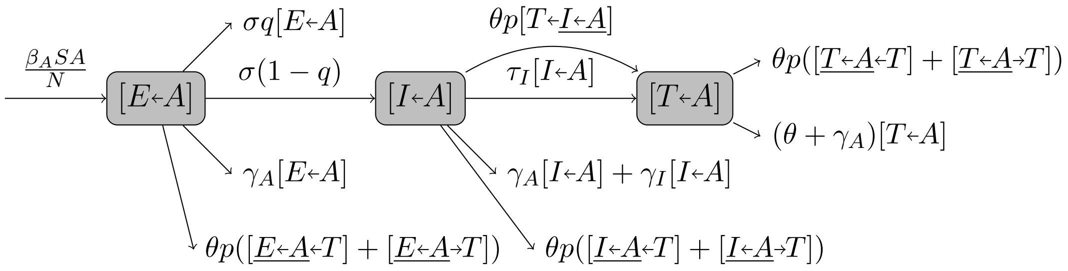

Figure 3.4: Pair dynamics for A infected pairs of the SEAIR model.

Similar to the SEIR dynamics, each individual infected by a symptomatic patient initially forms an $[E\leftarrow I]$ pair (Figure 3.5). If the infectee E shows symptoms, the pair $[E\leftarrow I]$ becomes $[I\leftarrow I]$; if E becomes asymptomatic at a rate σq, $[E\leftarrow I]$ becomes $[A\leftarrow I]$. The pair $[E\leftarrow I]$ becomes $[E\leftarrow T]$ when the infector I is diagnosed, via either contact tracing or voluntary testing. The $[E\leftarrow T]$ pair may becomes $[I\leftarrow T]$ or $[A\leftarrow T]$ depending on whether E becomes symptomatic or not. The pair $[A\leftarrow T]$ may also come from $[A\leftarrow I]$ when the infector I is diagnosed. Similarly, $[I\leftarrow T]$ can also come from $[I\leftarrow I]$ when the infector I is diagnosed. The pair $[I\leftarrow I]$ can become $[T\leftarrow I]$ when the infectee I is diagnosed.

These two flowcharts lead to the following system of pair dynamics.

$$
\begin{aligned}
[E\leftarrow I]' &= \beta_I S\frac{I}{N} - (\sigma + \tau_I + \gamma_I)[E\leftarrow I] - \theta p([\underline{E\leftarrow I}\rightarrow T] + [\underline{E\leftarrow I}\leftarrow T])\,, \\
[E\leftarrow A]' &= \beta_A S\frac{A}{N} - \sigma[E\leftarrow A] - \gamma_A[E\leftarrow A] - \theta p([\underline{E\leftarrow A}\rightarrow T] + [\underline{E\leftarrow A}\leftarrow T])\,, \\
[E\leftarrow T]' &= \tau[E\leftarrow I] + \theta p([\underline{E\leftarrow I}\rightarrow T] + [\underline{E\leftarrow I}\leftarrow T]) - (\sigma + \theta p)[E\leftarrow T]\,, \\
[A\leftarrow I]' &= \sigma q[E\leftarrow I] - (\gamma_A + \gamma_I + \tau_I)[A\leftarrow I] - \theta p([\underline{A\leftarrow I}\leftarrow T] + [\underline{A\leftarrow I}\rightarrow T] + [T\leftarrow \underline{A\leftarrow I}])\,, \\
[I\leftarrow A]' &= \sigma(1-q)[E\leftarrow A] - (\gamma_A + \gamma_I + \tau_I)[I\leftarrow A] - \theta p([\underline{I\leftarrow A}\leftarrow T] + [\underline{I\leftarrow A}\rightarrow T] \\
&\quad +[T\leftarrow \underline{I\leftarrow A}])\,, \\
[I\leftarrow I]' &= \sigma(1-q)[E\leftarrow I] - 2(\gamma_I + \tau_I)[I\leftarrow I] - \theta p([\underline{I\leftarrow I}\leftarrow T] + [\underline{I\leftarrow I}\rightarrow T] + [T\leftarrow \underline{I\leftarrow I}])\,, \\
[A\leftarrow T]' &= \theta p([\underline{A\leftarrow I}\leftarrow T] + [\underline{A\leftarrow I}\rightarrow T]) + \tau_I[A\leftarrow I] + \sigma q[E\leftarrow T] - (\theta + \gamma_A)[A\leftarrow T]
\end{aligned}
$$

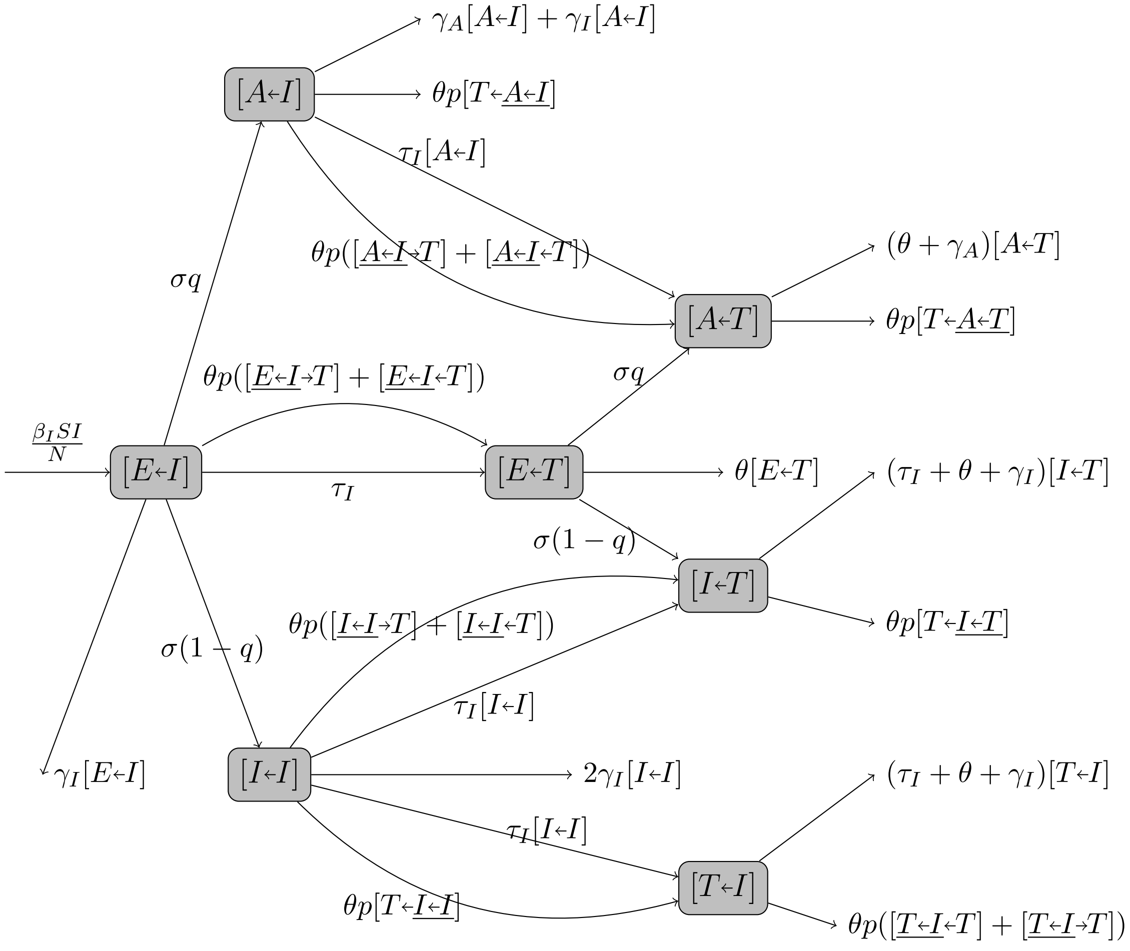

Figure 3.5: Pair dynamics for I infected pairs in the SEAIR model.

$$\begin{aligned}
& & & -\theta p[T{\leftarrow}\underline{A{\leftarrow}T}]\,, \\
[T{\leftarrow}A]' &=& & \theta p[T{\leftarrow}\underline{I{\leftarrow}A}] + \tau_I[I{\leftarrow}A] - (\theta + \gamma_A)[T{\leftarrow}A] - \theta p([\underline{T{\leftarrow}A}{\leftarrow}T] + [\underline{T{\leftarrow}A}{\rightarrow}T])\,, \\
[I{\leftarrow}T]' &=& & \sigma(1-q)[E{\leftarrow}T] + \theta p([\underline{I{\leftarrow}I}{\leftarrow}T] + [\underline{I{\leftarrow}I}{\rightarrow}T]) + \tau_I[I{\leftarrow}I] - (\tau_I + \theta + \gamma_I)[I{\leftarrow}T] \\
& & & -\theta p[T{\leftarrow}\underline{I{\leftarrow}T}]\,, \\
[T{\leftarrow}I]' &=& & \theta p[T{\leftarrow}\underline{I{\leftarrow}I}] + \tau_I[I{\leftarrow}I] - (\tau_I + \theta + \gamma_I)[T{\leftarrow}I] - \theta p([\underline{T{\leftarrow}I}{\leftarrow}T] + [\underline{T{\leftarrow}I}{\rightarrow}T])\,,
\end{aligned}$$

Using the same triple closure method as in section 3.2.1, the system is closed with the approximations

$$[\underline{E{\leftarrow}I}{\leftarrow}T] = [E{\leftarrow}I]\frac{[I{\leftarrow}T]}{I}, \;\; [\underline{E{\leftarrow}I}{\rightarrow}T] = [E{\leftarrow}I]\frac{[T{\leftarrow}I]}{I},$$

$$[\underline{E{\leftarrow}A}{\leftarrow}T] = [E{\leftarrow}A]\frac{[A{\leftarrow}T]}{A}, \quad [\underline{E{\leftarrow}A}{\rightarrow}T] = [E{\leftarrow}A]\frac{[T{\leftarrow}A]}{A},$$

$$[\underline{A{\leftarrow}I}{\leftarrow}T] = [A{\leftarrow}I]\frac{[I{\leftarrow}T]}{I}, \quad [\underline{A{\leftarrow}I}{\rightarrow}T] = [A{\leftarrow}I]\frac{[T{\leftarrow}I]}{I},$$

$$[T{\leftarrow}\underline{A{\leftarrow}I}] = [T{\leftarrow}A]\frac{[A{\leftarrow}I]}{A}, \quad [\underline{I{\leftarrow}A}{\leftarrow}T] = [I{\leftarrow}A]\frac{[A{\leftarrow}T]}{A},$$

$$[\underline{I{\leftarrow}A}{\rightarrow}T] = [I{\leftarrow}A]\frac{[T{\leftarrow}A]}{A}, \quad [T{\leftarrow}\underline{I{\leftarrow}A}] = [T{\leftarrow}I]\frac{[I{\leftarrow}A]}{I},$$

$$[\underline{I{\leftarrow}I}{\leftarrow}T] = [I{\leftarrow}I]\frac{[I{\leftarrow}T]}{I}, \quad [\underline{I{\leftarrow}I}{\rightarrow}T] = [I{\leftarrow}I]\frac{[T{\leftarrow}I]}{I},$$

$$[T{\leftarrow}\underline{I{\leftarrow}I}] = [T{\leftarrow}I]\frac{[I{\leftarrow}I]}{I}, \quad [\underline{T{\leftarrow}I}{\rightarrow}T] = [T{\leftarrow}I]\frac{[T{\leftarrow}I]}{I},$$

$$[\underline{T{\leftarrow}A}{\rightarrow}T] = [T{\leftarrow}A]\frac{[T{\leftarrow}A]}{I},$$

and

$$[\underline{T{\leftarrow}I}{\leftarrow}T] = [T{\leftarrow}I]\frac{[I{\leftarrow}T]}{I} = [T{\leftarrow}\underline{I{\leftarrow}T}], \quad [\underline{T{\leftarrow}A}{\leftarrow}T] = [T{\leftarrow}A]\frac{[A{\leftarrow}T]}{A} = [T{\leftarrow}\underline{A{\leftarrow}T}] \ .$$

In summary, the full SEAIR contact tracing model is given by the following system:

$$S' = -\beta_I S\frac{I}{N} - \beta_A S\frac{A}{N}\,, \tag{3.6a}$$

$$E' = \beta_A S\frac{A}{N} + \beta_I S\frac{I}{N} - \sigma E - \theta p[E{\leftarrow}T]\,, \tag{3.6b}$$

$$A' = \sigma q E - \theta p([A{\leftarrow}T] + [T{\leftarrow}A]) - \gamma_A A\,, \tag{3.6c}$$

$$I' = \sigma(1-q)E - (\gamma_I + \tau_I)I - \theta p([I{\leftarrow}T] + [T{\leftarrow}I])\,, \tag{3.6d}$$

$$Q_E' = \theta p[E{\leftarrow}T] - \sigma q Q_E - \sigma(1-q)Q_E\,, \tag{3.6e}$$

$$Q_A' = \theta p([A{\leftarrow}T] + [T{\leftarrow}A]) + \sigma q Q_E - \gamma_A Q_A\,, \tag{3.6f}$$

$$[E{\leftarrow}I]' = \beta_I S\frac{I}{N} - (\sigma + \tau_I + \gamma_I)[E{\leftarrow}I] - \theta p([E{\leftarrow}I]\frac{[T{\leftarrow}I]}{I} + [E{\leftarrow}I]\frac{[I{\leftarrow}T]}{I})\,, \tag{3.6g}$$

$$[E{\leftarrow}A]' = \beta_A S\frac{A}{N} - (\sigma + \gamma_A)[E{\leftarrow}A] - \theta p([E{\leftarrow}A]\frac{[T{\leftarrow}A]}{A} + [E{\leftarrow}A]\frac{[A{\leftarrow}T]}{A})\,, \tag{3.6h}$$

$$[E{\leftarrow}T]' = \tau_I[E{\leftarrow}I] + \theta p([E{\leftarrow}I]\frac{[T{\leftarrow}I]}{I} + [E{\leftarrow}I]\frac{[I{\leftarrow}T]}{I}) - (\sigma + \theta)[E{\leftarrow}T]\,, \tag{3.6i}$$

$$\begin{aligned}[A{\leftarrow}I]' = {} & \sigma q[E{\leftarrow}I] - (\gamma_A + \gamma_I + \tau_I)[A{\leftarrow}I] - \theta p([A{\leftarrow}I]\frac{[I{\leftarrow}T]}{I} + [A{\leftarrow}I]\frac{[T{\leftarrow}I]}{I} \\ & + [T{\leftarrow}A]\frac{[A{\leftarrow}I]}{A})\,,\end{aligned} \tag{3.6j}$$

$$
\begin{aligned}
[I{\leftarrow}A]' &= \sigma(1-q)[E{\leftarrow}A] - (\gamma_A + \gamma_I + \tau_I)[I{\leftarrow}A] - \theta p([I{\leftarrow}A]\frac{[A{\leftarrow}T]}{A} \\
&\quad + [I{\leftarrow}A]\frac{[T{\leftarrow}A]}{A} + [T{\leftarrow}I]\frac{[I{\leftarrow}A]}{I})\,, \qquad (3.6k) \\
[I{\leftarrow}I]' &= \sigma(1-q)[E{\leftarrow}I] - 2(\gamma_I + \tau_I)[I{\leftarrow}I] - \theta p([I{\leftarrow}I]\frac{[I{\leftarrow}T]}{I} \\
&\quad + [I{\leftarrow}I]\frac{[T{\leftarrow}I]}{I} + [T{\leftarrow}I]\frac{[I{\leftarrow}I]}{I})\,, \qquad (3.6l) \\
[A{\leftarrow}T]' &= \theta p([A{\leftarrow}I]\frac{[I{\leftarrow}T]}{I} + [A{\leftarrow}I]\frac{[T{\leftarrow}I]}{I}) + \tau_I[A{\leftarrow}I] + \sigma q[E{\leftarrow}T] \\
&\quad - (\theta + \gamma_A)[A{\leftarrow}T] - \theta p[T{\leftarrow}A]\frac{[A{\leftarrow}T]}{A}\,, \qquad (3.6m) \\
[T{\leftarrow}A]' &= \theta p[T{\leftarrow}I]\frac{[I{\leftarrow}A]}{I} + \tau_I[I{\leftarrow}A] - (\theta + \gamma_A)[T{\leftarrow}A] \\
&\quad - \theta p([T{\leftarrow}A]\frac{[A{\leftarrow}T]}{A} + [T{\leftarrow}A]\frac{[T{\leftarrow}A]}{A})\,, \qquad (3.6n) \\
[I{\leftarrow}T]' &= \sigma(1-q)[E{\leftarrow}T] + \theta p([I{\leftarrow}I]\frac{[I{\leftarrow}T]}{I} + [I{\leftarrow}I]\frac{[T{\leftarrow}I]}{I}) + \tau_I[I{\leftarrow}I] \\
&\quad - (\tau_I + \theta + \gamma_I)[I{\leftarrow}T] - \theta p[T{\leftarrow}I]\frac{[I{\leftarrow}T]}{I}\,, \qquad (3.6o) \\
[T{\leftarrow}I]' &= \theta p[T{\leftarrow}I]\frac{[I{\leftarrow}I]}{I} + \tau_I[I{\leftarrow}I] - (\tau_I + \theta + \gamma_I)[T{\leftarrow}I] \\
&\quad - \theta p([T{\leftarrow}I]\frac{[I{\leftarrow}T]}{I} + [T{\leftarrow}I]\frac{[T{\leftarrow}I]}{I})\,, \qquad (3.6p) \\
T' &= \tau_I I + \theta p([I{\leftarrow}T] + [T{\leftarrow}I]) + \sigma(1-q)Q_E - \theta T\,, \qquad (3.6q) \\
X' &= \theta T\,, \qquad (3.6r) \\
R' &= \gamma_A(A + Q_A) + \gamma_I I\,. \qquad (3.6s)
\end{aligned}
$$

Note that, if $q = 0$ and $A(0) = 0$, then $A(t) = 0$ for all t, and this SEAIR model simplifies to the SEIR model (Equation (3.3)).

Table 3.1: Parameter notation for models SEIR and SEAIR

Parameter	Definitions
β_I (β_A)	Transmission rate of I (A)
$1/\sigma$	Mean latent period
q	Fraction of susceptible individuals becoming A
$1/\theta$	Mean delay from diagnosis to triggering CT
p	Probability of an infectious contact being traced (coverage)
τ_I (τ_A)	Voluntary testing rate of I (A)
γ_I (γ_A)	Recovery rate of I (A)

3.2.3 Control Reproduction Number

The reproduction number represents the average number of secondary infections caused by a typical infectious individual. The basic reproduction number, $\mathcal{R}_0$, is defined as the reproduction number in a fully susceptible population with no interventions. In contrast, the control reproduction number, $\mathcal{R}_C$, reflects the reproduction number in a population where disease control measures are in place. Without control measures, $\mathcal{R}_C$ becomes $\mathcal{R}_0$. $\mathcal{R}_C$ serves as a disease threshold because the disease may spread if and only if $\mathcal{R}_C > 1$. Thus, to curtail the epidemic, control measures should reduce $\mathcal{R}_C < 1$. Hence, monitoring $\mathcal{R}_C$ is crucial for evaluating the effectiveness of disease control efforts and determining whether additional interventions are needed.

Systems (3.3) and (3.6) are undefined at disease-free equilibrium where $E = A = I = 0$, so we introduce a variable change

$$u_{[E\leftarrow I]} = \frac{[E\leftarrow I]}{E}, u_{[E\leftarrow A]} = \frac{[E\leftarrow A]}{E}, u_{[E\leftarrow T]} = \frac{[E\leftarrow T]}{E},$$

$$v_{[A\leftarrow I]} = \frac{[A\leftarrow I]}{I}, v_{[I\leftarrow A]} = \frac{[I\leftarrow A]}{I}, v_{[I\leftarrow I]} = \frac{[I\leftarrow I]}{I}, v_{[I\leftarrow T]} = \frac{[I\leftarrow T]}{I}, v_{[T\leftarrow I]} = \frac{[T\leftarrow I]}{I},$$

$$w_{[A\leftarrow I]} = \frac{[A\leftarrow I]}{A}, w_{[I\leftarrow A]} = \frac{[I\leftarrow A]}{A}, w_{[A\leftarrow T]} = \frac{[A\leftarrow T]}{A}, w_{[T\leftarrow A]} = \frac{[T\leftarrow A]}{A},$$

and

$$f = \frac{E}{I}, g = \frac{A}{I}.$$

The system (3.6) can be rewritten as Equation (D.1) in Appendix D, where we calculate the control reproduction numbers $\mathcal{R}_C$ for two models.

For the SEAIR model (3.6),

$$\mathcal{R}_C = \left[\frac{\beta_A q}{\theta p(w^*_{[A\leftarrow T]} + w^*_{[T\leftarrow A]}) + \gamma_A} + \frac{\beta_I(1-q)}{\gamma_I + \tau_I + \theta p(v^*_{[I\leftarrow T]} + v^*_{[T\leftarrow I]})} \right] \frac{\sigma}{\sigma + \theta p u^*_{[E\leftarrow T]}}, \quad (3.7)$$

where $w^*_{[A\leftarrow T]}$ and $w^*_{[T\leftarrow A]}$ represent the equilibrium variables $w_{[A\leftarrow T]}$ and $w_{[T\leftarrow A]}$ at the disease free equilibrium. Without contact tracing, where the tracing coverage $p = 0$, $\mathcal{R}_C$ reduces to the basic reproduction number,

$$\mathcal{R}_0 = \frac{\beta_A q}{\gamma_A} + \frac{\beta_I(1-q)}{\gamma_I + \tau_I}. \quad (3.8)$$

For the SEIR model (3.3), $q = 0$, then the reproduction numbers (3.7) and (3.8) simplify as below,

$$\mathcal{R}_C = \frac{\beta_I \sigma}{(\sigma + \theta p u^*_{[E \leftarrow T]})(\gamma_I + \tau_I + \theta p (v^*_{[I \leftarrow T]} + v^*_{[T \leftarrow I]}))}, \tag{3.9}$$

$$\mathcal{R}_0 = \frac{\beta_I}{\gamma_I + \tau_I}. \tag{3.10}$$

3.2.4 Model justification

To determine whether our SEAIR contact tracing model can accurately reflect the impact of contact tracing on disease transmission, we develop an agent-based contact tracing model that incorporates asymptomatic transmission, a latent period, contact tracing, isolation and quarantine, to see if our model agrees with agent-based simulations.

For the agent-based model, we consider a population with N individuals, and I_0 individuals are randomly selected as symptomatic patients (I) at the beginning of disease transmission, the others are labelled susceptible (S). To conduct contact tracing, each infectious individual keeps track of their contacts, and adds them to a list. There are five types of events, four of which are associated with infectious individuals.

- Transmission event. We assume that the population is randomly mixed, so the individuals are uniformly distributed, the contacts are randomly chosen in the population. If the contact is susceptible, the contact becomes exposed (E). Each infected individual has a contact list, initially this list is empty. If the transmission event happens, the contact is added to the contact list of the infector, and the infector is also added to the list of the infectee. There is an exponentially distributed waiting time with a rate β_I between symptomatic transmission events, and a rate β_A between asymptomatic transmission events.

- Recovery event. If infectious individuals recover, they are labelled recovered (R), the contact list and all remaining events associated with them are cleared. A recovery event has a waiting time distribution with a density $f_I(t)$ or $f_A(t)$, for symptomatic or asymptomatic individuals, respectively.

- Voluntary test event. An infectious individual tests positive and becomes diagnosed (T). The waiting time between voluntary test events is distributed with a density $f_T(t)$.

- Contact tracing event. The contacts in the list of diagnosed individual are traced with a coverage probability p. The traced contacts are diagnosed if they are symptomatic, and quarantined if they are asymptomatic. The diagnosed individuals are then labelled traced (X), and the contact list is cleared. The waiting time between contact tracing events is distributed with a density $f_X(t)$.

Each exposed individual is assigned one type of event as follows.

- Becoming infectious event. When latent patients become infectious, they become asymptomatic (A) with a probability q, or symptomatic (I) with a probability $1 - q$. A becoming-infectious event has a waiting time distribution with a density $f_E(t)$.

The event times are calculated as the current time plus the waiting time of the event. ODE models assume exponentially distributed waiting times for transitions between compartments. To compare with our SEAIR contact tracing model, the density functions $f_E(t)$, $f_I(t)$, $f_A(t)$, $f_T(t)$ and $f_X(t)$ are assumed to be exponential with rates σ, γ_I, γ_A, τ_I, θ, respectively. Our SEAIR model agrees with the agent-based model very well (Figure 3.6). Specifically, these two models produce the same exponential growth rate in the initial phase. This consistency demonstrates that our SEAIR model is both reasonable and effective in capturing the effects of asymptomatic patients and contact tracing on disease dynamics, particularly during the exponential growth phase. The ODE model can be extended to incorporate realistic distributions using either age-of-infection or multiple sub-stages for the latent and infectious classes. However, these extensions are beyond the scope of this paper. For our model, some parameter values are motivated by COVID-19, where $\beta_A = \beta_I/3$ [78], $\sigma = 0.27$ [79], $\gamma_A = 0.2$ [80], $\gamma_I = 0.1$ [81], $q = 0.3$ [82]. Here, we take $\theta = 2$ and $p = 0.2$ as an example. Additionally, we experiment with altering values of θ and p, and the curves simulated with different values all consistently reflect similar results. We use the R package *ABM* for agent-based simulations, and the R code for these simulations has been published. More details are provided in the Data Availability section.

3.3 Simulation Study

To evaluate the effectiveness of contact tracing using the SEIR model (3.3) or the SEAIR model (3.6), we must calibrate the models to data. However, it is challenging

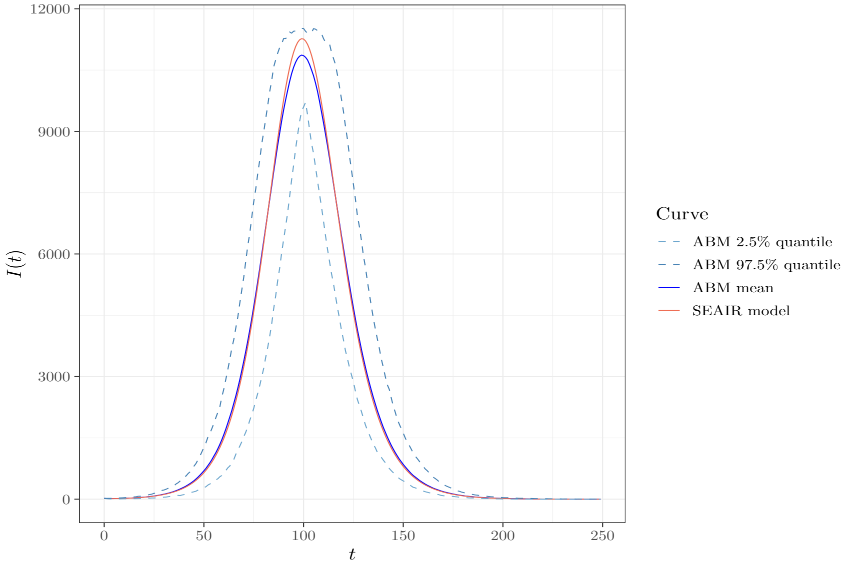

Figure 3.6: The comparison of $I(t)$ numerically solved from our SEAIR model with the average of 100 runs of the agent based model with the same parameter values and initial conditions, where $\beta_I = 0.6$, $\beta_A = 0.2$, $\theta = 2$, $p = 0.2$ $\tau_I = 0.15$, $\sigma = 0.27$, $\gamma_A = 0.2$, $\gamma_I = 0.1$, $q = 0.3$, $N = 300000$ and $I(0) = 20$.

to calibrate the models to the exponential growth stage of an epidemic, because an observed exponentially growing epidemic curve can be generated by an infinite number of combinations of parameter values, including the transmission rate β_I, the testing rate τ_I and the contact tracing parameters such as coverage p and delay θ, all of which are influenced by various NPIs. Thus, the case count data alone are insufficient to identify all parameters during the exponential growth stage. We use a simulation study to determine the data needed to estimate model parameters. We also evaluate the difference in the approximate effectiveness of contact tracing between using the SEIR model (3.3) and using the SEAIR model (3.6).

3.3.1 Data

Firstly, we identify the types of data that can be matched to our models. The new cases per unit time correspond to the diagnosis terms, which are the terms entering T. Specifically, voluntary testing corresponds to $\tau_I I$, and contact tracing corresponds to $\theta p([T \leftarrow I]+[I \leftarrow T])+\sigma(1-q)Q_E$. Among these, the quarantined cases are represented by $\sigma(1-q)Q_E$, and the remaining cases are isolated symptomatic cases. Additionally, symptom onset corresponds to the $\sigma(1-q)E$ term that enters I from E.

Since the case count data are insufficient for parameter estimation, we need data that include contact tracing information. Because the cases identified through voluntary testing and contact tracing add up to the new cases, we need data from one of these sources. In addition, we may use data on cases that are isolated or have been quarantined via contact tracing to improve the estimates. Since these cases contribute to the cases identified by contact tracing, only one of these data source is needed. Symptom onset data may provide information on disease progression.

To determine whether previously quarantined case counts and symptom onset counts are necessary for parameter estimation, we generate the following four datasets, as summarized in Table 3.2.

Table 3.2: Datasets used to determine which data are required for parameter estimation

	New cases	Voluntary test	Quarantined	Symptom onset
Data1	✓	✓		
Data2	✓	✓	✓	
Data3	✓	✓		✓
Data4	✓	✓	✓	✓

To assess whether our model can distinguish the effect of contact tracing from other control measures, such as social distancing, we implement three intervention periods. We assume that these measures alter the transmission rate [83].

1. Before Day 40, no control measures were implemented, and the transmission rate was $\beta_{I_1} = 0.6$;
2. From Day 40 to Day 59, a strong control measure was implemented that reduced the transmission rate to $\beta_{I_2} = 0.3$;
3. From Day 60 to Day 80, the control measure was relaxed, with the transmission rate increasing to $\beta_{I_3} = 0.45$.

In addition, $\beta_A = \beta_I/3$ [78] in each period, and the other parameter values are the same as those shown in Figure 3.6. Figure 3.7 shows the four types of data generated by an agent-based simulation. The simulated time span is 80 days.

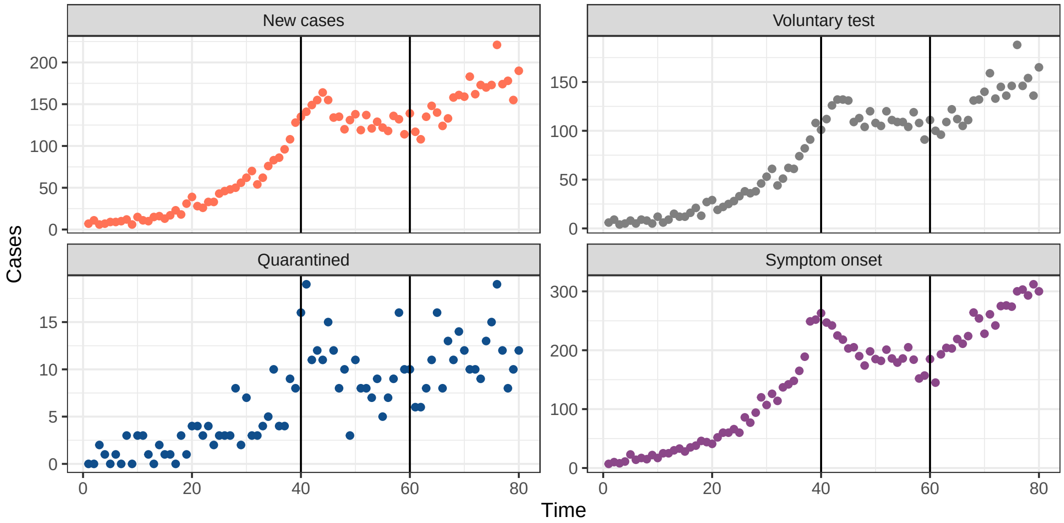

Figure 3.7: Cases generated by an agent based model over an 80 day period. The parameters are $\beta_{I_1} = 0.6$, $\beta_{I_2} = 0.3$, $\beta_{I_3} = 0.45$, $\sigma = 0.27$, $q = 0.3$, $\theta = 2$, $p = 0.2$, $\gamma_I = 0.1$, $\gamma_A = 0.2$ and $\tau_I = 0.15$. The initial conditions are $N = 300000$ and $I(0) = 20$.

Table 3.3: The comparison of estimated parameters (95% credible intervals) for four different data combinations and the values in the agent based model (ABM) simulation study.

	ABM	Data1	Data2	Data3	Data4
			SEIR Model		
β_{I_1}	0.6	0.48 (0.47,0.49)	0.48 (0.47,0.49)	0.49 (0.48,0.50)	0.48 (0.47,0.50)
β_{I_2}	0.3	0.26 (0.25,0.27)	0.26 (0.25,0.27)	0.26 (0.25,0.28)	0.26 (0.25,0.27)
β_{I_3}	0.45	0.36 (0.35,0.37)	0.36 (0.35,0.37)	0.35 (0.34,0.36)	0.35 (0.33,0.36)
θ	2	1.86 (1.51,2.32)	1.77 (1.23,2.32)	2.01 (1.73,2.40)	1.94 (1.77,2.12)
p	0.2	0.17 (0.16,0.19)	0.18 (0.16,0.19)	0.17 (0.16,0.18)	0.17 (0.16,0.18)
τ_I	0.15	-	-	0.16 (0.15,0.17)	0.16 (0.15,0.17)
			SEAIR Model		
β_{I_1}	0.6	0.58 (0.57,0.59)	0.58 (0.57,0.59)	0.60 (0.58,0.61)	0.60 (0.58,0.61)
β_{I_2}	0.3	0.32 (0.31,0.32)	0.32 (0.31,0.32)	0.33 (0.32,0.34)	0.33 (0.32,0.34)
β_{I_3}	0.45	0.43 (0.42,0.44)	0.43 (0.42,0.44)	0.44 (0.43,0.46)	0.44 (0.43,0.46)
θ	2	2.51 (2.10,2.79)	2.36 (2.14,2.67)	2.53 (2.28,2.67)	2.24 (2.08,2.37)
p	0.2	0.20 (0.19,0.21)	0.20 (0.19,0.21)	0.20 (0.19,0.21)	0.20 (0.19,0.21)
τ_I	0.15	-	-	0.16 (0.15,0.17)	0.16 (0.15,0.17)

3.3.2 Fitting Results

We fit both the SEIR model (Equation (3.3)) and the SEAIR model (Equation (3.6)) to the four datasets in Table 3.2 using the Bayesian MCMC method with wide normal priors centered at the parameter values used in the simulation. We use the R package *mcmc* for model calibration. The R code used to perform the simulation study, including data generation and model calibration, is provided in the Data Availability section to ensure reproducibility.

Table 3.3 displays the posterior means and 95% credible intervals for the two models estimated from each dataset. If the symptom onset data are not used (Data1 and Data2), the MCMC runs do not converge unless the value of the test rate τ_I is provided. Providing either the symptom onset data or τ_I allows all parameters to be identified. For the SEAIR model, including previously quarantined cases (Data2 and Data4) reduces the width of the credible intervals for the parameter θ.

The SEIR model consistently underestimates the transmission rates and the contact tracing coverage, while the SEAIR model correctly estimates all parameters.

3.4 Application to the COVID-19 pandemic in Ontario

In this section, we calibrate our contact tracing models (3.3) and (3.6) to the early stage of the COVID-19 pandemic in Ontario, focusing on the period from March 16 to May 1, 2020, to evaluate the effectiveness of contact tracing in the province. Starting on February 5, Public Health Ontario advised close contacts of COVID-19 cases to self-isolate as part of public health management [84]. On April 9, contact tracing efforts were strengthened with the introduction of phone calls to contacts, which aimed to improve tracing coverage and effectiveness [85].

Ontario published anonymized COVID-19 cases data on the provincial government website [86]. This dataset includes each individual patient's infection information, such as the test date, report date, symptom onset date, and case requisition information (e.g., travel, no epidemiological link, close contact, etc.). Note that some of this information, such as case requisition details, was removed since April 13, 2023. We aggregate daily counts of new cases, new symptom onsets, and new cases identified as "close contact" (as a proxy for contact tracing). Figure 3.8 shows three types of COVID-19 data in this period.

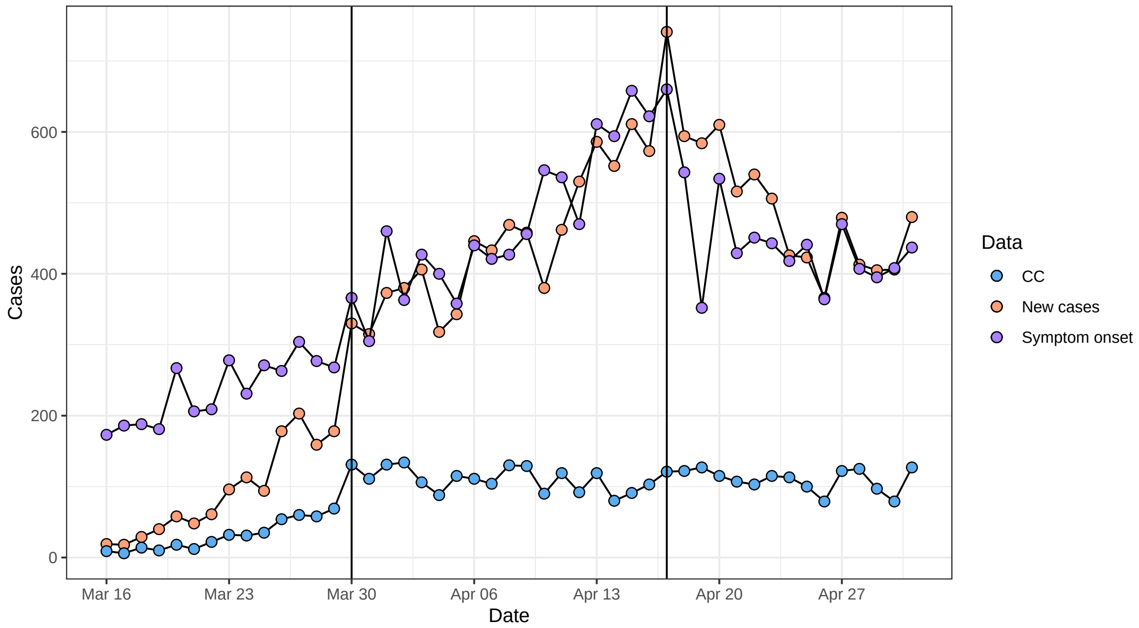

Figure 3.8: COVID-19 data for Ontario from March 16 to May 1, 2020. The blue dots represent confirmed cases due to close contacts (contact tracing), orange dots represent daily new cases, and purple dots represent cases showing symptoms per day.

During this period, the Ontario Ministry of Health implemented various NPIs, which influenced both the transmission rate and the testing policy. Detailed information about these measures is published by the Canadian Institute for Health Information [77]. Based on trends observed in the data, we identify three distinct intervention periods: March 16-29, March 30-April 16, and April 17-May 1. We assume that the transmission rate, β_I, and the test rate, τ_I, vary across these periods.

3.4.1 Parameter Estimation

We set $\beta_{A_i} = \beta_{I_i}/3$ (i=1,2,3) [78], $q = 0.3$ [82], and $\gamma_A = 0.2$ [80]. Assuming that most symptomatic cases during the early stage of COVID-19 were identified, we set $\gamma_I = 0$. We fit our contact tracing models (3.3) and (3.6) to the dataset shown in Figure 3.8 using the Bayesian MCMC method to estimate the parameters listed in Table 3.4. This table provides the posterior means and the 95% credible intervals for the estimated parameters of both models. Note that we use a overly-simplified likelihood function, assuming that the errors on the data points are independent. These assumptions may result in narrower credible intervals with relatively poor probabilities containing the true value. This approach and its implications are discussed further in Chapter 5, where we demonstrate how these assumptions influence the precision of the estimates.

To evaluate the potential impact of the introduction of phone calls to contacts on April 9, we considered the scenario θ and p became larger after April 9. We calibrated this alternative model to data, however, the results showed negligible differences, with the posterior means of the parameter estimates nearly overlapping.

Figure 3.9 shows the comparison of the fitted curves with the Ontario COVID-19 data. This indicates that the estimated parameter values fit the data well. As in the simulation study, the SEIR model (3.3) underestimates the transmission rates and the rate σ for leaving the latent stage. The voluntary test rates estimated by the two models are similar. The contact tracing coverage p is estimated to be close to 30% in both models, although the SEIR model yields a slightly smaller value.

Table 3.4: Estimated parameter values (the posterior means) and 95% credible intervals in brackets of the contact tracing models for the Ontario COVID-19 data

	Prior Distribution	SEIR model	SEAIR model
β_{I_1}	Normal(0.3,0.2)	0.22 (0.21,0.24)	0.30 (0.28,0.32)
β_{I_2}	Normal(0.25,0.2)	0.20 (0.19,0.21)	0.27 (0.25,0.30)
β_{I_3}	Normal(0.15,0.2)	0.14 (0.13,0.15)	0.20 (0.18,0.22)
θ	Normal(0.5,0.2)	0.90 (0.79,1.02)	1.15 (0.95,1.35)
p	Uniform (0,1)	0.27 (0.26,0.28)	0.29 (0.28,0.30)
σ	Normal(0.2,0.1)	0.58 (0.52,0.65)	0.75 (0.67,0.83)
τ_{I_1}	Normal(0.2,0.1)	0.081 (0.075,0.087)	0.085 (0.077,0.094)
τ_{I_2}	Normal(0.2,0.1)	0.123 (0.115,0.132)	0.131 (0.120,0.146)
τ_{I_3}	Normal(0.2,0.1)	0.130 (0.120,0.141)	0.141 (0.128,0.158)

The control reproduction numbers (3.7) and (3.9), along with the prevalence ($A+I$ for the SEAIR model and I for the SEIR model), using the estimated parameter values from Table 3.4, are plotted as the red curves in Figure 3.10. This figure also includes a scenario study (see Subsection 3.4.2). It shows that both the SEIR and SEAIR models give similar $\mathcal{R}_C$ predictions, although the SEIR model slightly overestimates $\mathcal{R}_C$ during the first intervention period (without significant interventions). The SEIR model also significantly underestimates the prevalence. Compared to the scenario without contact tracing (the blue curves in Figure 3.10), contact tracing moderately reduces $\mathcal{R}_C$ and significantly reduces the prevalence. For both models, contact tracing reduces $\mathcal{R}_C$ by approximately 25%, although this reduction is slightly smaller in

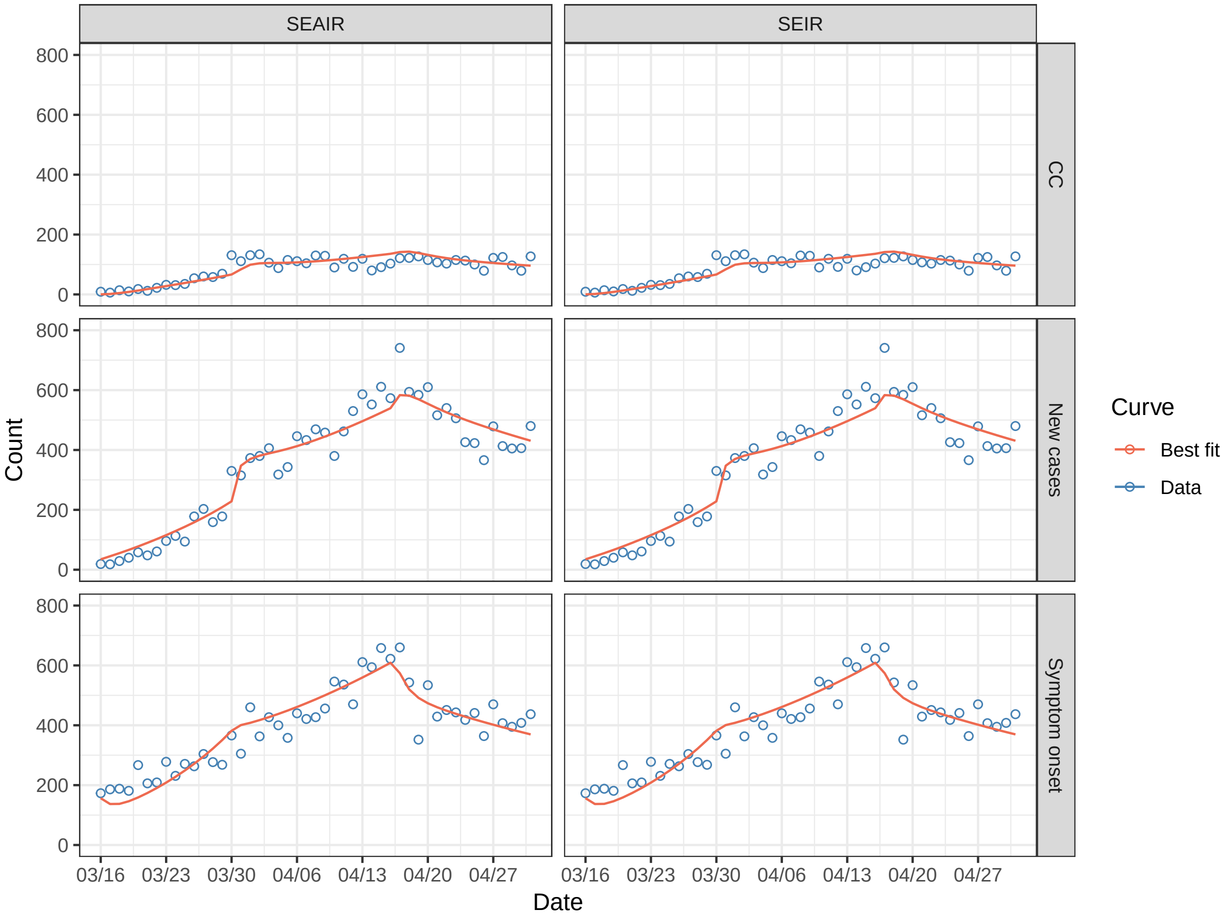

Figure 3.9: Comparison of the fitted curves with the Ontario COVID-19 data from March 16 to May 1, 2020 (confirmed cases due to close contacts, new cases and symptom onset data). The blue dots represent the case count data (top panels: close contacts, middle panels: new cases, bottom panels: symptom onset) and the red lines are the fitted curves. The first column is the fitting results of the SEAIR model, and the second column is the SEIR model.

a period with a larger transmission rate β_I. However, this reduction is gradually achieved by the end of the first period.

3.4.2 Scenario Study

To show the effect of contact tracing, we vary the tracing coverage p, and study how $\mathcal{R}_C$ and prevalence depend on p; see Figure 3.10. Here we vary p while keeping that other parameters fixed as in Table 3.4, to compare four different scenarios:

$p.1$ without contact tracing ($p = 0$);

$p.2$ the point estimate parameter values in Table 3.4;

$p.3$ the tracing coverage p is increased to 0.6

$p.4$ p is increased to 0.9.

Both $\mathcal{R}_C$ and the prevalence depend significantly on p (Figure 3.10). If the coverage p is roughly doubled to 60%, then the outbreak could be controlled in period 2. If it were tripled, then it could have been controlled in period 1.

The dependence of $\mathcal{R}_c$ and the prevalence on the contact tracing rate θ is shown in Figure 3.11, where $1/\theta$ is the mean delay between diagnosis and contact tracing. Similarly, we vary the value of θ and fix the others as in Table 3.4, to consider the following five scenarios:

$\theta.1$ without contact tracing ($\theta = 0$);

$\theta.2$ the point estimate values in Table 3.4;

$\theta.3$ the delay was prolonged to two days($\theta = 0.5$);

$\theta.4$ the delay was shortened to half a day ($\theta = 2$);

$\theta.5$ the delay was shortened to three hours $\theta = 8$.

We find that neither $\mathcal{R}_C$ nor the prevalence significantly depends on θ near the point estimate values in Table 3.4 (Figure 3.11).

All code and datasets used in this study, including scripts for parameter estimation and scenario simulations, are available in the Data Availability section.

3.5 Concluding Remarks

We aim to determine whether the effect of contact tracing and other NPIs can be disentangled and evaluated separately during the early stage of an epidemic. To do so, we extend the SIR contact tracing model [42] to include the latent stage and asymptomatic transmissions, and develop contact tracing SEIR and SEAIR models. The SEAIR model agrees very well with agent-based simulations, while the SEIR model is a special case of the SEAIR model with the fraction of asymptomatic cases $q = 0$.

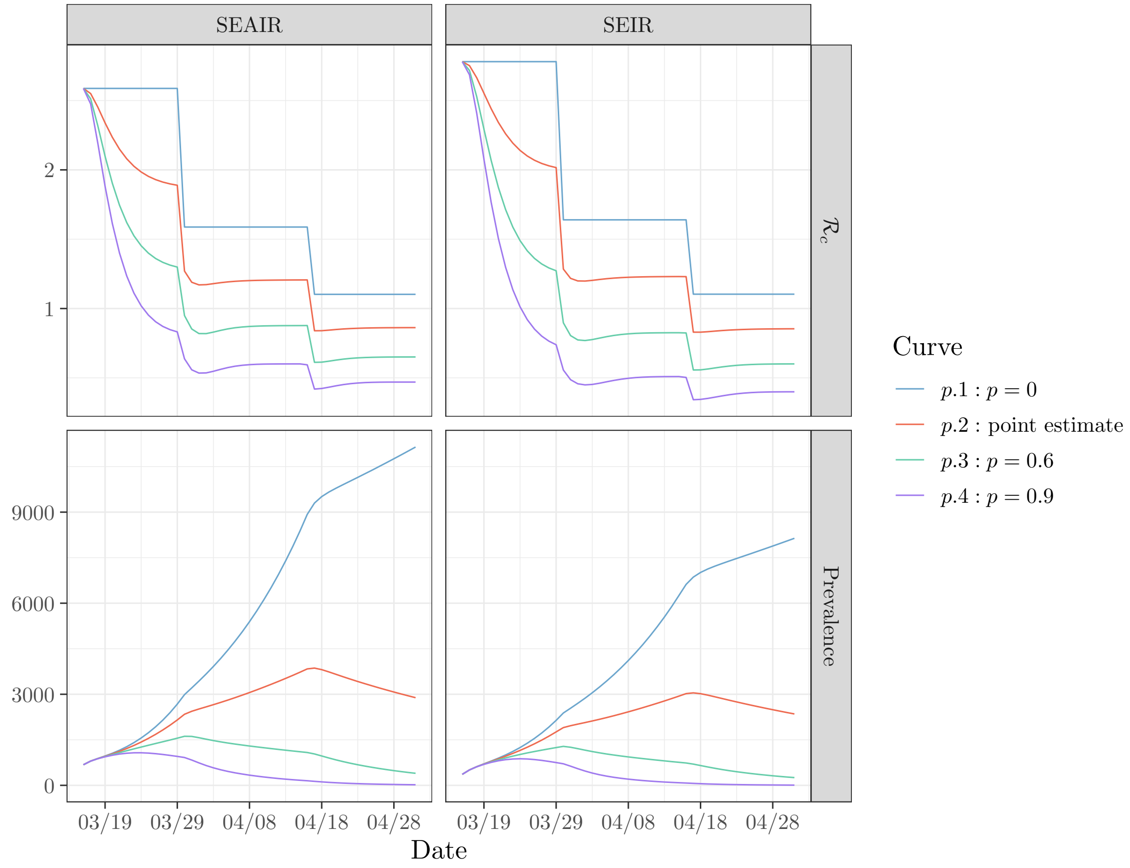

Figure 3.10: The dependence of the control reproduction number $\mathcal{R}_C$ (top panels) and prevalence (bottom panels) on the tracing coverage p. All the other parameter values are listed in Table 3.4. These curves correspond to the four scenarios $p.1 - p.4$.

Our model captures the key features of the underlying contact tracing process. This is demonstrated by comparing the results of our model with those of an agent-based contact tracing model. It is important to develop our ODE models because they allow us to perform theoretical analysis on disease dynamics such as identifying the disease threshold. It is also faster to calibrate our ODE model to data than to calibrate the agent-based model.

Since new case count data in the early stage of an epidemic typically grow exponentially, these data alone cannot disentangle the effects of different NPIs because different strengths of disease interventions may give the same exponential growth. Thus, we need extra data to separate their effects. These data must include information about contact tracing. We use a simulation study to generate different datasets

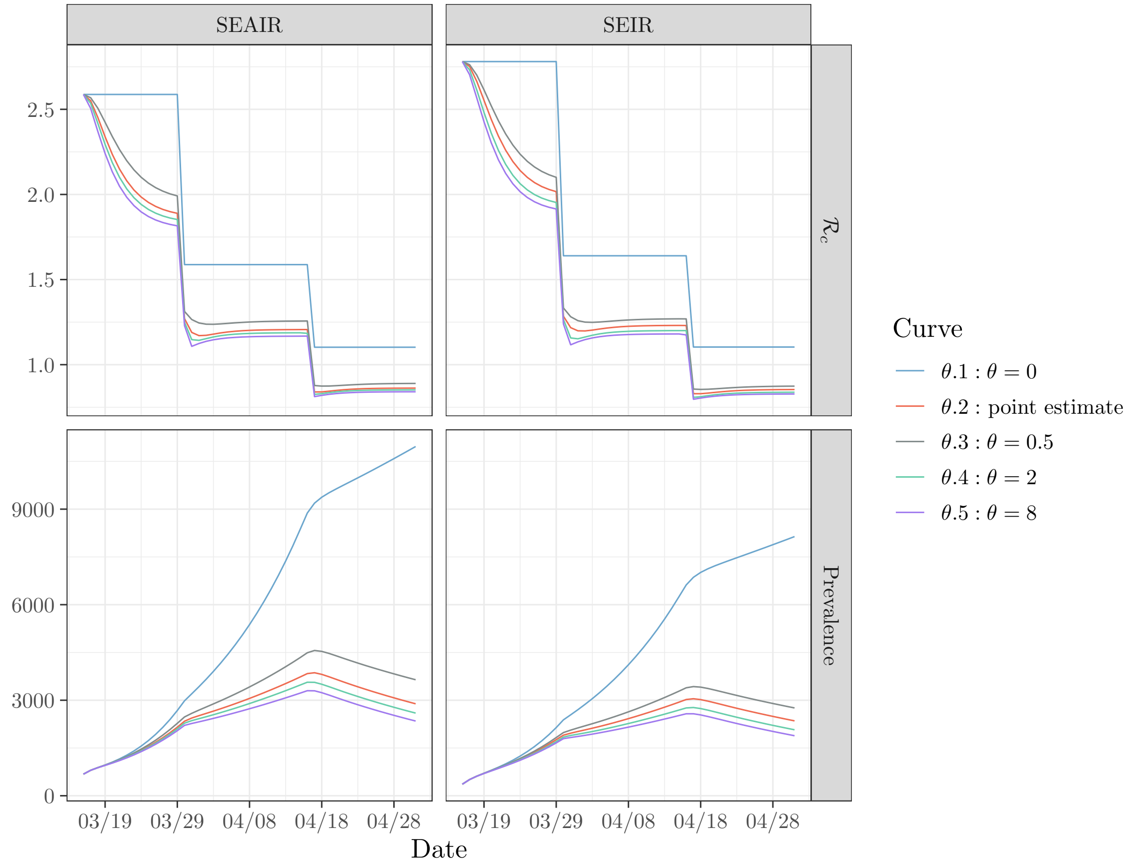

Figure 3.11: The dependence of the control reproduction number $\mathcal{R}_C$ (top panels) and prevalence (bottom panels) on the contact tracing rate θ. These curves correspond to five scenarios $\theta.1 - \theta.5$.

from the agent-based model, to determine the data needed to evaluate the effect of different control measures. We find that, in addition to new case counts, it is crucial to use voluntary test counts (alternatively, cases identified via contact tracing) and symptom onset counts to distinguish the effect of contact tracing from other control measures. On the other hand, the previously quarantined case counts are not crucial, but slightly improve the accuracy of parameter estimation.

In the early stage of an epidemic, disease features such as asymptomatic transmission cannot be easily determined Therefore,SEIR models are commonly used to study the epidemic. We evaluate whether SEIR models can provide similar results to the SEAIR model. We find that the SEIR model slightly underestimates the parameter values. Thus, if we have information about the fraction of asymptomatic cases, the reduction of transmission rate for asymptomatic patients, and the recovery rate of the asymptomatic individuals, then the SEAIR model should be used. Otherwise, using the SEIR model can still identify contact tracing parameters.

We apply our contact tracing models to the early stage of the Ontario COVID-19 pandemic during March 16–May 1, 2020. We use daily cases, symptom onsets, and cases identified as close contacts (as an approximation to contact tracing). We find that approximately 29% of diagnosed cases were identified via contact tracing, which moderately reduced the reproduction number and significantly reduced the prevalence. The effectiveness of contact tracing is significantly affected by the tracing coverage. However, it is not sensitive to the tracing delay ($1/\theta$) near the estimated parameter values, possibly because the estimated delay is short compared to the COVID-19 incubation period. The SEIR model slightly overestimates the control reproduction number, but significantly underestimates the prevalence. The estimated effects of contact tracing by these two models are similar.

Although we assume that asymptomatic cases are not identified in Ontario during the study period due to the testing policy, our model can be extended to include the testing of asymptomatic cases. We can also consider different testing frequencies (for example, testing once a day or once every three days) to analyze which testing frequency can improve the effectiveness of contact tracing. We assume that all symptomatic patients are diagnosed before recovery (i.e., the recovery rate $\gamma_I = 0$), which we believe is realistic in the early stage of the pandemic. However, our model can still be applied if $\gamma_I > 0$. Our contact tracing models do not include antiviral treatments and vaccination, as they were not available during the study period. However,incorporating them into our model would be an interesting extension, particularly for re-emerging infectious diseases. The triple closure method used in our model is overly simple. A more realistic closure, introduced in [35], requires information about the distribution of the number of contacts of an infectious individual. Including this information would make our models more precise, and is an interesting future research direction. Our ODE model implicitly assumes exponentially distributed infectious and latent periods, which is not realistic. To incorporate realistic distributions for the infectious and latent periods, this model can be extended to consider.

Data Availability

We have published the data and R codes in a GitHub repository:
`https://github.com/junlingm/ContactTracing-SEAIR/`

Chapter 4

Stochasticity in the early stage of an epidemic

4.1 Introduction

Infectious disease outbreaks have profound impacts on public health and society. Rapid estimation of key disease parameters, particularly during the early stages of transmission when the number of newly confirmed cases grows exponentially, enables timely analysis and prediction of disease spread facilitating the implementation of effective control measures [87, 88].

Deterministic epidemic models are widely used to study disease dynamics [59, 89, 90]. These models provide valuable insights into the underlying mechanisms of disease transmission. For the model's predictions to be applicable in real-world scenarios, such as forecasting future cases, it is essential to calibrate them to actual epidemic data. This process involves estimating key disease parameters, such as the transmission rate and recovery rate, based on observed data. Proper calibration ensures that the model accurately reflects the true dynamics of the disease, leading to more reliable predictions and informed decision-making.

Two common approaches for parameter estimation are maximum likelihood estimation (MLE) and Bayesian methods such as Markov Chain Monte Carlo (MCMC). Both approaches use a likelihood function, which represents the probability of observing the data given a set of parameter values. Constructing this likelihood function necessitates an understanding of the stochasticity inherent in the epidemic process, particularly the time evolution of case distributions. An accurate likelihood function allows for the precise evaluation of uncertainty in model parameters, which in turn ensures reliable assessments of uncertainty in model forecasts.

To construct the likelihood functions, appropriate statistical models are selected based on the properties of the observed data. For example, when modeling confirmed case counts, the Poisson distribution is often used as a starting point because it is the simplest counting process with a single parameter [91]. However, the Poisson distribution assumes that the mean is equal to the variance, making it unsuitable for overdispersed data (where the variance exceeds the mean). For epidemic data, overdispersion is very common [92, 93]. Ignoring this phenomenon can give unreliable interval estimates of the parameters, leading to misleading analytical conclusions.

The negative binomial distribution, which has two parameters, is widely used for handling overdispersed count data [94–97]. Consequently, the negative binomial distribution is often applied in epidemiology to study confirmed case counts and secondary transmission cases [98–100]. Advanced extensions of the negative binomial distribution, such as mixtures with the inverse Gaussian distribution [101] or the Lindley distribution [102], have also been proposed to improve the fit of the model. These models are more commonly applied in ecological and biodiversity studies than in epidemiology.

Despite its common use in epidemiological studies, the theoretical justification of the negative binomial likelihood for epidemic data remains limited. This raises an important question: What is the true distribution of case counts? Although deterministic models are useful for analyzing disease dynamics, they do not capture the random fluctuations observed in epidemiological data during disease spread. To address this limitation, Bartlett [103] in 1949 introduced a stochastic epidemic model for closed populations, and derived partial differential equations for the probability generating functions (PGFs) of two variables: the number of susceptible individuals and the number of infectious individuals at any given time. Subsequently, Bailey [104] extended Bartlett's work by formulating master equations and providing more detailed results for the general stochastic SIR epidemic process, as well as other stochastic processes, such as the birth-and-death process.

Building on the birth-and-death process with immigration, Kobayashi [8] developed a statistical SIR model for infectious diseases, demonstrating that the time-dependent probability distribution of the number of infectious individuals follows a negative binomial distribution [105]. However, this model overlooks important factors, such as the latent period and asymptomatic transmission. Tritch and Allen [106] used a multi-type branching process to approximate the dynamics of exposed and infectious individuals in a stochastic Susceptible-Exposed-Infectious-Recovered model. They derived the PGF of two variables: the number of exposed individuals and the number of infectious individuals at time t. This PGF satisfies a system of two differential equations. However, since this system cannot be solved analytically, this limits the theoretical understanding of the distribution of cases and affects its applicability to the construction of accurate likelihood functions for parameter estimation.

Many infectious diseases, such as COVID-19 and influenza, have a latent period. However, a theoretical understanding of the case distribution in models that incorporate this latent period remains limited. Our study uses a stochastic linear Susceptible-Exposed-Infectious-Removed (SEIR) model to study the distributions of new cases in the exponential growth phase of an epidemic, to help determine the proper likelihood functions for parameter estimation. In Section 4.2, we establish the master equation for the joint process $(E(t), I(t))$ and derive the partial differential equations for its PGF. In Section 4.3, we derive an approximate PGF and analytical approximations for the probability distributions of the number of infectious individuals $I(t)$. Subsequently, in Section 4.4, we derive the distribution of daily new cases. Conclusions are given in Section 4.5.

4.2 A Stochastic Linear SEIR Model

An SEIR epidemic model divides the population into four compartments: susceptible (S), exposed (E), infectious (I) and removed (R). We use the symbols S, E, I and R to denote the number of individuals in each compartment. This model assumes no population dynamics and no disease-related deaths, so the total population size remains constant at $N = S + E + I + R$. We assume that infectious individuals are diagnosed before recovery and are removed. Figure 4.1 illustrates the state changes of individuals in the model. Here β represents the transmission rate, γ is the diagnosis rate, and exposed individuals become infectious at a rate of σ (i.e., the mean latent period is $1/\sigma$).

The SEIR model assumes that the number of infections per unit time is given by $\beta\frac{SI}{N}$, accounting for the depletion of the susceptible population as infections occur. During the early stage of an epidemic, the proportion of the population that has been infected is small, so $S \approx N$. This approximation simplifies the nonlinear infection term $\beta\frac{SI}{N}$ to the linear term βI. The rest of the model equations remain unchanged,

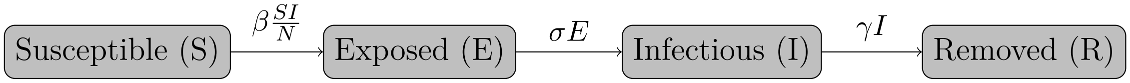

Figure 4.1: The dynamics of the SEIR model.

resulting in a linear SEIR model. This linearization captures the key dynamics of the early exponential growth phase of the epidemic while significantly simplifying mathematical analysis. In addition, we assume $\beta > \gamma$. This ensures that the basic reproduction number, $\mathcal{R}_0 = \beta/\gamma$, is greater than 1. As a result, each infectious individual generates more than one secondary infection on average. This leads to a sustained outbreak rather than the disease dying out. In this section, we use a stochastic linear SEIR model to analyze the time evolution of the distribution of case counts.

The state of the linear SEIR model can be characterized by the number of exposed and infectious individuals at time t, denoted as $(E(t), I(t))$. The probability mass function (PMF) of the process $(E(t), I(t))$ is defined as

$$P_{ij}(t) = Pr[E(t) = i, I(t) = j], \quad \text{for } i, j \in \{0, 1, 2, \ldots, n\}.$$

For the state $(E(t), I(t))$, there are six possible transitions:

$$\begin{aligned}
&(i-1, j) \xrightarrow{\beta j} (i, j), \\
&(i, j+1) \xrightarrow{\gamma(j+1)} (i, j), \\
&(i+1, j-1) \xrightarrow{\sigma(i+1)} (i, j), \\
&(i, j) \xrightarrow{\beta j} (i+1, j), \\
&(i, j) \xrightarrow{\gamma j} (i, j-1), \\
&(i, j) \xrightarrow{\sigma i} (i-1, j+1).
\end{aligned}$$

Hence, for $i, j \in \{1, 2, \ldots, n\}$, the master equation can be written as below

$$\dot{P}_{ij}(t) = \beta j P_{i-1,j}(t) + \gamma(j+1) P_{i,j+1}(t) + \sigma(i+1) P_{i+1,j-1}(t) - (\sigma i + \beta j + \gamma j) P_{ij}(t).$$

For the boundary case $i = j = 0$, we have $\dot{P}_{00}(t) = \gamma P_{01}(t)$.

However, the master equation governing the time evolution of this joint probability distribution forms a large system of coupled ordinary differential equations, which is challenging to analyze due to its high dimensionality. The PGF provides an alternative representation of the joint distribution $P_{ij}(t)$, simplifying the analysis [107]. Therefore, we use the PGF to represent the distribution P_{ij}. The PGF is defined as

$$G(X,Y,t) = \sum_{i=0}^{n}\sum_{j=0}^{n} X^i Y^j P_{i,j}(t) := \sum_{ij} X^i Y^j P_{i,j}(t).$$

When $t=0$, $G(X,Y,0) = X^{E_0}Y^{I_0}$. Here, X corresponds to the number of exposed individuals in E, and Y corresponds to the number of infectious individuals in I.

To derive the equation that governs the dynamics of $G(X,Y,t)$, we take partial derivatives:

$$\begin{aligned}
\frac{\partial G}{\partial t} =& \sum_{i,j} X^i Y^j \dot{P}_{i,j}(t)\\
=& \sum_{i,j} X^i Y^j [\beta j P_{i-1,j}(t) + \gamma(j+1)P_{i,j+1}(t) + \sigma(i+1)P_{i+1,j-1}(t)\\
& - (\sigma i + \beta j + \gamma j)P_{ij}(t)]\\
=& \beta \sum_{i,j} X^i Y^j j P_{i-1,j}(t) + \gamma \sum_{i,j} X^i Y^j (j+1) P_{i,j+1}(t) + \sigma \sum_{i,j} X^i Y^j (i+1) P_{i+1,j-1}(t)\\
& - (\beta+\gamma)\sum_{i,j} X^i Y^j j P_{i,j}(t) - \sigma \sum_{i,j} X^i Y^j i P_{i,j}(t)\\
=& \beta XY \sum_{i,j} X^{i-1} Y^{j-1} j P_{i-1,j}(t) + \gamma \sum_{i,j} X^i Y^j (j+1) P_{i,j+1}(t)\\
& + \sigma Y \sum_{i,j} X^i Y^{j-1}(i+1)P_{i+1,j-1}(t) - (\beta+\gamma)Y \sum_{i,j} X^i Y^{j-1} j P_{i,j}(t)\\
& - \sigma X \sum_{i,j} X^{i-1} Y^j i P_{i,j}(t)\\
=& \sigma(Y-X)\frac{\partial G}{\partial X} + (\beta XY + \gamma - \beta Y - \gamma Y)\frac{\partial G}{\partial Y}.
\end{aligned}$$

That is,

$$\frac{\partial G}{\partial t} + \sigma(X-Y)\frac{\partial G}{\partial X} + (\beta Y + \gamma Y - \beta XY - \gamma)\frac{\partial G}{\partial Y} = 0, \tag{4.1}$$

with the boundary condition

$$G(X,Y,0) = X^{E_0}Y^{I_0}.$$

4.2.1 Model Solutions

Equation (4.1) can be solved using the method of characteristics: we look for a solution of the form $G(X(t), Y(t), t)$, where

$$\frac{dG}{dt} = \frac{\partial G}{\partial t} + \frac{\partial G}{\partial X}\frac{\partial X}{\partial t} + \frac{\partial G}{\partial Y}\frac{\partial Y}{\partial t}.$$

Thus, by letting

$$\frac{\partial X}{\partial t} = \sigma(X - Y), \tag{4.2a}$$

$$\frac{\partial Y}{\partial t} = \beta Y + \gamma Y - \beta XY - \gamma, \tag{4.2b}$$

the PDE (4.1) becomes

$$\frac{dG}{dt} = 0.$$

This implies that G is constant along the line of characteristics, i.e., solutions of (4.2). To find the value of $G(X, Y, t)$, we start at (X, Y) and trace along the line of characteristics backward in time to find the initial conditions $X(0) = X_0$ and $Y(0) = Y_0$. Specifically, (X_0, Y_0) satisfies the following system:

$$\frac{\partial X_0}{\partial t} = -\sigma(X_0 - Y_0), \tag{4.3a}$$

$$\frac{\partial Y_0}{\partial t} = -(\beta + \gamma)Y_0 + \beta X_0 Y_0 + \gamma, \tag{4.3b}$$

with the initial conditions $X_0(0) = X$ and $Y_0(0) = Y$. Then, the solution of (4.1) can be written as

$$G(X, Y) = X_0^{E_0} Y_0^{I_0}. \tag{4.4}$$

However, the system (4.3) is nonlinear, making it impossible to obtain exact solutions. Therefore, we approximate the solutions to approximate the PGF. Once (X_0, Y_0) is determined, the approximate PGF will be given by (4.4).

4.3 Approximation of the Probability Distribution of $I(t)$

In this section, we derive an approximate PGF for the joint process $(E(t), I(t))$ and use it to approximate the probability distribution of $I(t)$.

4.3.1 Methods for Approximating the PGF

Corollary 1 in Appendix E shows that a finite probability distribution is uniquely determined by its moments. The moments of the distribution of $I(t)$ are obtained by taking derivatives of the PGF at $(X, Y) = (1, 1)$. Therefore, we approximate the PGF around $(X, Y) = (1, 1)$.

The point $(1, 1)$ is an equilibrium of the system (4.2). At this equilibrium point, the characteristic polynomial is given by

$$\lambda^2 - (\sigma + \gamma)\lambda + \sigma(\gamma - \beta) = 0.$$

Since $\gamma - \beta < 0$, one eigenvalue is positive and the other one is negative, indicating that $(1, 1)$ is a saddle point. We will approximate the line of characteristics, i.e., the solutions of (4.2), around $(1, 1)$. Since $(1, 1)$ is a saddle, solutions near it remain close to the unstable manifold of the saddle. The trajectories will follow this unstable manifold. Therefore, we will approximate the unstable manifold and use it to derive the approximation of the PGF.

We will derive a polynomial approximation to the unstable manifold. To do so, we shift the equilibrium $(1, 1)$ of system (4.2) to $(0, 0)$, and then perform a variable change to study the system along its eigenvectors. To shift, let $x = 1 - X$ and $y = 1 - Y$, so the initial conditions become $x_0 = 1 - X_0$ and $y_0 = 1 - Y_0$. Therefore, when we trace the solutions $(x(t), y(t))$ backward in time, (x_0, y_0) satisfies the following equations:

$$\frac{\partial x_0}{\partial t} = -\sigma(x_0 - y_0), \tag{4.5a}$$

$$\frac{\partial y_0}{\partial t} = \beta x_0 - \gamma y_0 - \beta x_0 y_0 + \gamma. \tag{4.5b}$$

The corresponding Jacobian matrix is given by

$$J = \begin{bmatrix} -\sigma & \sigma \\ \beta & -\gamma \end{bmatrix}.$$

The eigenvalues satisfy the quadratic equation

$$\lambda^2 + (\sigma+\gamma)\lambda + \sigma\gamma - \sigma\beta = 0,$$

so the eigenvalues

$$\lambda_{1,2} = \frac{-(\sigma+\gamma) \pm \sqrt{(\sigma-\gamma)^2 + 4\sigma\beta}}{2}, \tag{4.6}$$

where $\lambda_1 > 0$ and $\lambda_2 < 0$. The corresponding eigenvectors are

$$\begin{bmatrix} \sigma \\ \sigma+\lambda_1 \end{bmatrix}, \begin{bmatrix} \sigma \\ \sigma+\lambda_2 \end{bmatrix}.$$

Hence, The Jordan canonical form is

$$J = \begin{bmatrix} \sigma & \sigma \\ \sigma+\lambda_1 & \sigma+\lambda_2 \end{bmatrix} \begin{bmatrix} \lambda_1 & 0 \\ 0 & \lambda_2 \end{bmatrix} \begin{bmatrix} \sigma & \sigma \\ \sigma+\lambda_1 & \sigma+\lambda_2 \end{bmatrix}^{-1}.$$

To approximate the unstable manifold, we diagonalize the linear part of the system (4.5). Let

$$\begin{aligned} \begin{bmatrix} u \\ v \end{bmatrix} &= \begin{bmatrix} \sigma & \sigma \\ \sigma+\lambda_1 & \sigma+\lambda_2 \end{bmatrix}^{-1} \begin{bmatrix} x_0 \\ y_0 \end{bmatrix} \\ &= \frac{1}{\sigma(\lambda_2-\lambda_1)} \begin{bmatrix} \sigma+\lambda_2 & -\sigma \\ -(\sigma+\lambda_1) & \sigma \end{bmatrix} \begin{bmatrix} x_0 \\ y_0 \end{bmatrix} \\ &= \frac{1}{\sigma(\lambda_2-\lambda_1)} \begin{bmatrix} (\sigma+\lambda_2)x_0 - \sigma y_0 \\ -(\sigma+\lambda_1)x_0 + \sigma y_0 \end{bmatrix}, \end{aligned}$$

so

$$\begin{bmatrix} x_0 \\ y_0 \end{bmatrix} = \begin{bmatrix} \sigma & \sigma \\ \sigma+\lambda_1 & \sigma+\lambda_2 \end{bmatrix} \begin{bmatrix} u \\ v \end{bmatrix} = \begin{bmatrix} \sigma u + \sigma v \\ (\sigma+\lambda_1)u + (\sigma+\lambda_2)v \end{bmatrix}. \tag{4.7}$$

Thus,

$$\begin{aligned}\frac{d}{dt}\begin{bmatrix} u \\ v \end{bmatrix} &= \begin{bmatrix} \lambda_1 u \\ \lambda_2 v \end{bmatrix} + \begin{bmatrix} \sigma & \sigma \\ \sigma+\lambda_1 & \sigma+\lambda_2 \end{bmatrix}^{-1}\begin{bmatrix} 0 \\ -\beta x_0 y_0 \end{bmatrix} \\ &= \begin{bmatrix} \lambda_1 u \\ \lambda_2 v \end{bmatrix} + \frac{1}{\sigma(\lambda_2-\lambda_1)}\begin{bmatrix} \sigma+\lambda_2 & -\sigma \\ -(\sigma+\lambda_1) & \sigma \end{bmatrix}\begin{bmatrix} 0 \\ -\beta x_0 y_0 \end{bmatrix}.\end{aligned}$$

That is

$$u' = \lambda_1 u + \frac{1}{\lambda_2-\lambda_1}\beta[\sigma u+\sigma v][(\sigma+\lambda_1)u+(\sigma+\lambda_2)v], \tag{4.8a}$$

$$v' = \lambda_2 v - \frac{1}{\lambda_2-\lambda_1}\beta[\sigma u+\sigma v][(\sigma+\lambda_1)u+(\sigma+\lambda_2)v]. \tag{4.8b}$$

Thus, in this two-dimensional system, we find a polynomial approximation to the unstable manifold, namely, $v = f(u) = \sum\limits_{i=1}^{\infty} a_i u^i$. The coefficients a_i are determined from the following calculations. From (4.8a),

$$\begin{aligned} v' &= f'(u)u' \\ &= \sum_{i=1}^{\infty} a_i i u^{i-1}\left(\lambda_1 u + \frac{1}{\lambda_2-\lambda_1}\beta[\sigma u + \sigma\sum_{i=1}^{\infty} a_i u^i][(\sigma+\lambda_1)u+(\sigma+\lambda_2)\sum_{i=1}^{\infty} a_i u^i]\right)\end{aligned} \tag{4.9}$$

On the other hand, from (4.8b),

$$v' = \lambda_2 \sum_{i=1}^{\infty} a_i u^i - \frac{1}{\lambda_2-\lambda_1}\beta[\sigma u + \sigma\sum_{i=1}^{\infty} a_i u^i][(\sigma+\lambda_1)u+(\sigma+\lambda_2)\sum_{i=1}^{\infty} a_i u^i] \tag{4.10}$$

Comparing the coefficients of (4.9) and (4.10) for each degree of u:

- First order:

  $$a_1\lambda_1 = a_1\lambda_2, \text{ i.e., } a_1 = 0.$$

- Second order:

  $$2a_2\lambda_1 = \lambda_2 a_2 - \frac{1}{\lambda_2-\lambda_1}\beta\sigma(\sigma+\lambda_1),$$

  that is,

  $$a_2 = \frac{\beta\sigma(\sigma+\lambda_1)}{(2\lambda_1-\lambda_2)(\lambda_1-\lambda_2)}.$$

Therefore,

$$v = f(u) \approx a_2 u^2.$$

From (4.8a), we approximate u as a polynomial with a squared term:

$$u' \approx \lambda_1 u - \frac{\beta\sigma(\sigma+\lambda_1)}{\lambda_1-\lambda_2}u^2 = \lambda_1 u\left(1-\frac{u}{K}\right), \tag{4.11}$$

where

$$K = \frac{\lambda_1(\lambda_1-\lambda_2)}{\beta\sigma(\sigma+\lambda_1)},$$

with the initial condition

$$u_0 = \frac{(\sigma+\lambda_2)x-\sigma y}{\sigma(\lambda_2-\lambda_1)} = \frac{(\sigma+\lambda_2)(1-X)-\sigma(1-Y)}{\sigma(\lambda_2-\lambda_1)},$$

where (x, y) is the initial point corresponding to (x_0, y_0).

The equation for u in (4.11) is a logistic equation, thus we obtain

$$u = \frac{Ku_0}{u_0+(K-u_0)e^{-\lambda_1 t}} = \frac{u_0 e^{\lambda_1 t}}{u_0(e^{\lambda_1 t}-1)/K+1}.$$

Hence, from (4.7), we have

$$\begin{aligned} x_0 &\approx \sigma u + \sigma a_2 u^2, \\ y_0 &\approx (\sigma+\lambda_1)u + (\sigma+\lambda_2)a_2 u^2. \end{aligned}$$

Here, u^2 is negligible around $(X, Y) = (1, 1)$. Therefore, the PGF can be approximated as

$$\begin{aligned} G(X,Y,t) &= X_0^{E_0} Y_0^{I_0} \\ &= (1-x_0)^{E_0}(1-y_0)^{I_0} \\ &\approx (1-\sigma u)^{E_0}\left[1-(\sigma+\lambda_1)u\right]^{I_0}, \end{aligned} \tag{4.12}$$

where $u = \frac{Ku_0}{u_0+(K-u_0)e^{-\lambda_1 t}}$, $u_0 = \frac{(\sigma+\lambda_2)(1-X)-\sigma(1-Y)}{\sigma(\lambda_2-\lambda_1)}$, $K = \frac{\lambda_1(\lambda_1-\lambda_2)}{\beta\sigma(\sigma+\lambda_1)}$ and $\lambda_{1,2}$ are defined in (4.6).

4.3.2 The Probability Distribution of $I(t)$

To approximate the marginal distribution of $I(t)$, we set $X = 1$. The approximate PGF of $I(t)$ is given by:

$$\begin{aligned} G(1, Y, t) &\approx (1 - \sigma u)^{E_0} \left[1 - (\sigma + \lambda_1)u)\right]^{I_0} \\ &= \left[\frac{1 + (A - B)(1 - Y)}{1 + A(1 - Y)}\right]^{E_0} \left[\frac{1 + (A - C)(1 - Y)}{1 + A(1 - Y)}\right]^{I_0} \\ &= \left[\frac{1}{1 + A - AY}\right]^{E_0 + I_0} \left[1 - (B - A) + (B - A)Y\right]^{E_0} \left[1 - (C - A) + (C - A)Y\right]^{I_0}, \end{aligned} \tag{4.13}$$

where

$$A = \frac{e^{\lambda_1 t} - 1}{K(\lambda_1 - \lambda_2)}, \; B = \frac{\sigma e^{\lambda_1 t}}{\lambda_1 - \lambda_2}, \; \text{and } C = \frac{(\sigma + \lambda_1)e^{\lambda_1 t}}{\lambda_1 - \lambda_2}$$

are positive and increasing with t.

If $0 < B - A < 1$ and $0 < C - A < 1$, the approximate PGF of $I(t)$ can be decomposed into four components representing two negative binomial processes and two binomial-distributed processes:

$$G(1, Y, t) \approx G_{NB}(E_0, \frac{1}{1 + A})G_{Bin}(E_0, B - A)G_{NB}(I_0, \frac{1}{1 + A})G_{Bin}(I_0, C - A). \tag{4.14}$$

This decomposition is inspired by Kobayashi's work on the SIR model based on the birth-and-death process [8]. Similarly, the marginal PGF for $E(t)$ can be decomposed into two distinct birth-and-death processes.

We generate 80,000 sample paths of $I(t)$ using a stochastic linear SEIR model with initial conditions $E_0 = I_0 = 10$ and $R_0 = 0$. The parameter values are motivated by early estimates from COVID-19 studies. We set the transmission rate to $\beta = 0.4$ [108], the diagnosis rate to $\gamma = 0.2$ [109], and assume a latent period of 5 days, corresponding to a progression rate of $\sigma = 0.2$ [110]. We compare the time evolution of the first four moments (mean, variance, skewness, and kurtosis) of $I(t)$ obtained from the 80,000 simulations with theoretical values derived from the approximate PGF (4.13), as shown in Figure 4.2. The simulated and theoretical mean, variance, skewness and kurtosis show excellent agreement throughout the entire time period. This result suggests that the approximate PGF captures both the central tendency and variability of the stochastic dynamics well, especially at later stages.

We compare the simulated probability distributions of $I(t)$ with the approximate

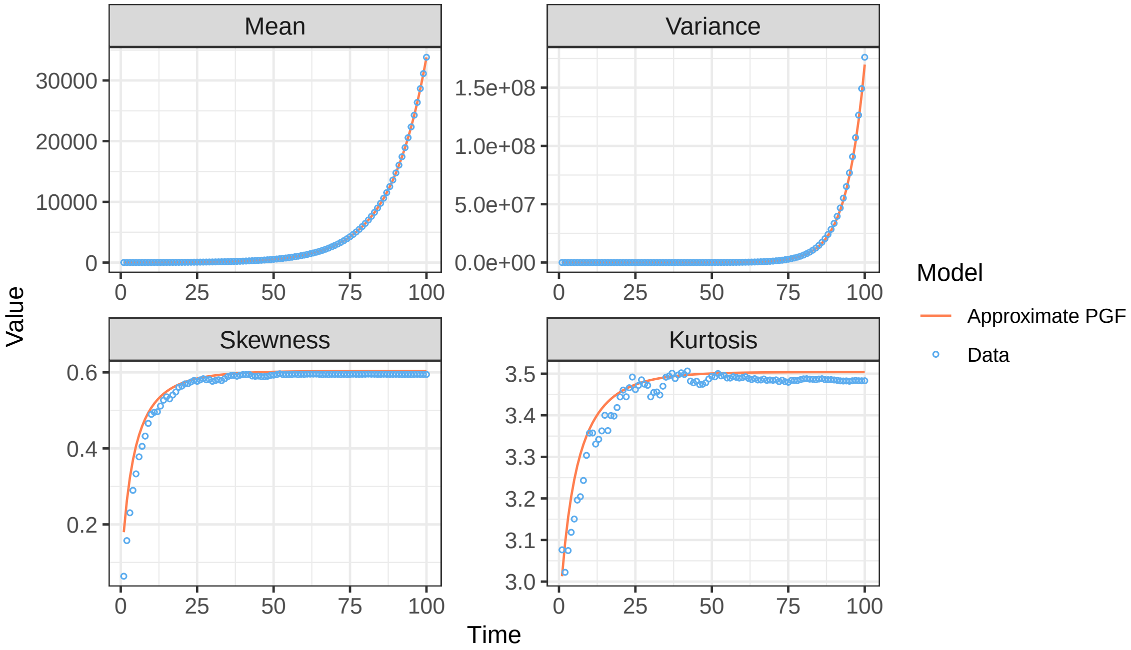

Figure 4.2: Comparison of the time evolution of the first four moments (mean, variance, skewness, and kurtosis) of $I(t)$, derived from 80,000 sets of simulated data and from the approximate PGF. Parameter values are motivated by COVID-19: $\beta = 0.4$, $\sigma = 0.2$, and $\gamma = 0.2$, with initial conditions $E_0 = I_0 = 10$ and initial number of diagnosed individuals $R_0 = 0$. Note that the vertical scales differ across panels.

probability distributions. Numerical simulations reveal that the probability distribution of $I(t)$ can be further simplified as a single distribution. To capture the variability in $I(t)$, we consider two approximation scenarios based on the relationship between its mean $\mathbb{E}[I(t)]$ and variance $\mathrm{Var}[I(t)]$, which are derived in Appendix F as given in (F.1) and (F.2), respectively. When the variance is less than the mean, we approximate the distribution using a binomial distribution; when the variance exceeds the mean, we use a negative binomial distribution. These choices are motivated by their common use in modeling count data with underdispersion or overdispersion in epidemiological studies [92, 111, 112]:

- Binomial Approximation ($\mathbb{E}[I(t)] > \mathrm{Var}[I(t)]$): When the mean of $I(t)$ exceeds its variance, the distribution can be approximated by a single binomial distribution with parameters determined by $\mathbb{E}[I(t)]$ and $\mathrm{Var}[I(t)]$. Specifically,

  $$I(t) \sim Bin(N_I, P_I),$$

  where $P_I = 1 - \frac{\mathrm{Var}[I(t)]}{\mathbb{E}[I(t)]}$ and $N_I = \frac{\mathbb{E}[I]}{P_I}$.

- Negative Binomial Approximation ($\mathbb{E}[I(t)] < \mathrm{Var}[I(t)]$): When the variance of $I(t)$ exceeds its mean, the distribution can instead be approximated by a single negative binomial distribution. Specifically,

  $$I(t) \sim NB(r_I, p_I),$$

  where $p_I = \frac{\mathbb{E}[I(t)]}{\mathrm{Var}[I(t)]}$ and $r_I = \frac{\mathbb{E}[I(t)]p_I}{1-p_I}$.

By substituting the parameter values used to generate the data into the expressions for A, B, and C, we observe that when $t < 7$, $0 < B - A < 1$ and $0 < C - A < 1$. Under these conditions, the distribution of $I(t)$ can be approximated as the convolution of two negative binomial distributions and two binomial distributions, as shown in (4.14). Furthermore, when $t \geq 4$, $\mathbb{E}[I(t)] > \mathrm{Var}[I(t)]$. Thus, the distribution of $I(t)$ is approximated as a single binomial for $t < 4$ and as a single negative binomial for $t \geq 4$. In Figure 4.3, we compare the empirical distributions of $I(t)$ from simulations (red circles) with the corresponding approximate probability distributions (histograms). The results show that the single distribution curve nearly overlaps with the convolution of the four distributions. The approximate PGF of $I(t)$ fits this case well when $t = 3$, but exhibits a large error compared to the actual distribution when $t = 1$.

However, when $t \geq 7$, either $B - A < 0$ or $C - A < 0$. In this case, we observe that $\text{Var}[I(t)] > \mathbb{E}[I(t)]$, so the distribution of $I(t)$ is approximated with a single negative binomial distribution. Figure 4.4 shows the comparison between the approximate negative binomial distribution and the actual distribution of $I(t)$ data, demonstrating that the negative binomial distribution closely fits the actual distribution curve.

4.4 The Probability Distribution of Daily New Cases

Let $C(t)$ represent the number of new daily cases on day t. We assume that each infectious individual is detected with a probability γ per day. Conditional on $I(t)$, the distribution of $C(t)$ follows a binomial distribution:

$$C(t) \mid I(t) \sim Bin(I(t), \gamma).$$

From this, the conditional mean and variance are:

$$\begin{aligned} \mathbb{E}[C(t)|I(t)] =& I(t)\gamma, \\ \text{Var}[C(t)|I(t)] =& I(t)\gamma(1-\gamma). \end{aligned}$$

Using the law of total expectation and variance [113], we derive the following:

$$\mathbb{E}[C(t)] = \mathbb{E}[\mathbb{E}[C(t)|I(t)]] = \gamma\mathbb{E}[I(t)],$$

and

$$\begin{aligned} \text{Var}[C(t)] &= \text{Var}[\mathbb{E}[C(t)|I(t)]] + \mathbb{E}[\text{Var}[C(t)|I(t)]] \\ &= \text{Var}[I(t)\gamma] + \mathbb{E}[I(t)\gamma(1-\gamma)] \\ &= \gamma^2\text{Var}[I(t)] + \gamma(1-\gamma)\mathbb{E}[I(t)]. \end{aligned}$$

Since $C(t)$ is conditionally binomially distributed given $I(t)$, and $I(t)$ can be approximated by a binomial or a negative binomial distribution, these hierarchical models lead to mixture distributions. Based on the properties of hierarchical models [114], the marginal distribution of $C(t)$ depends on the distributional properties of $I(t)$. Thus, there are two scenarios:

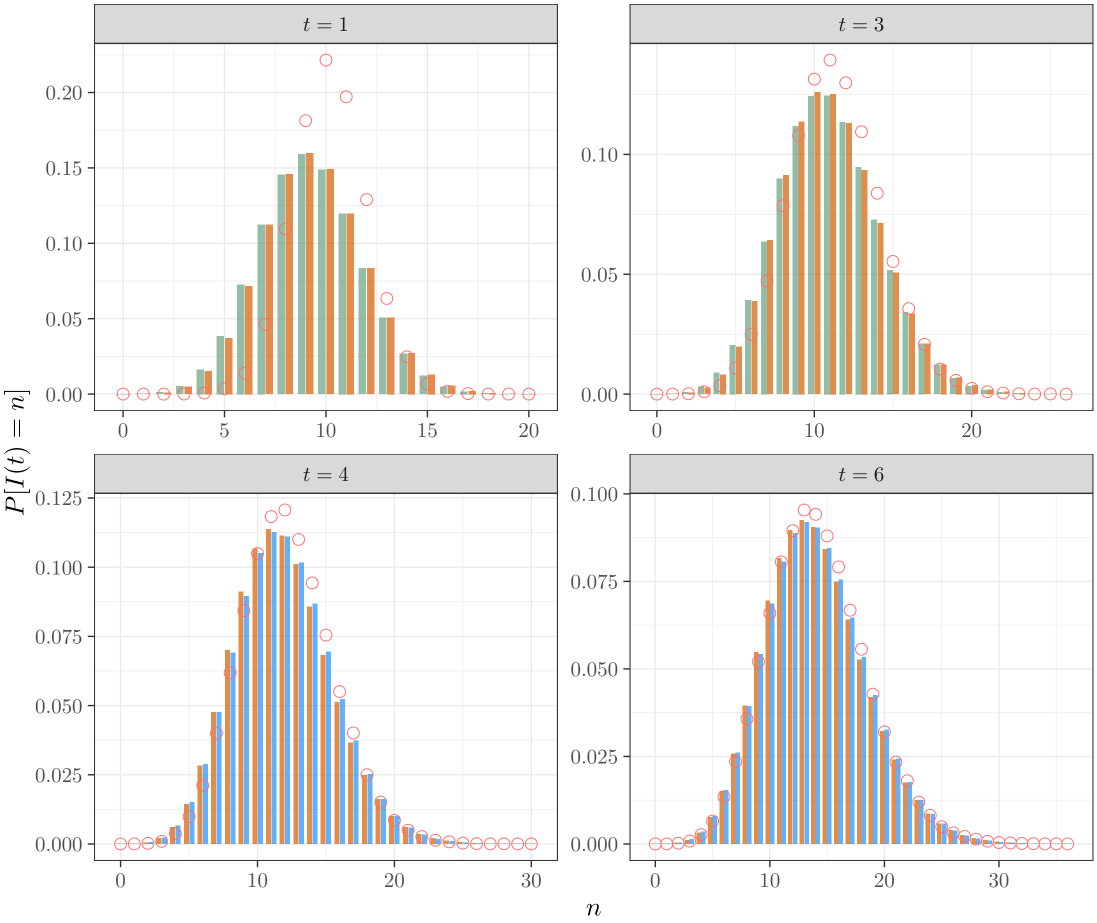

Figure 4.3: Comparison of the probability distribution of $I(t)$ with the approximate probability distributions. The red dots represent the frequencies of simulated $I(t)$ from 80,000 realizations, while the histogram shows the probability mass function of the approximated distribution. The orange bars represent the convolution of two binomial and two negative binomial distributions, the green bars in the top panels represent a single binomial distribution, and the blue bars in the bottom panels represent a single negative binomial distribution. The Parameter values are COVID-19 motivated: $\beta = 0.4$, $\sigma = 0.2$ and $\gamma = 0.2$, with initial conditions $E_0 = I_0 = 10$ and the initial diagnosed individuals $R_0 = 0$. Note that the vertical scales are different.

- If $I(t) \sim Bin(N_I, P_I)$: Then

$$C(t) \sim Bin(N_C, P_C),$$

where $P_C = 1 - \frac{\mathrm{Var}[C(t)]}{\mathbb{E}[C(t)]}$ and $N_C = \frac{\mathbb{E}[C(t)]}{P_C}$.

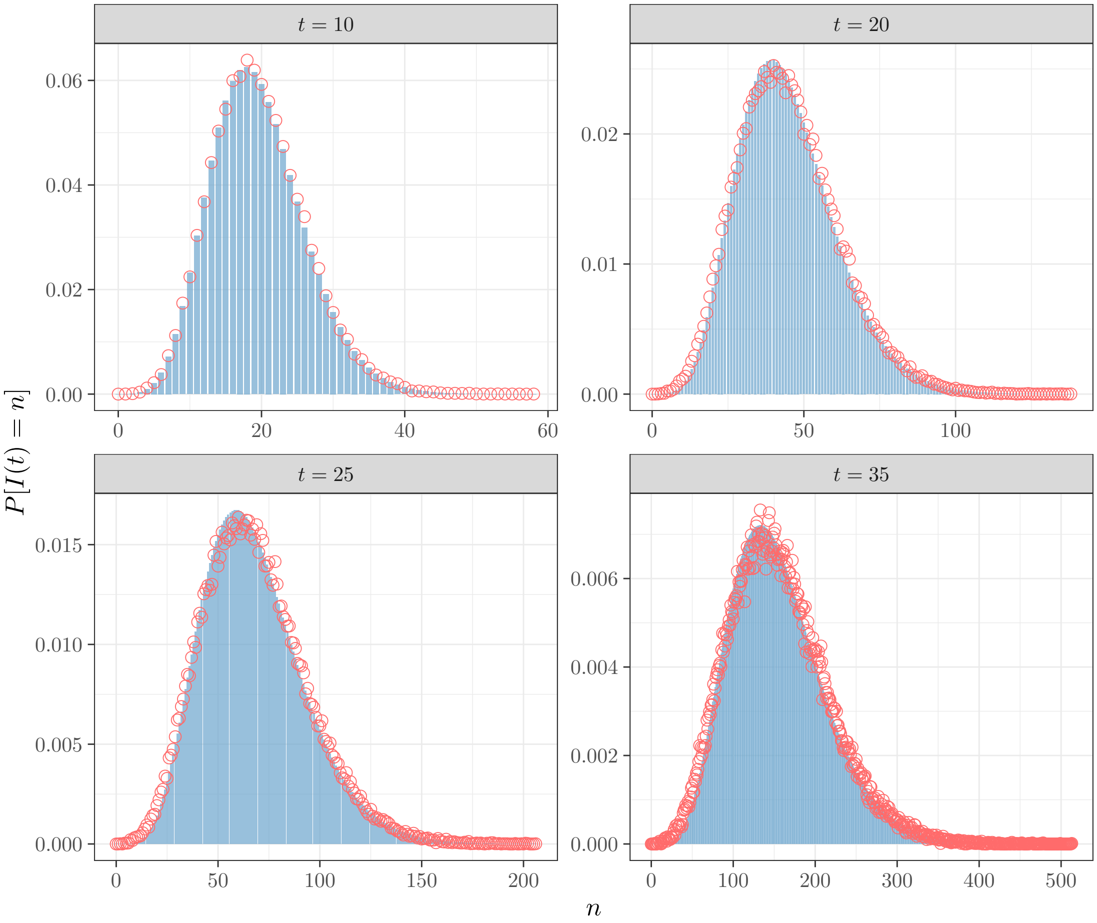

Figure 4.4: Comparison of the probability distribution of $I(t)$ with the approximated negative binomial distribution. The red dots represent the frequencies of simulated values from the 80,000 realizations falling exactly on each integer n, while the histogram shows the probability mass function of the approximate negative binomial distribution. The same parameter values and initial conditions as in Figure 4.3 are used. Note that the vertical scales are different.

- If $I(t) \sim Negbin(r_I, p_I)$: Then

$$C(t) \sim NB(r_C, p_C),$$

where $p_C = \frac{\mathbb{E}[C(t)]}{\mathrm{Var}[C(t)]}$ and $r_C = \frac{\mathbb{E}[C(t)]p_C}{1-p_C}$.

We also generate 80,000 datasets for $C(t)$ using the same parameters as in Figure 4.3. Similarly, we approximate the distribution of $C(t)$ using a binomial distribution for $t \leq 4$, and a negative binomial distribution for $t > 4$. Figures 4.5 and 4.6 compare the approximate distributions with the actual distributions in these cases, respectively. The approximate distributions fit the data very well.

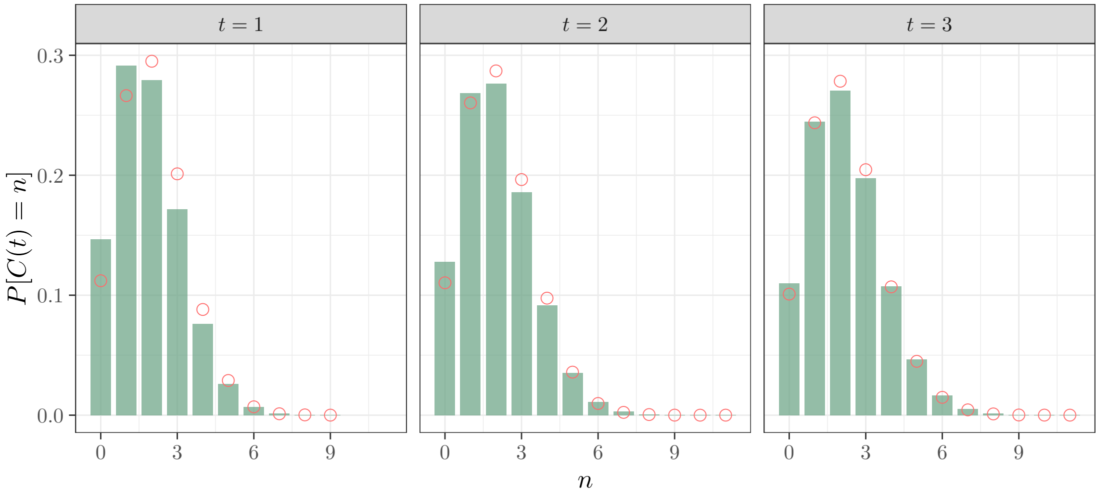

Figure 4.5: Comparison of the probability distribution of $C(t)$ with the approximated binomial distribution. The red dots represent the frequencies of simulated values from the 80,000 realizations falling exactly on each integer n. The green bars represent the approximated binomial distribution. The same parameter values and initial conditions as in Figure 4.3 are used.

4.5 Concluding Remarks

To understand the probability distribution of daily new cases, we consider a stochastic linear SEIR model. Through theoretical analysis, we derive the approximate PGF of the joint process $(E(t), I(t))$. From this, we obtain the approximate PGF of the number of infectious individuals, $I(t)$, and calculate its mean and variance. This approximate PGF captures the moments of the distribution of $I(t)$.

Other methods can also be used to derive the moment equations of the stochastic model. For example, one can start from the continuous-time Markov chain representation and apply the random time change method using unit-rate Poisson processes [115, 116], or describe the model trajectories using stochastic differential equations driven by Poisson random measures [117, 118]. These frameworks allow one to derive exact moment equations via Dynkin's martingale [119] by choosing suitable test functions. In principle, such moment equations can be solved sequentially, as higher-order moments depend on the lower-order ones. However, in practice, the system of equations becomes increasingly intractable as the moment order increases.

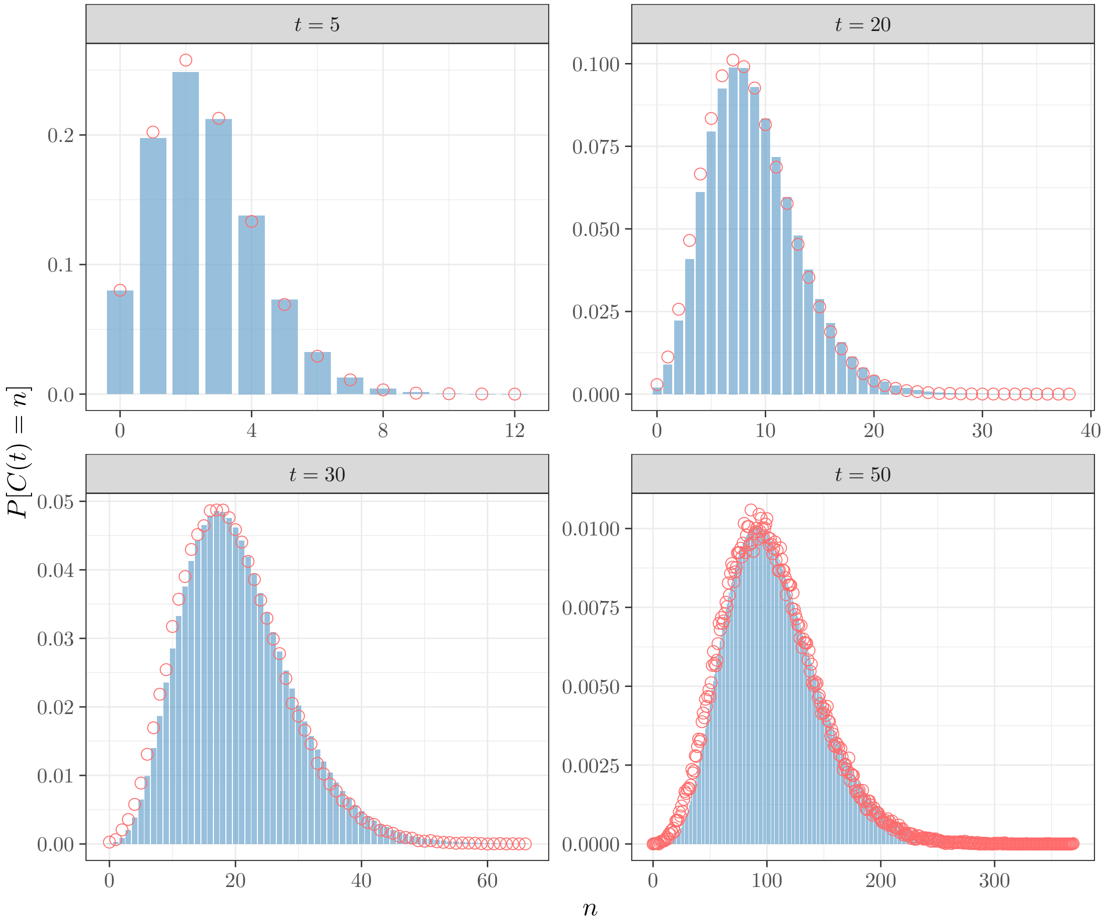

Figure 4.6: Comparison of the probability distribution of $C(t)$ with the approximated negative binomial distribution. The red dots represent the frequencies of simulated values from the 80,000 realizations falling exactly on each integer n. The blue bars represent the approximated negative binomial distribution. The same parameter values and initial conditions as in Figure 4.3 are used. Note that the vertical scales are different.

Our method offers a practical and accurate approximation for the PGF, from which the full distribution, including the mean, variance, and higher moments of $I(t)$, can be effectively captured, especially during the early phase of the epidemic.

We find that the process $I(t)$ can be decomposed into two distinct birth-and-death processes, each represented as a combination of a negative binomial distribution process and a binomial distribution process. Consequently, the distribution of $I(t)$ can be approximated as the convolution of four distributions, with probability parameters dependent on the SEIR model parameters and time t.

However, as t increases, the probability parameters of the binomial distributions may become negative. To simplify the analysis and enhance practicality, we consider two approximation scenarios for $I(t)$ based on the relationship between its mean and variance: When $\mathbb{E}[I(t)] > \mathrm{Var}[I(t)]$, the distribution can be approximated by a single binomial distribution; when $\mathbb{E}[I(t)] < \mathrm{Var}[I(t)]$, the distribution can be approximated by a single negative binomial distribution. Using a stochastic linear SEIR model, we generate 1,000 datasets of $I(t)$ and find that the simulated distributions align well with the theoretical approximations. When $t = 1$, the approximate binomial distribution exhibits an error compared to the actual distribution. This may be due to our approximation of the unstable manifold near the equilibrium point $(1, 1)$ to estimate the PGF. When the time is too small, the starting point near $(1, 1)$ has not yet converged to the unstable manifold.

Assuming that $C(t)$, the number of new daily cases, follows a binomial distribution conditional on $I(t)$, we derive formulas for the mean and variance of $C(t)$. By the properties of hierarchical models, the marginal distribution of $C(t)$ is determined by the distribution of $I(t)$. If $I(t)$ can be approximated by a binomial distribution, then $C(t)$ will be a binomial random variable. However, if $I(t)$ follows a negative binomial distribution, then $C(t)$ will follow a negative binomial distribution. Comparisons between the simulated and theoretical distributions demonstrate that the approximations fit the data well.

Through numerical simulations, we find that the variance of both the number of infectious individuals and the daily new cases is smaller than the mean only when t is very small. When we assume that the observations are independent, a negative binomial distribution is a suitable choice for modelling the number of new cases if the observation period is long. However, if the data are collected sequentially with small time steps, where each step depends on the previous time unit, a binomial distribution is more appropriate. This distinction allows for a more flexible modelling approach, depending on the step size of the epidemic progression. Therefore, a more reasonable likelihood function can be established to improve the accuracy of parameter estimation and better capture the underlying epidemic dynamics.

The case counts on a given day depend on case counts from previous days through the prevalence $I(t)$. As a result, regression methods such as negative binomial regression may not be appropriate, as they assume independent observations. Moreover, the prevalence is usually unobservable. Thus, calculating the likelihood requires taking expectations over the prevalence, which poses a significant computational challenge for the maximum likelihood method. Bayesian methods, such as hidden Markov models, are more suitable for parameter estimation using case count data. Our results provide a good approximation to the distribution of $I(t)$ and $E(t)$ given $I(t-1)$ and $E(t-1)$ in hidden Markov models. Since the model at each time step depends on data from the previous steps, our results are well-suited for sequential updates as new data become available. This allows for iterative refinement of parameter estimates as the outbreak evolves, which is important for real-time epidemic tracking.

Our analysis of the prevalence and new case distributions relies on a linear stochastic SEIR model. This linear assumption is most accurate during the early stages of an outbreak, when the number of infected individuals is small and the number of susceptible individuals remains roughly constant. However, as the outbreak progresses, especially when a significant portion of the population becomes infected or the basic reproduction number $\mathcal{R}_0$ is high, nonlinear effects become more pronounced, and the linear approximation may no longer accurately capture the full dynamics. Therefore, the applicability of our method is primarily limited to the initial growth phase of an outbreak. Extending the approach to incorporate nonlinear effects remains an important direction for future work.

Chapter 5

Estimation of the exponential growth rate of an outbreak

5.1 Introduction

In the early stages of an outbreak, the number of infections generally grows exponentially. The exponential growth rate is a fundamental measure in infectious disease epidemiology, describing how quickly the number of cases increases. It serves as a direct indicator of the speed of disease transmission and provides a basis for estimating the basic reproduction number, $\mathcal{R}_0$ [23, 120–122]. Furthermore, the growth rate plays a key role in evaluating the effectiveness of control measures, since a reduction in its value indicates the success of interventions such as NPIs, contact tracing, or vaccination [123–125]. Accurately estimating this rate enables public health officials to optimize response strategies, efficiently allocate medical resources, and anticipate the future burden of disease, ensuring a timely and effective outbreak response.

Statistical methods have been widely used to estimate the exponential growth rate of an outbreak, including the least squares method [126], MLE [127, 128], and Bayesian MCMC [129]. A common approach is to apply a linear regression model using the least squares method, which involves taking the logarithm of observed case counts and fitting a straight line to the data over time [122, 130, 131]. This method is simple and computationally efficient, but assumes constant variance and normally distributed errors, which may not hold in real-world outbreak data.

Poisson regression models are another commonly used approach for parameter estimation via the maximum likelihood method [132, 133]. In this approach, the number of new cases is assumed to follow a Poisson distribution, and infection events are modeled as having exponentially distributed waiting times. However, Poisson regression assumes that the variance is equal to the mean, which may not be realistic in the presence of overdispersion, where case counts exhibit greater variability than expected under a Poisson distribution. To address overdispersion and underdispersion in count data, Bayesian Conway–Maxwell–Poisson regression models have been proposed [134]. These models use Bayesian inference via the Metropolis–Hastings algorithm and have been evaluated through data analysis and simulations. Negative binomial regression models are often used to fit overdispersed data, such as the case counts and the secondary transmission cases [98–100]. However, these methods are dependent on data collected during the early stages of an epidemic, where the exponential growth phase is short and available data are limited [125].

On the other hand, in some cases, observations are not independent but instead correlated over time, which can affect the accuracy of the estimation results. For example, in the SEIR model discussed in Chapter 4, we assume that daily new cases are obtained through the detection of infectious individuals. Therefore, the observations of daily new cases are not independent. The Hidden Markov Model (HMM) is another approach commonly used to describe systems that evolve over time in a way that is partially observable [135, 136]. The model assumes that the system is in one of a set of hidden states at any given time, but these states cannot be directly observed. Instead, only the observable outputs or observations, which are probabilistically related to the hidden states, are available. Since epidemic processes are usually only partially observed through routine surveillance data, HMMs are often applied in epidemiology [137–139].

Both MLE and MCMC methods require a clear understanding of the distribution of case counts to establish appropriate likelihood functions for parameter estimation. In Chapter 4, we found through theoretical analysis and simulation studies that when time is very small, the binomial distribution can approximate the probability distribution of new cases per day. However, as the outbreak progresses through the exponential growth phase, the data quickly exhibit overdispersion. At this stage, the negative binomial distribution provides a better fit for the probability distribution of case counts. Building on this finding, in this chapter, we consider two different models for estimating the exponential growth rate: the negative binomial regression model and the HMM. We compare the performance of different likelihood functions in terms of estimation accuracy.

5.2 Negative Binomial Regression Model

Through the simulation study in Chapter 4, we observe that although the number of new cases does not initially follow a negative binomial distribution at the onset of disease spread, identifying the exact start of an outbreak is often challenging. By the time the spread is detected in the population, the number of cases is typically in an exponential growth phase. Therefore, under the assumption that observations are independent, it is reasonable to model the distribution of cases as a negative binomial distribution.

5.2.1 Methods

In the negative binomial regression model, the daily new cases, $C(t)$, follow a negative binomial distribution:

$$C(t) \sim NB(r, p),$$

where r is the size parameter, and p is the probability parameter.

The expected value of $C(t)$ is modeled as an exponential growth function:

$$\mathbb{E}[C(t)] = c_0 e^{\lambda t},$$

where c_0 is the initial value and λ is the growth rate. Unlike a Poisson distribution, a negative binomial distribution cannot be uniquely determined by its mean, because the mean $\mathbb{E}[C(t)] = \frac{r(1-p)}{p}$. Thus, either p or r needs to be estimated together with model parameters c_0 and λ, while the other may then be inferred from the mean. We consider two parameterization approaches to construct the likelihood function:

Method 1: Negative binomial likelihood with a constant probability parameter Estimate p and express the size parameter r in terms of p and $\mathbb{E}[C(t)]$:

$$r_t = \mathbb{E}[C(t)] \frac{p}{1-p} = \frac{c_0 e^{\lambda t} p}{1-p}.$$

Using the PMF of the negative binomial distribution (see Example 1.4.2), the corresponding likelihood function is:

$$\mathcal{L}_1[C(t) \mid p, c_0, \lambda] = \prod_{t=1}^{T} \binom{C(t) + r_t - 1}{C(t)} p^{r_t} (1-p)^{C(t)}. \tag{5.1}$$

Method 2: Negative binomial likelihood with a constant size parameter estimate r and express the probability parameter p in terms of r and $\mathbb{E}[C(t)]$:

$$p_t = \frac{r}{r + \mathbb{E}[C(t)]} = \frac{r}{r + c_0 e^{\lambda t}}.$$

Consequently, the likelihood function is:

$$\mathcal{L}_2[C(t) \mid r, c_0, \lambda] = \prod_{t=1}^{T} \binom{C(t) + r - 1}{C(t)} p_t^r (1 - p_t)^{C(t)}. \tag{5.2}$$

5.2.2 Accuracy of Exponential Growth Rate Estimation

To compare the accuracy of these two methods in estimating the exponential growth rate λ, we conduct a simulation study. Using a stochastic linear SEIR model, we generate 100 datasets of $C(t)$ with a fixed set of parameter values (the same values used in Figure 4.3) over a time range of 0 to 90. Here, the transmission rate is denoted by β, $1/\sigma$ represents the mean latent period, and infectious individuals are detected at a rate γ and move to compartment R. We fix the detection rate $\gamma = 0.2$ and estimate λ within a Bayesian framework, employing the *nimble* package with MCMC sampling and assuming normal priors centered on the true parameter values.

We consider different fitting windows, where a fitting window refers to the time period of observed data used for estimation. Specifically, we test nine fitting windows, with time periods ranging from $[0, 10]$ to $[0, 90]$ in increments of 10. For each window, we fit 100 datasets and calculate the mean, variance, and average 95% credible interval width of the estimated λ across the 100 results.

Figure 5.1 presents the fitting results of the two methods across different fitting windows. The left panel compares the mean of the point estimates of λ . As more data points are used, the point estimates converge more closely to the true value. However, when the fitting window is short, Method 1 exhibits a larger bias. The middle panel compares the variance of the point estimates of λ. As the fitting window increases, the variance decreases and approaches zero. The last panel shows the average width of the credible intervals for λ. The width decreases as the fitting window becomes wider. Both methods show the same trend.

When estimating the growth rate λ, a key question is whether our credible intervals truly capture the underlying growth rate or if they only reflect the specific outbreak we observed. Real epidemics are just one outcome of a random process. Different

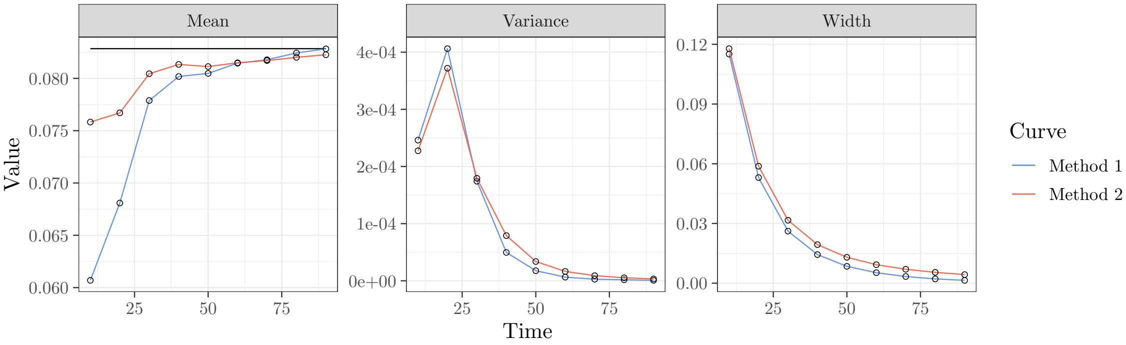

Figure 5.1: Comparison of the mean, variance, and 95% credible interval width of the estimated exponential growth rate λ across different fitting windows. The blue dots represent the estimation results using Method 1, where p is a constant, while the red dots correspond to Method 2, where r is a constant. In the left panel, the horizontal line indicates the true value $\lambda \approx 0.084$, computed using the fixed parameters, which are the same as those in Figure 4.3.

outbreaks can have different observed growth rates, even if they follow the same transmission rules. If our credible intervals ignore this randomness, they may be too narrow or too wide. Narrow intervals can miss the true value too often, while wide intervals reduce precision. To check if our credible intervals are reliable, we use coverage probability, which measures how often they contain the true growth rate over many realizations. A good method should have a coverage probability that matches the nominal confidence level. This ensures our estimates are accurate and useful. To estimate the coverage probability , we use 100 datasets to estimate the parameters for each fitting window. The coverage probability is then estimated by calculating the proportion of the 95% credible intervals that contain the true value across the 100 estimates.

Table 5.1 compares the estimated coverage probability of λ for these two methods. The coverage for both methods is significantly lower than 95%. Although the coverage reaches 100% when using data from the time period $[0, 10]$, this is due to the small number of data points, which results in overly wide credible intervals.

5.3 Hidden Markov Model

In the negative binomial regression model, we assume that the observed data are independent. However, in reality, they are not. The number of daily new cases, $C(t)$,

Table 5.1: Dependence of the estimated coverage probability of the growth rate λ on the end time of the fitting windows.

Time Period	Method 1	Method 2
[0,90]	61%	68%
[0,80]	60%	68%
[0,70]	52%	76%
[0,60]	60%	76%
[0,50]	48%	65%
[0,40]	61%	68%
[0,30]	60%	76%
[0,20]	68%	85%
[0,10]	100%	100%

depends on whether the infectious individuals $I(t)$ are detected at a rate γ, and $I(t)$ depends on $I(t-1)$. At the same time, $C(t-1)$ also depends on $I(t-1)$. Thus $C(t)$ and $C(t-1)$ are not independent.

Theoretically, $I(t)$ and $C(t)$ have the same exponential growth rate provided that each infectious individual has the same probability of detection. Thus it might be easier to estimate the growth rate from $I(t)$. However, obtaining data for $I(t)$ is difficult, as it is not directly observed. Therefore, we consider $I(t)$ as a latent statistical variable (an unobserved state), and use the Hidden Markov Model to capture the dependencies in the data. The HMM allows us to model the hidden state $I(t)$ while using observable data $C(t)$ to infer it. We can estimate the unobserved state transitions over time and account for the dependencies between the hidden and observable states.

5.3.1 Methods

Here, we model the expected value of $I(t)$ as exponential growth:

$$\mathbb{E}[I(t)|I(t-1)] = I(t-1)e^{\lambda}.$$

This is a step-by-step model, where the time step is 1. Given by $I(t)$, the observed cases is assumed to be binomial distribution

$$C(t) \mid I(t) \sim Bin(I(t), \gamma).$$

To establish the likelihood function, we need to specify the distribution for $I(t)$.

When we assume that $I(t)$ follows a negative binomial distribution:

$$I(t) \sim \mathrm{NB}(r, p),$$

we can establish the likelihood function in two different ways, as follows:

Method 3: HMM with negative binomial likelihood and a constant probability parameter Like Method 1, we assume p is a constant and estimate it with other model parameters. The size parameter r can be written in terms of p and $\mathbb{E}[I(t)]$:

$$r_t = \mathbb{E}[I(t)]\frac{p}{1-p} = \frac{I(t-1)e^{\lambda}p}{1-p}.$$

The completed likelihood functions is given by

$$\begin{aligned} \mathcal{L}_3(C|\lambda, p, I_0, \gamma) &= \prod_{t=1}^{T}\left[NB(I(t)|r_t, p) \cdot Bin(C(t)|I(t), \gamma)\right] \\ &= \prod_{t=1}^{T}\binom{I(t)+r_t-1}{I(t)}p^{r_t}(1-p)^{I(t)}\binom{I(t)}{C(t)}\gamma^{C(t)}(1-\gamma)^{I(t)-C(t)}. \end{aligned} \tag{5.3}$$

Method 4: HMM with negative binomial likelihood and a constant size parameter Like Method 2, we assume that r is a constant and and estimate it with other model parameters. We express the probability parameter p in terms of r and $\mathbb{E}[I(t)]$:

$$p_t = \frac{r}{r+\mathbb{E}[I(t)]} = \frac{r}{r+I(t-1)e^{\lambda}}.$$

Then, the likelihood function is:

$$\begin{aligned} \mathcal{L}_4(C|\lambda, r, I_0, \gamma) &= \prod_{t=1}^{T}\left[NB(I(t)|r, p_t) \cdot Bin(C(t)|I(t), \gamma)\right] \\ &= \prod_{t=1}^{T}\binom{I(t)+r-1}{I(t)}p_t^{r}(1-p_t)^{I(t)}\binom{I(t)}{C(t)}\gamma^{C(t)}(1-\gamma)^{I(t)-C(t)}. \end{aligned} \tag{5.4}$$

5.3.2 Additional Methods

In Chapter 4, we found that when t is large, the distribution of $I(t)$ can be approximated by a negative binomial distribution. However, when t is small, the variance of $I(t)$ is less than its mean and can be approximated by a binomial distribution. For this HMM, we assume that the time step is 1, so its distribution may follow a binomial distribution.

Method 5: HMM with a binomial likelihood and a constant probability parameter We assume that $I(t)$ follows a binomial distribution,

$$I(t) \sim Bin(N_t, P),$$

and the size parameter N_t is proportional to $I(t-1)$, i.e., $N_t = aI(t-1)$, where a is a constant and $a > 1$. Then, the probability is

$$P = \frac{\mathbb{E}[I(t)]}{N_t} = \frac{I(t-1)e^{\lambda}}{aI(t-1)} = \frac{e^{\lambda}}{a}.$$

The likelihood function can be written as:

$$\begin{aligned}\mathcal{L}_5(C|\lambda, a, I_0, \gamma) &= \prod_{t=1}^{T} [Bin(I(t)|N_t, P) \cdot Bin(C(t)|I(t), \gamma)] \\ &= \binom{N_t}{I(t)} P^{I(t)}(1-P)^{N_t - I(t)} \binom{I(t)}{C(t)} \gamma^{C(t)}(1-\gamma)^{I(t)-C(t)}. \qquad (5.5)\end{aligned}$$

The negative binomial distribution is suitable for handling overdispersed data, while the binomial distribution is appropriate for underdispersed data. For completeness, we also consider the Poisson distribution, which has equal mean and variance.

Method 6: HMM with Poisson likelihood If $I(t)$ follows a Poisson distribution,

$$I(t) \sim \text{Poisson}(\mathbb{E}[I(t)]),$$

where $\mathbb{E}[I(t)] = I(t-1)e^{\lambda}$. Using the PMF of Poisson distribution (see Example 1.4.1), the likelihood function is given by

$$\begin{aligned}\mathcal{L}_6(C|\lambda, I_0, \gamma) &= \prod_{i=t}^{T} [\text{Poisson}(I(t)|\mathbb{E}[I(t)]) \cdot Bin(C(t)|I(t), \gamma)] \\ &= \frac{\mathbb{E}[I(t)]^{I(t)} e^{-\mathbb{E}[I(t)]}}{I(t)!} \binom{I(t)}{C(t)} \gamma^{C(t)}(1-\gamma)^{I(t)-C(t)}. \qquad (5.6)\end{aligned}$$

5.3.3 Accuracy of Exponential Growth Rate Estimation

To compare the accuracy of these four likelihood functions for estimating the growth rate λ, we fit the data of $C(t)$ using a Bayesian HMM with the *nimble* package. The model assumes an exponential growth phase where infections $I(t)$ evolve based on past values, and observed cases $C(t)$ follow a binomial sampling process. We fix $\gamma = 0.2$.

We compare the estimated coverage of the true value of λ within the 95% credible interval for the four methods. Across different fitting windows, the coverage for all methods is approximately 100%. Thus, the coverage probability alone cannot distinguish the performance of these methods.

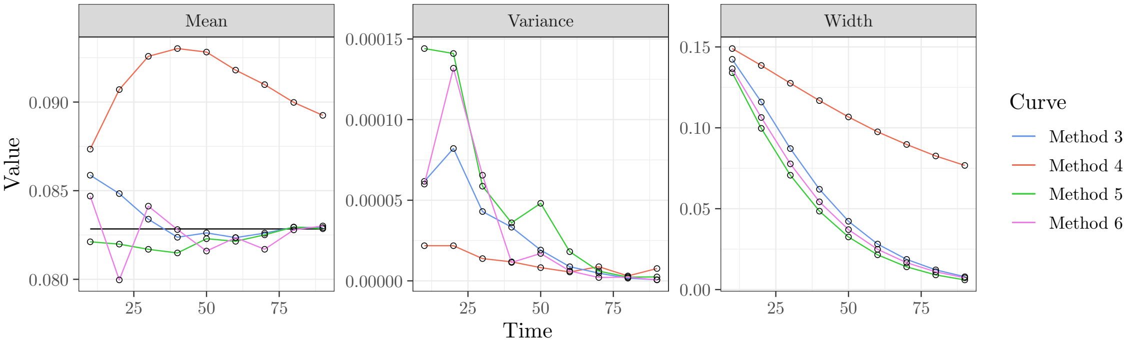

Figure 5.2: Dependence of the estimated exponential growth rate λ on the end time of the fitting window. The curves represent different methods: blue (Method 3, negative binomial with a constant p), red (Method 4, negative binomial with a constant r), green (Method 5, binomial distribution), and pink (Method 6, Poisson distribution). For the left panel, the horizontal line represents the true λ.

Figure 5.2 shows the dependence of the point estimation results of λ on the end time of the fitting windows. The left panel displays the mean of 100 point estimates across different fitting windows. Here, Method 4 exhibits the largest deviation from the true value of λ, while the other three methods follow a similar trend. As the number of data points in the fitting window increases, the estimated value of λ approaches the true value. The middle panel illustrates the variance of the 100 point estimates across different fitting windows. The variances are generally small and tend to decrease as the number of data points increases. The right panel shows how the average width of the 95% credible interval for λ depends on the end time of the fitting window. All curves exhibit the same trend: as the end time increases, the credible interval narrows. However, the credible interval estimated using Method 4 remains significantly wider than those obtained from the other likelihood functions.

Therefore, when estimating the exponential growth rate within the HMM framework, $I(t)$ is not suitable for assuming a negative binomial distribution with a constant size parameter r. However, assuming that $I(t)$ follows a negative binomial distribution with a constant probability parameter p provides a good estimate of λ. Additionally, as our model progresses step by step, the estimation results assuming that $I(t)$ follows either a binomial or Poisson distribution are also comparable.

This comparison is done assuming a fixed transmission rate β and a fixed latent period $1/\sigma$. However, there are infinite combinations of β and σ that result in the same exponential growth rate, so our method cannot identify β and σ individually. Do the results depend on the combinations of β and σ? This question is addressed in the following subsection.

5.3.4 Dependence of the Estimation Results on β and σ

In this subsection, we fix $\lambda \approx 0.084$ and vary σ from 0.2 to 1 in increments of 0.2, adjusting β accordingly. The corresponding parameter values are shown in Table 5.2. For each set of parameters, we generate 100 datasets of $C(t)$. Figure 5.2 illustrates that the point estimates from Method 3 (which assumes $I(t)$ follows a negative binomial distribution with a constant r) exhibit a large error relative to the true value of λ. Therefore, we focus our comparison on the remaining three methods.

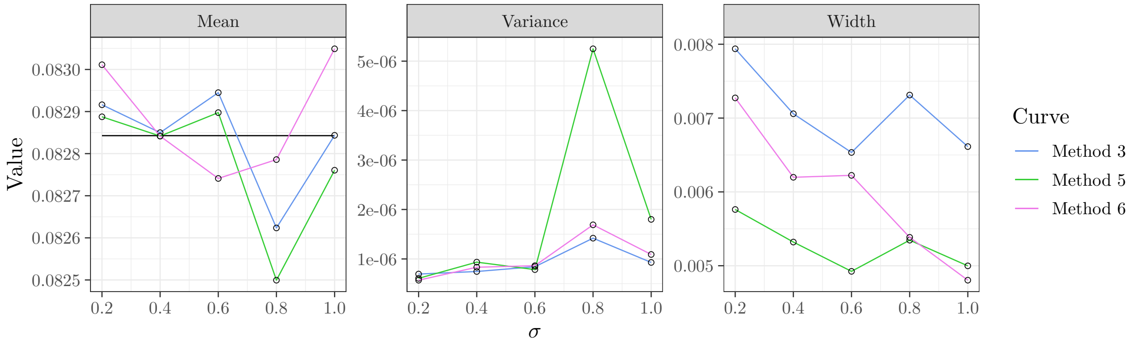

Figure 5.3: Dependence of the estimated exponential growth rate λ on model parameters. The curves represent different methods: green (Method 3, negative binomial with a constant p), green (Method 5, binomial distribution), and pink (Method 6, Poisson distribution).

Table 5.2: Dependence of the estimated coverage probability of the growth rate λ on the parameters β and σ.

σ	β	Method 3	Method 5	Method 6
0.2	0.4	100%	100%	100%
0.4	0.341	100%	100%	68%
0.6	0.322	100%	99%	68%
0.8	0.312	100%	98%	68%
1	0.306	100%	99%	60%

Figure 5.3 illustrates the dependence of the point estimates of λ on the parameters. Similarly, we compare the mean, variance, and average width of the 95% credible intervals for the 100 point estimates. Overall, there is minimal difference between the estimation results from the three methods. While the estimates fluctuate slightly for data generated by different parameter pairs, the observed differences are relatively small.

We compare the estimated coverage probability of the true λ within the 95% credible intervals for the three methods in Table 5.2. Method 3 and Method 5 exhibit high coverage. However, when assuming that the distribution of $I(t)$ follows a Poisson distribution, Method 6 provides lower coverage.

5.4 Concluding Remarks

In this study, we explore various statistical methods to build likelihood functions for estimating the exponential growth rate, λ, in the early stages of an outbreak. Estimating λ is crucial for understanding disease transmission dynamics and informing public health interventions. Based on the approximate distributions of the number of infected individuals $I(t)$ and the number of new cases per day $C(t)$ derived in Chapter 4, we consider both traditional methods, such as negative binomial regression, and more complex models like hidden Markov models.

For the negative binomial regression model, the distribution has two parameters: the size parameter r and the probability parameter p. We construct the likelihood function in two ways: assuming p is constant or assuming r is constant. We generate 100 sets of $C(t)$ data over a 90-day period. These data are generated by fixing a set of parameter values through a random SEIR model. We compare the results of the two likelihood functions for estimating λ with respect to the end time of the fitting window (with the start time fixed at 0). As more data are included, both methods converge to the true λ. However, the coverage of the 95% confidence interval for the true λ is below the expected 95%. This is likely because the model assumes independent observations, while in reality, the data depend on the hidden state $I(t)$.

The HMM add complexity by accounting for the hidden state $I(t)$. Although unobservable, this state affects the observed cases $C(t)$. Because time dependence is considered, the value of $I(t)$ depends on previous time steps. The time step is set to 1. In constructing the likelihood function, we assume that $I(t)$ follows a negative binomial distribution. We also consider the possibility that $I(t)$ follows a binomial distribution or a Poisson distribution. We then compare these likelihood functions.

Our estimation results show that, except for Method 4 (where $I(t)$ follows a negative binomial distribution with a constant size parameter r), all other methods within the HMM framework provide robust estimates of λ. Method 4 produces larger estimation errors and wider credible intervals. The other three methods ($I(t)$ follows a negative binomial distribution with a constant probability parameter p, a binomial distribution, or a Poisson distribution) demonstrate better accuracy in parameter estimation.

Since the exponential growth rate depends on β and σ, different combinations of these parameters can result in the same λ. To study whether the results of parameter estimation depend on the parameter values, we vary σ. We then calculate the corresponding β to maintain the same λ as in the previous simulation study. We randomly generate 100 sets of $C(t)$ data with different parameter combinations and fit them to the model. We find that the credible intervals generated by the likelihood function assuming that $I(t)$ follows a Poisson distribution have low coverage. In contrast, assuming $I(t)$ follows a negative binomial distribution with a constant probability parameter p or a binomial distribution yields better accuracy in parameter estimation.

Chapter 6

Conclusions

The early stage of an epidemic is a critical period when the trajectory of disease spread is highly uncertain, and timely interventions can have the greatest impact. During this stage, cases often grow exponentially, and multiple control measures, such as contact tracing and non-pharmaceutical interventions, are implemented simultaneously. As a result, disentangling and assessing the effectiveness of contact tracing and other interventions is challenging. Some key model parameters cannot be identified solely from case data, as different parameter combinations can produce similar exponential growth curves. Moreover, the initial growth rate serves as a key indicator of transmission speed and is often used to evaluate the effectiveness of control measures. Accurately estimating this growth rate is therefore essential for optimizing intervention strategies.

This dissertation contributes to the mathematical epidemiology of infectious disease modelling in three key areas: (1) developing a novel approach to integrating contact tracing into compartmental models while balancing realism and analytical tractability to disentangle the effects of contact tracing and other NPIs, (2) identifying critical data sources for estimating key contact tracing parameters to evaluate the effectiveness of contact tracing, and (3) enhancing parameter estimation techniques by refining likelihood functions and evaluating statistical methods for estimating epidemic growth rates. These findings have significant implications for public health policy, particularly in designing effective contact tracing strategies and improving the precision of outbreak forecasting.

In Chapter 2, we propose a novel framework for modeling contact tracing. In a randomly mixed population, we assume that infection-causing contacts form a transmission tree. The nodes represent infectious individuals, and the directed edges indicate who-infected-who. We apply the concept of edge dynamics from network models to track contacts in randomly mixed population. This framework extends the traditional SIR compartment model to include contact tracing. It combines the convenience of random mixing models with the accuracy of network-based contact tracing, eliminating the need for detailed contact network information.

We calculate the control reproduction number $\mathcal{R}_C$ for our SIR contact tracing model and examine its dependence on key parameters. Theoretical analysis in Appendix C shows that increasing contact tracing coverage p or testing rate τ lowers $\mathcal{R}_C$. This confirms the expected impact of identifying and isolating more infectious individuals. Numerical analysis reveals that $\mathcal{R}_C$ is more sensitive to the testing rate than to contact tracing coverage. This suggests that increasing the availability of tests improves the overall effectiveness of contact tracing. Our results also indicate that when the transmission rate is high, contact tracing alone may not be enough to control the disease. This highlights the need for additional public health interventions. The implementation of contact tracing is limited by resources, so we study the effect of tracing capacity on $\mathcal{R}_C$. We find that contact tracing is most effective in the early stages of an epidemic but becomes saturated as case numbers increase. When the tracing capacity is limited, its effectiveness decreases. Expanding tracing capacity significantly delays and suppresses the epidemic peak, emphasizing the importance of resource allocation.

Using COVID-19 as a case study, we extend our simplistic SIR contact tracing model to incorporate the latent period and asymptomatic transmission. In Chapter 3, we introduce the SEIR and SEAIR contact tracing models to offer a more realistic framework. Since disease features like asymptomatic transmission are difficult to identify early on, SEIR models are commonly used. We also compare the differences between these models in evaluating the effect of contact tracing. When calibrating the models with new case data to estimate parameters, we find that different combinations of parameters can produce the same exponential growth curve, making it difficult to identify the model parameters. To determine which data are necessary for parameter estimation, we conduct a simulation study. We find that additional data, such as voluntary test counts, cases identified through contact tracing, and symptom onset counts, are essential. Previously quarantined case counts offer only a slight improvement in accuracy. Our study also shows that the SEIR model underestimates the model parameters, while the SEAIR model provides more accurate results.

We apply our contact tracing models to the early stage of the Ontario COVID-

19 pandemic, from March 16 to May 1, 2020. We use daily case counts, symptom onsets, and cases identified through contact tracing to estimate parameters. The parameters estimated by the SEIR model are slightly lower than those estimated by the SEAIR model. We calculate $\mathcal{R}_C$ for both models and analyze its dependence on contact tracing parameters: the contact tracing rate θ and tracing coverage p. Our analysis reveals that contact tracing identified approximately 29% of diagnosed cases, moderately reducing the reproduction number and significantly decreasing prevalence. The effectiveness of contact tracing is primarily influenced by tracing coverage, with little impact from tracing delays. While the SEIR model slightly overestimates the control reproduction number, it underestimates prevalence. Similar effects of contact tracing are observed in both models.

Maximum likelihood estimation and Bayesian MCMC methods are both commonly used for parameter estimation. To improve the accuracy of parameter estimation in infectious disease models, it is essential to understand the distribution of new cases and develop an appropriate likelihood function based on their probability distribution. Since many diseases have a latent period, in Chapter 4, we analyze the distribution of the number of infectious individuals $I(t)$ and the number of daily new cases $C(t)$ using a stochastic linear SEIR model.

We establish the master function for the process $(E(t), I(t))$ and derive the approximate probability generating function (PGF) for this process. This approximate PGF allows for the calculation of the mean and variance of the number of infectious individuals, $I(t)$. The process $I(t)$ is found to decompose into two distinct birth-and-death processes and can be approximated as the convolution of four distributions: two negative binomial distributions and two binomial distributions. However, as time progresses, the parameters of the binomial distributions may become negative. Numerical simulations show that there are two approximation scenarios for $I(t)$ based on its mean and variance. When $\mathbb{E}[I(t)] > \mathrm{Var}[I(t)]$, the distribution can be approximated by a single binomial distribution; when $\mathbb{E}[I(t)] < \mathrm{Var}[I(t)]$, the distribution can be approximated by a single negative binomial distribution.

We assume that the number of daily new cases, $C(t)$, is detected from the infectious individuals, so it can be modeled as a binomial distribution conditional on $I(t)$. Hence, the distribution of $C(t)$ depends on whether $I(t)$ is binomial or negative binomial. Numerical simulations reveal that the variance of infectious individuals and new cases is smaller than the mean only for small t. For long observation periods, a negative binomial distribution fits the data, while for short time steps, a binomial distribution is more appropriate. These findings help develop a more accurate likelihood function for better parameter estimation and epidemic modeling.

In Chapter 5, we compare the performance of different statistical methods for establishing the likelihood function to estimate the initial exponential growth rate λ. Based on the findings in Chapter 4, we begin by considering the negative binomial regression model. The negative binomial distribution has two parameters: the size parameter r and the probability parameter p. We construct the likelihood function in two ways: assuming p is constant or assuming r is constant. We randomly generate 100 sets of daily new cases $C(t)$ and use these data to estimate λ. We find that the coverage of the 95% confidence interval for the true λ is below the expected 95%. This is likely because the model assumes independent observations, while in reality, the data depend on the hidden state $I(t)$.

The hidden Markov model accounts for the hidden state $I(t)$ (which influences $C(t)$) and includes time dependence. In this framework, we establish the likelihood functions assuming that $I(t)$ follows a negative binomial distribution in two ways: assuming p is constant or r is constant. For comparison, we also consider the likelihood functions assuming that $I(t)$ follows binomial and Poisson distributions. The results show that, except for the case where $I(t)$ follows a negative binomial distribution with constant r, the other methods provide accurate estimates of λ.

Different combinations of model parameters can lead to the same initial growth rate; this phenomenon is called nonidentifiability. Finally, we fix the growth rate λ and vary the model parameters to generate data to test whether the accuracy of λ estimation depends on the parameters. The results show that assuming $I(t)$ follows a Poisson distribution leads to poor coverage in credible intervals, while assuming a negative binomial or binomial distribution provides better accuracy in parameter estimation.

Future research can extend our models in several directions to make them more realistic. Our SEIR and SEAIR model framework is based on assumptions about how contact tracing was implemented in the early stages of COVID-19 in Canada. For example, our model assumes that testing is based on symptoms, meaning asymptomatic patients are not tested. However, these models can be extended to include testing for asymptomatic cases and varying testing frequencies, for example, blanket testing or testing all traced cases. In addition, the heterogeneity of contacts should be considered. Different types of contacts, such as close contacts and community contacts, have varying levels of traceability. Close contacts are generally easier to trace, while community contacts, which are often more dispersed and less predictable, present challenges in terms of traceability. Addressing this heterogeneity in future models could lead to a more accurate representation of the contact tracing process and improve the design of intervention strategies. Moreover, as control measures are implemented, the growth rate of an epidemic changes. Extending the statistical methods developed in this study to identify change points in the growth rate and quantifying these changes would offer valuable information on the effectiveness of interventions over time.

Appendix A

SIR Contact Tracing Model-Flowchart of the Full Pair Dynamics

The flowchart in Figure 2.3 includes only the dynamics of the pairs $[I{\leftarrow}I]$, $[I{\leftarrow}T]$ and $[T{\leftarrow}I]$. The pairs $[I{\leftarrow}X]$, $[I{\leftarrow}R]$, $[T{\leftarrow}T]$, $[T{\leftarrow}X]$ and $[T{\leftarrow}R]$ are not tracked in that flowchart, even though they are valid states. In Figure A.1, we give the full flowchart for all these pairs. The equations in (2.1) can be read from this flowchart with the relationships $I = [I{\leftarrow}I] + [I{\leftarrow}T] + [I{\leftarrow}X] + [I{\leftarrow}R]$ and $T = [T{\leftarrow}I] + [T{\leftarrow}T] + [T{\leftarrow}X] + [T{\leftarrow}R]$.

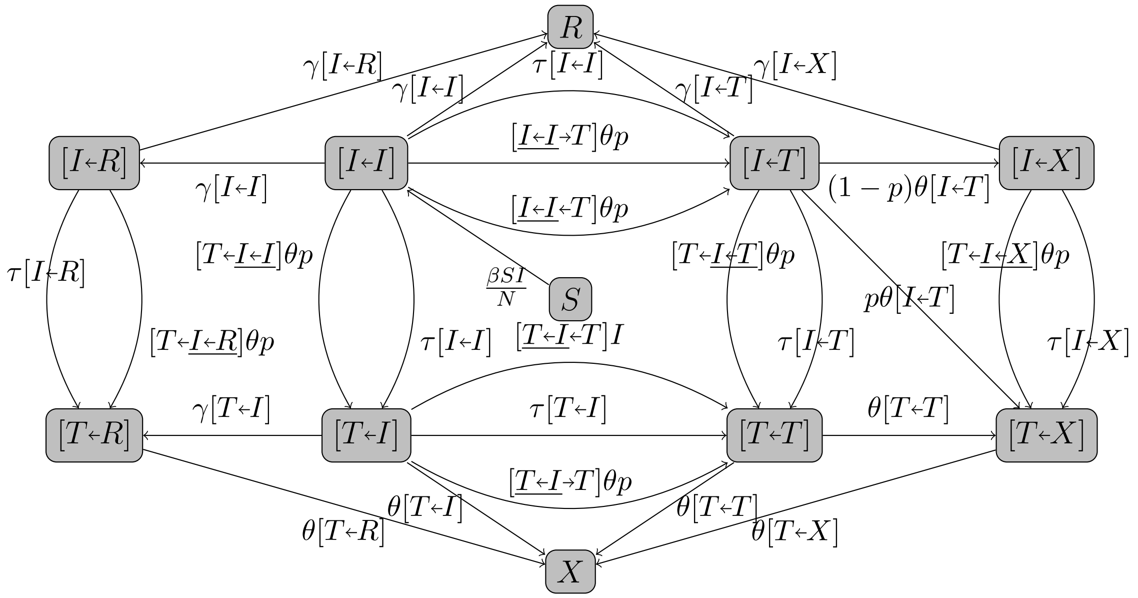

Figure A.1: The full flowchart of the pair dynamics for Model (2.1).

Appendix B

SIR Contact Tracing Model-Uniqueness and Stability of Disease-Free Equilibrium

Here we show that the system (2.2) has a unique biologically meaningful disease-free equilibrium (DFE) that is globally asymptotically stable in the disease-free invariant set $\mathcal{H}$.

Equation (2.4) gives a unique positive root w^*. We will show that equation (2.5) has two positive roots, and only one is in the invariant region $\mathcal{H}$ (i.e., biologically meaningful). This is true if

$$F(1-u^*) = \tau u^* + \theta p u^* w^* + (\theta p u^* - \beta - \theta)(1-u^*) + \theta p (1-u^*)^2 < 0, \tag{B.1}$$

and thus the larger root satisfies $v^* > 1 - u^*$ and is outside of $\mathcal{H}$, while the smaller root satisfies $v^* < 1 - u^*$ and is inside $\mathcal{H}$. To show that (B.1) is true, note that from (2.2e),

$$\tau u^* + \theta p u^* w^* = (\beta + \theta) w^*.$$

In addition, adding (2.2c) and (2.2e) gives,

$$\beta - \beta u^* - \gamma u^* = (\beta + \theta) w^*.$$

The above two equations give

$$\tau u^* + \theta p u^* w^* = \beta - \beta u^* - \gamma u^*. \tag{B.2}$$

Thus,

$$\begin{aligned} F(1-u^*) &= \beta - \beta u^* - \gamma u^* + \theta p(1-u^*) - (\beta+\theta)(1-u^*), \\ &= -\gamma u^* - \theta(1-p)(1-u^*) < 0. \end{aligned}$$

This implies that there is a unique biologically meaningful disease-free equilibrium $(N, 0, u^*, v^*, w^*)$ in $\mathcal{H}$.

To study the stability of the DFE, we linearize this model about the DFE $(N, 0, u^*, v^*, w^*)$, and restrict to the invariant set $\mathcal{H}$. The dynamics of the linearized system is only determined by the equations of I, u, v and w. From (2.2c), (2.2d), (2.2e),

$$u' = \beta - \beta u - (\tau+\gamma)u - \theta p u w := f(u,w)\,, \tag{B.3a}$$

$$v' = \tau u + \theta p u(v+w) - (\beta+\theta)v + \theta p v^2\,, \tag{B.3b}$$

$$w' = \tau u - (\beta+\theta)w + \theta p u w := g(u,w)\,. \tag{B.3c}$$

Note that u and w are independent of v. We thus first study (B.3a) and (B.3c). At the positive equilibrium point (u^*, w^*) where $0 \le u^* \le 1$, the Jacobian of the (u, w) system is

$$J = \begin{bmatrix} -(\beta+\tau+\gamma+\theta p w^*) & -\theta p u^* \\ \tau + \theta p w^* & \theta p u^* - (\beta+\theta) \end{bmatrix}.$$

The trace

$$tr(J) = -(\beta+\tau+\gamma+\theta p w^*) + \theta p u^* - (\beta+\theta) < 0,$$

and the determinant

$$det(J) = (\beta+\theta)(\beta+\tau+\gamma+\theta p w^*) - (\beta+\gamma)\theta p u^* > 0.$$

Hence, this DFE is locally asymptotically stable.

We use the Bendixon criterion to show the global stability of the DFE. Because $p \le 1$ and $u \le 1$,

$$\frac{\partial f}{\partial u} + \frac{\partial g}{\partial w} = -(\beta+\tau+\gamma+\theta p w) - (\beta+\theta) + \theta p u < 0,$$

and thus the (u, w) system has no periodic solution in the invariant set $\mathcal{H}$. Thus, in $\mathcal{H}$, all solutions satisfy $u(t) \to u^*$ and $w(t) \to w^*$ as $t \to \infty$. To study the behaviour of $v(t)$, substitute (u^*, w^*) into the equation for v:

$$v' = \tau u^* + \theta p u^* w^* + (\theta p u^* - \beta - \theta)v + \theta p v^2.$$

Note that v^* is the smaller root of $F(v) = 0$, $F'(v^*) < 0$, and thus v^* is locally asymptotically stable. Because this is a one-dimensional autonomous equation, all solutions in the invariant set $\mathcal{H}$ approach the biologically meaningful DFE $(N, 0, u^*, v^*, w^*)$.

Appendix C

SIR Contact Tracing Model-The dependence of $\mathcal{R}_c$ on p and τ

Here we prove that $\mathcal{R}_c$ is a decreasing function of the tracing coverage p and the testing rate τ. To show the dependence on p, we calculate $\partial w^*/\partial p$ from equation (2.4).

$$\frac{\partial w^*}{\partial p} = -\frac{\partial G/\partial p}{\partial G/\partial w^*},$$

where

$$\partial G/\partial p = (\beta+\theta)\theta w^* \left(w^* - \frac{\beta}{\beta+\theta} \right),$$

and $\partial G/\partial w^* > 0$ (because G has a positive root and a negative root, thus w^* is the larger root of (2.4)). To determine the sign of $\partial G/\partial p$, we need to calculate the sign of $w^* - \frac{\beta}{\beta+\theta}$. Consider

$$G(\frac{\beta}{\beta+\theta}) = (\beta+\theta)\theta p(\frac{\beta}{\beta+\theta})^2 + [(\beta+\theta)(\beta+\tau+\gamma) - \beta\theta p]\frac{\beta}{\beta+\theta} - \beta\tau = \beta(\beta+\gamma) > 0\,,$$

and

$$\left.\frac{\partial G}{\partial w^*}\right|_{\frac{\beta}{\beta+\theta}} = \theta p\beta + (\beta+\theta)(\beta+\tau+\gamma) > 0\,.$$

Thus, $\beta/(\beta+\theta) > w^*$. Hence, $\partial G/\partial p < 0$, giving $\frac{\partial w^*}{\partial p} > 0$, therefore, the value of w^* increases as p increases.

Similarly, we calculate $\partial v^*/\partial p$ from (2.5). Equation (B.3c) gives

$$\theta p u^* w^* + \tau u^* = (\beta+\theta)w^*.$$

Substituting this into (2.5) gives

$$F = \theta p v^{*2} + (\theta p u^* - \beta - \theta)v^* + (\beta + \theta)w^* = 0. \tag{C.1}$$

Thus, taking the total derivative of F gives

$$\frac{\partial v^*}{\partial p} = -\frac{\frac{\partial F}{\partial u^*}\frac{\partial u^*}{\partial p} + \frac{\partial F}{\partial w^*}\frac{\partial w^*}{\partial p} + \frac{\partial F}{\partial p}}{\partial F/\partial v^*}.$$

Here,

$$\frac{\partial F}{\partial p} = \theta(v^*)^2 + \theta u^* v^*, \quad \frac{\partial F}{\partial u^*} = \theta p v^*, \quad \frac{\partial F}{\partial w^*} = \beta + \theta,$$

and $\partial F/\partial v^* < 0$ (because v^* is the smaller root of (C.1)). The sign of $\partial v^*/\partial p$ is determined by the sign of its numerator. From (2.3),

$$\begin{aligned}\frac{\partial u^*}{\partial p} &= -\frac{\beta\theta p}{(\beta+\tau+\gamma+\theta p w^*)^2}\frac{\partial w^*}{\partial p} - \frac{\beta\theta w^*}{(\beta+\tau+\gamma+\theta p w^*)^2} \\ &= -\frac{\theta p u^*}{\beta+\tau+\gamma+\theta p w^*}\frac{\partial w^*}{\partial p} - \frac{\theta w^* u^*}{\beta+\tau+\gamma+\theta p w^*}.\end{aligned}$$

Thus,

$$\begin{aligned}\frac{\partial F}{\partial u^*}\frac{\partial u^*}{\partial p} + \frac{\partial F}{\partial w^*}\frac{\partial w^*}{\partial p} + \frac{\partial F}{\partial p} &= -\frac{(\theta p)^2 v^* u^*}{\beta+\tau+\gamma+\theta p w^*}\frac{\partial w^*}{\partial p} - \frac{\theta^2 p v^* w^* u^*}{\beta+\tau+\gamma+\theta p w^*} \\ &\quad +(\beta+\theta)\frac{\partial w^*}{\partial p} + \theta(v^*)^2 + \theta u^* v^*.\end{aligned}$$

Note that,

$$-\frac{(\theta p)^2 v^* u^*}{\beta+\tau+\gamma+\theta p w^*}\frac{\partial w^*}{\partial p} + \theta\frac{\partial w^*}{\partial p} = \frac{\beta+\tau+\gamma+\theta p w^* - \theta p^2 u^* v^*}{\beta+\tau+\gamma+\theta p w^*}\theta\frac{\partial w^*}{\partial p} > 0 \tag{C.2}$$

in the case of $\mathcal{R}_c > 1$, i.e., $\beta > \gamma + \tau + \theta p(u^* + v^*)$. In addition,

$$\frac{\theta^2 p u^* v^* w^*}{\beta+\tau+\gamma+\theta p w^*} \le \theta u^* v^*\,,$$

and thus

$$\frac{\partial F}{\partial u^*}\frac{\partial u^*}{\partial p} + \frac{\partial F}{\partial w^*}\frac{\partial w^*}{\partial p} + \frac{\partial F}{\partial p} > 0.$$

This gives $\partial v^*/\partial p > 0$. Therefore, if $\mathcal{R}_c > 1$, both v^* and w^* are increasing functions of p. Thus,

$$\frac{\partial \mathcal{R}_c}{\partial p} < 0.$$

We use a similar approach to prove that $\mathcal{R}_c$ is a decreasing function of τ for $R_c > 1$. From equation (2.4),

$$\frac{\partial w^*}{\partial \tau} = -\frac{\partial G/\partial \tau}{\partial G/\partial w^*},$$

where

$$\partial G/\partial \tau = (\beta + \theta)w^* - \beta,$$

and $\partial G/\partial w^* > 0$. Because $\beta/(\beta + \theta) > w^*$, $\partial G/\partial \tau < 0$. Thus,

$$\frac{\partial w^*}{\partial \tau} = -\frac{\partial G/\partial \tau}{\partial G/\partial w^*} > 0.$$

To calculate $\partial v^*/\partial p$, we rewrite (2.5). From (B.2),

$$F = \theta p v^{*2} + (\theta p u^* - \beta - \theta)v^* + \beta - \beta u^* - \gamma u^* = 0.$$

Thus,

$$\frac{\partial v^*}{\partial \tau} = -\frac{\frac{\partial F}{\partial u^*}\frac{\partial u^*}{\partial \tau}}{\partial F/\partial v^*}.$$

Here,

$$\frac{\partial F}{\partial u^*} = \theta p v^* - \beta - \gamma, \quad \partial F/\partial v^* < 0.$$

To determine the sign of $\partial v^*/\partial \tau$, we calculate the sign of its numerator. From (2.3),

$$\begin{aligned} \frac{\partial u^*}{\partial \tau} &= -\frac{\beta\theta p}{(\beta + \tau + \gamma + \theta p w^*)^2}\frac{\partial w^*}{\partial \tau} - \frac{\beta}{(\beta + \tau + \gamma + \theta p w^*)^2} \\ &= -\frac{\theta p u^*}{\beta + \tau + \gamma + \theta p w^*}\frac{\partial w^*}{\partial \tau} - \frac{u^*}{\beta + \tau + \gamma + \theta p w^*}. \end{aligned}$$

Thus,

$$\frac{\partial F}{\partial u^*}\frac{\partial u^*}{\partial \tau} = (\beta + \gamma - \theta p v^*)\left[\frac{\theta p u^*}{\beta + \tau + \gamma + \theta p w^*}\frac{\partial w^*}{\partial \tau} + \frac{u^*}{\beta + \tau + \gamma + \theta p w^*}\right].$$

In the case of $\mathcal{R}_c > 1$ (i.e., $\beta > \gamma + \tau + \theta p(u^* + v^*)$),

$$\frac{\partial F}{\partial u^*}\frac{\partial u^*}{\partial \tau} > 0.$$

Thus, $\frac{\partial v^*}{\partial \tau} > 0$. Hence, if $\mathcal{R}_c > 1$, v^* and w^* are increasing functions of τ. Thus

$$\frac{\partial \mathcal{R}_c}{\partial \tau} < 0.$$

Appendix D

SEAIR Contact Tracing Model-Control Reproduction Number

With the variable change in subsection 3.2.3, the SEAIR model (3.6) can be rewritten as below:

$$S' = -\beta_I S \frac{I}{N} - \beta_A S \frac{A}{N}\,, \tag{D.1a}$$

$$E' = \beta_A S \frac{A}{N} + \beta_I S \frac{I}{N} - \sigma E - \theta p u_{[E\leftarrow T]} E\,, \tag{D.1b}$$

$$A' = \sigma q E - \theta p (w_{[A\leftarrow T]} + w_{[T\leftarrow A]}) A - \gamma_A A\,, \tag{D.1c}$$

$$I' = \sigma(1-q)E - (\gamma_I + \tau_I) I - \theta p (v_{[I\leftarrow T]} + v_{[T\leftarrow I]}) I\,, \tag{D.1d}$$

$$Q_E' = \theta p u_{[E\leftarrow T]} E - \sigma q Q_E - \sigma(1-q) Q_E\,, \tag{D.1e}$$

$$Q_A' = \theta p (w_{[A\leftarrow T]} + w_{[T\leftarrow A]}) A + \sigma q Q_E - \gamma_A Q_A - \tau_A Q_A\,, \tag{D.1f}$$

$$\begin{aligned} u_{[E\leftarrow I]}' = {} & \frac{\beta_I}{f} - u_{[E\leftarrow I]}(\tau_I + \gamma_I) - \theta p u_{[E\leftarrow I]} (v_{[I\leftarrow T]} + v_{[T\leftarrow I]}) \\ & - u_{[E\leftarrow I]} [\beta_A \frac{g}{f} + \frac{\beta_I}{f} - \theta p u_{[E\leftarrow T]}]\,, \end{aligned} \tag{D.1g}$$

$$\begin{aligned} u_{[E\leftarrow A]}' = {} & \beta_A \frac{g}{f} - \theta p u_{[E\leftarrow A]} (w_{[A\leftarrow T]} + w_{[T\leftarrow A]}) - u_{[E\leftarrow A]} [\gamma_A + \beta_A \frac{g}{f} + \frac{\beta_I}{f} \\ & - \theta p u_{[E\leftarrow T]}]\,, \end{aligned} \tag{D.1h}$$

$$\begin{aligned} u_{[E\leftarrow T]}' = {} & \tau_I u_{[E\leftarrow I]} + \theta p u_{[E\leftarrow I]} (v_{[I\leftarrow T]} + v_{[T\leftarrow I]}) - u_{[E\leftarrow T]} \theta \\ & - u_{[E\leftarrow T]} [\beta_A \frac{g}{f} + \frac{\beta_I}{f} - \theta p u_{[E\leftarrow T]}]\,, \end{aligned} \tag{D.1i}$$

$$v'_{[A\leftarrow I]} = \sigma q f u_{[E\leftarrow I]} - \gamma_A v_{[A\leftarrow I]} - \theta p v_{[A\leftarrow I]} w_{[T\leftarrow A]} - v_{[A\leftarrow I]}\sigma(1-q)f\,, \tag{D.1j}$$

$$\begin{aligned} v'_{[I\leftarrow A]} = {} & \sigma(1-q)fu_{[E\leftarrow A]} - \gamma_A v_{[I\leftarrow A]} - \theta p v_{[I\leftarrow A]}(w_{[A\leftarrow T]} + w_{[T\leftarrow A]}) \\ & - v_{[I\leftarrow A]}[\sigma(1-q)f - \theta p v_{[I\leftarrow T]}]\,, \end{aligned} \tag{D.1k}$$

$$\begin{aligned} v'_{[I\leftarrow I]} = {} & \sigma(1-q)fu_{[E\leftarrow I]} - (\gamma_I + \tau_I)v_{[I\leftarrow I]} - \theta p v_{[I\leftarrow I]} v_{[T\leftarrow I]} \\ & - v_{[I\leftarrow I]}\sigma(1-q)f\,, \end{aligned} \tag{D.1l}$$

$$\begin{aligned} v'_{[I\leftarrow T]} = {} & \sigma(1-q)fu_{[E\leftarrow T]} + \theta p v_{[I\leftarrow I]}(v_{[I\leftarrow T]} + v_{[T\leftarrow I]}) + \tau_I v_{[I\leftarrow I]} - \theta v_{[I\leftarrow T]} \\ & - v_{[I\leftarrow T]}[\sigma(1-q)f - \theta p v_{[I\leftarrow T]}]\,, \end{aligned} \tag{D.1m}$$

$$v'_{[T\leftarrow I]} = \theta p v_{[T\leftarrow I]} v_{[I\leftarrow I]} + \tau_I v_{[I\leftarrow I]} - \theta v_{[T\leftarrow I]} - v_{[T\leftarrow I]}\sigma(1-q)f\,, \tag{D.1n}$$

$$\begin{aligned} w'_{[A\leftarrow I]} = {} & \sigma q u_{[E\leftarrow I]}\frac{f}{g} + \theta p u_{[E\leftarrow I]}\frac{f}{g}(v_{[I\leftarrow T]} + v_{[T\leftarrow I]}) - (\sigma + \theta p)u_{[E\leftarrow T]}\frac{f}{g} \\ & - w_{[A\leftarrow I]}[\sigma q\frac{f}{g} - \theta p(w_{[A\leftarrow T]} + w_{[T\leftarrow A]}) - \gamma_A]\,, \end{aligned} \tag{D.1o}$$

$$\begin{aligned} w'_{[I\leftarrow A]} = {} & \sigma(1-q)u_{[E\leftarrow A]}\frac{f}{g} - (\gamma_I + \tau_I)w_{[I\leftarrow A]} - \theta p w_{[I\leftarrow A]} v_{[T\leftarrow I]} \\ & - w_{[I\leftarrow A]}\sigma q\frac{f}{g}\,, \end{aligned} \tag{D.1p}$$

$$\begin{aligned} w'_{[A\leftarrow T]} = {} & \theta p w_{[A\leftarrow I]}(v_{[I\leftarrow T]} + v_{[T\leftarrow I]}) + \tau_I w_{[A\leftarrow I]} + \sigma q u_{[E\leftarrow T]}\frac{f}{g} - \theta w_{[A\leftarrow T]} \\ & - w_{[A\leftarrow T]}[\sigma q\frac{f}{g} - \theta p w_{[A\leftarrow T]}]\,, \end{aligned} \tag{D.1q}$$

$$w'_{[T\leftarrow A]} = \theta p w_{[I\leftarrow A]} v_{[T\leftarrow I]} + \tau_I w_{[I\leftarrow A]} - \theta w_{[T\leftarrow A]} - w_{[T\leftarrow A]}\sigma q\frac{f}{g}\,, \tag{D.1r}$$

$$\begin{aligned} f' = {} & \beta_A g + \beta_I - \sigma f - \theta p f u_{[E\leftarrow T]} \\ & - f[\sigma(1-q)f - (\gamma_I + \tau_I) - \theta p(v_{[I\leftarrow T]} + v_{[T\leftarrow I]})]\,, \end{aligned} \tag{D.1s}$$

$$\begin{aligned} g' = {} & \sigma q f - \theta p g(w_{[A\leftarrow T]} + w_{[T\leftarrow A]}) - \gamma_A g \\ & - g[\sigma(1-q)f - (\gamma_I + \tau_I) - \theta p(v_{[I\leftarrow T]} + v_{[T\leftarrow I]})]\,, \end{aligned} \tag{D.1t}$$

$$T' = \tau_A Q_A + \tau_I I + \theta p(v_{[I\leftarrow T]} + v_{[T\leftarrow I]})I + \sigma(1-q)Q_E - \theta T\,, \tag{D.1u}$$

$$X' = \theta T\,, \tag{D.1v}$$

$$R' = \gamma_A(A + Q_A) + \gamma_I I\,. \tag{D.1w}$$

This is a very complex system and it is difficult to directly calculate the disease-free equilibrium of the model. Numerical simulations indicate that this model has a unique non-negative disease-free equilibrium

$$(N, 0, 0, 0, 0, 0, u^*_{[E\leftarrow I]}, u^*_{[E\leftarrow A]}, u^*_{[E\leftarrow T]}, v^*_{[A\leftarrow I]}, v^*_{[I\leftarrow A]}, v^*_{[I\leftarrow I]},$$

$$v^*_{[I\leftarrow T]}, v^*_{[T\leftarrow I]}, w^*_{[A\leftarrow I]}, w^*_{[I\leftarrow A]}, w^*_{[A\leftarrow T]}, w^*_{[T\leftarrow A]}, 0, 0, 0, 0, 0).$$

We use the next generation matrix method [140] to calculate its control reproduction number. We consider the infected classes E, A and I.

$$F = \begin{bmatrix} 0 & \beta_A & \beta_I \\ 0 & 0 & 0 \\ 0 & 0 & 0 \end{bmatrix},$$

$$V = \begin{bmatrix} \sigma + \theta p u^*_{[E\leftarrow T]} & 0 & 0 \\ -\sigma q & \gamma_A + \theta p(w^*_{[A\leftarrow T]} + w^*_{[T\leftarrow A]}) & 0 \\ -\sigma(1-q) & 0 & \gamma_I + \tau_I + \theta p(v^*_{[I\leftarrow T]} + v^*_{[T\leftarrow I]}) \end{bmatrix}.$$

Let

$$a = \frac{\sigma q}{(\sigma + \theta p u^*_{[E\leftarrow T]})(\gamma_A + \theta p(w^*_{[A\leftarrow T]} + w^*_{[T\leftarrow A]}))},$$

$$b = \frac{\sigma(1-q)}{(\sigma + \theta p u^*_{[E\leftarrow T]})(\gamma_I + \tau_I + \theta p(v^*_{[I\leftarrow T]} + v^*_{[T\leftarrow I]}))}.$$

Then,

$$FV^{-1} = \begin{bmatrix} \beta_A a + \beta_I b & \frac{\beta_A}{\gamma_A + \theta p(w^*_{[A\leftarrow T]} + w^*_{[T\leftarrow A]})} & \frac{\beta_I}{\gamma_I + \tau_I + \theta p(v^*_{[I\leftarrow T]} + v^*_{[T\leftarrow I]})} \\ 0 & 0 & 0 \\ 0 & 0 & 0 \end{bmatrix}.$$

Since $\mathcal{R}_C$ is the spectral radius of FV^{-1}, it follows that $\mathcal{R}_C = \beta_A a + \beta_I b$, which gives (3.7).

When $q = 0$, the SEAIR model simplifies to the SEIR model, and the control reproduction number of the SEIR model is given by (3.9).

Appendix E

The Stochastic Linear SEIR Model-Uniqueness Theorem

Theorem 1. *Let f be a probability measure having finite moments $a_k = \int_{-\infty}^{\infty} s^k f(s)ds$ of all orders. If the power series $\sum\limits_k a_k \frac{r^k}{k!}$ has a positive radius of convergence, then f is the only probability measure with the moments $a_1, a_2, \ldots$.*

This theorem is stated and proved in [141].

Corollary 1. *For a discrete random variable with a finite probability distribution, its distribution is uniquely determined by its moments.*

Proof. Consider a discrete finite random variable taking values in $\{0, 1, \ldots, n\}$. The moments are given by

$$a_k = \sum_{s=0}^{n} s^k p(s),$$

where $p(s)$ is the probability mass function.

Consider the power series $\sum\limits_k a_k \frac{r^k}{k!}$. Define

$$b_k = a_k \frac{r^k}{k!}.$$

Then, we examine the ratio test:

$$\lim_{k\to\infty} \left| \frac{b_{k+1}}{b_k} \right| = \lim_{k\to\infty} \left| \frac{a_{k+1} r^{k+1}}{(k+1)!} \cdot \frac{k!}{a_k r^k} \right|.$$

Since

$$a_{k+1} = \sum_{s=0}^{n} s^{k+1} p(s) = \sum_{s=0}^{n} s s^k p(s) \leq \sum_{s=0}^{n} n s^k p(s) = n a_k,$$

we obtain

$$\lim_{k\to\infty} \left| \frac{b_{k+1}}{b_k} \right| \leq \lim_{k\to\infty} \left| \frac{nr}{k+1} \right| = 0.$$

By the ratio test for series, this power series converges everywhere. Therefore, by Theorem 1, the distribution is uniquely determined by its moments. □

Appendix F

The Stochastic Linear SEIR Model-Derivation of the mean and variance of $I(t)$

From the approximate PGF formula (4.12) derived in Section 4.2,

$$\begin{aligned} X_0 &\approx 1 - \sigma u, \\ Y_0 &\approx 1 - (\sigma + \lambda_1) u. \end{aligned}$$

When $X = 1$, $u = \frac{Ku_0}{u_0 + (K - u_0)e^{-\lambda_1 t}}$ and $u_0 = \frac{-\sigma(1-Y)}{\sigma(\lambda_2 - \lambda_1)}$. Here, $K = \frac{\lambda_1(\lambda_1 - \lambda_2)}{\beta\sigma(\sigma + \lambda_1)}$ and $\lambda_{1,2} = \frac{-(\sigma+\gamma) \pm \sqrt{(\sigma-\gamma)^2 + 4\sigma\beta}}{2}$.

Then, we obatin

$$\begin{aligned} \left.\frac{dX_0}{du}\right|_{Y=1} &= -\sigma, \\ \left.\frac{dY_0}{du}\right|_{Y=1} &= -(\sigma + \lambda_1), \\ \left.\frac{du}{du_0}\right|_{Y=1} &= \left.\left(\frac{K}{u_0 + (K - u_0)e^{-\lambda_1 t}} - \frac{Ku_0(1 - e^{-\lambda_1 t})}{[u_0 + (K - u_0)e^{-\lambda_1 t}]^2} \right)\right|_{Y=1} = e^{\lambda_1 t}, \\ \left.\frac{du_0}{dY}\right|_{Y=1} &= \frac{1}{\lambda_2 - \lambda_1}. \end{aligned}$$

Thus,

$$\begin{aligned}\frac{d^2u}{du_0^2}\bigg|_{Y=1} &= \left(\frac{-K(1-e^{-\lambda_1 t})}{[u_0+(K-u_0)e^{-\lambda_1 t}]^2} - \frac{K(1-e^{-\lambda_1 t})}{[u_0+(K-u_0)e^{-\lambda_1 t}]^2}\right)\bigg|_{Y=1} \\ &\quad + \left(\frac{2Ku_0(1-e^{-\lambda_1 t})^2}{[u_0+(K-u_0)e^{-\lambda_1 t}]^3}\right)\bigg|_{Y=1} \\ &= \frac{-2e^{2\lambda_1 t}(1-e^{-\lambda_1 t})}{K},\end{aligned}$$

so

$$\begin{aligned}\frac{d^2X_0}{dY^2}\bigg|_{Y=1} &= \left(\frac{d^2X_0}{du^2}\left(\frac{du}{du_0}\cdot\frac{du_0}{dY}\right)^2 + \frac{dX_0}{du}\cdot\frac{d^2u}{du_0^2}\left(\frac{du_0}{dY}\right)^2 + \frac{dX_0}{du}\cdot\frac{du}{du_0}\cdot\frac{d^2u_0}{dY^2}\right)\bigg|_{Y=1} \\ &= \frac{2\sigma e^{2\lambda_1 t}(1-e^{-\lambda_1 t})}{K(\lambda_2-\lambda_1)^2} \\ &= \frac{2\sigma e^{\lambda_1 t}(e^{\lambda_1 t}-1)}{K(\lambda_2-\lambda_1)^2},\end{aligned}$$

and

$$\begin{aligned}\frac{d^2Y_0}{dY^2}\bigg|_{Y=1} &= \left(\frac{d^2Y_0}{du^2}\left(\frac{du}{du_0}\cdot\frac{du_0}{dY}\right)^2 + \frac{dY_0}{du}\cdot\frac{d^2u}{du_0^2}\left(\frac{du_0}{dY}\right)^2 + \frac{dY_0}{du}\cdot\frac{du}{du_0}\cdot\frac{d^2u_0}{dY^2}\right)\bigg|_{Y=1} \\ &= \frac{2(\sigma+\lambda_2)e^{\lambda_1 t}(e^{\lambda_1 t}-1)}{K(\lambda_2-\lambda_1)^2}.\end{aligned}$$

Therefore,

$$\begin{aligned}\mathbb{E}[I(t)] &= \frac{d}{dY}G(1,Y,t)\bigg|_{Y=1} \\ &= \left(E_0X_0^{E_0-1}\frac{dX_0}{dY}Y_0^{I_0} + I_0Y_0^{I_0-1}\frac{dY_0}{dY}X_0^{E_0}\right)\bigg|_{Y=1} \\ &= \left(E_0X_0^{E_0-1}\frac{dX_0}{du}\frac{du}{du_0}\frac{du_0}{dY}Y_0^{I_0} + I_0Y_0^{I_0-1}\frac{dY_0}{du}\frac{du}{du_0}\frac{du_0}{dY}X_0^{E_0}\right)\bigg|_{Y=1} \\ &= [E_0\sigma + I_0(\sigma+\lambda_1)]\,\frac{e^{\lambda_1 t}}{\lambda_1-\lambda_2}, \qquad \text{(F.1)}\end{aligned}$$

and

$$\mathrm{Var}[I(t)] = \frac{d^2}{dY^2}G(1,Y,t)\bigg|_{Y=1} + \frac{d}{dY}G(1,Y,t)\bigg|_{Y=1} - \left(\frac{d}{dY}G(1,Y,t)\bigg|_{Y=1}\right)^2$$

$$
\begin{aligned}
&= \frac{d}{dY}\left(E_0 X_0^{E_0-1}\frac{dX_0}{dY}\cdot Y_0^{I_0} + I_0 Y_0^{I_0-1}\frac{dY_0}{dY}\cdot X_0^{E_0}\right)\Bigg|_{Y=1} \\
&\quad + \mathbb{E}[I(t)] - \mathbb{E}^2[I(t)] \\
&= [E_0(E_0-1)X_0^{E_0-2}\left(\frac{dX_0}{dY}\right)^2 Y_0^{I_0} + E_0 X_0^{E_0-1}\frac{d^2X_0}{dY^2}Y_0^{I_0} \\
&\quad + E_0 X_0^{E_0-1}\frac{dX_0}{dY}I_0 Y_0^{I_0-1}\frac{dY_0}{dY} + I_0(I_0-1)Y_0^{I_0-2}\left(\frac{dY_0}{dY}\right)^2 X_0^{E_0} \\
&\quad + I_0 Y_0^{I_0-1}\frac{d^2Y_0}{dY^2}X_0^{E_0} + I_0 Y_0^{I_0-1}\frac{dY_0}{dY}E_0 X_0^{E_0-1}\frac{dX_0}{dY}]\Bigg|_{Y=1} \\
&\quad + \mathbb{E}[I(t)] - \mathbb{E}^2[I(t)] \\
&= E_0(E_0-1)\left(\frac{\sigma e^{\lambda_1 t}}{\lambda_1-\lambda_2}\right)^2 + E_0\left[\frac{2\sigma e^{\lambda_1 t}(e^{\lambda_1 t}-1)}{K(\lambda_2-\lambda_1)^2} + \right] \\
&\quad + I_0(I_0-1)\left(\frac{(\sigma+\lambda_1)e^{\lambda_1 t}}{\lambda_1-\lambda_2}\right)^2 + I_0\left[\frac{2(\sigma+\lambda_2)e^{\lambda_1 t}(e^{\lambda_1 t}-1)}{K(\lambda_2-\lambda_1)^2}\right] \\
&\quad + \frac{2E_0 I_0 \sigma(\sigma+\lambda_1)e^{2\lambda_1 t}}{(\lambda_1-\lambda_2)^2} + \mathbb{E}[I(t)] - (\mathbb{E}[I(t)])^2. \qquad \text{(F.2)}
\end{aligned}
$$

Bibliography

[1] Dye C, Gay N. Modeling the SARS epidemic. Science. 2003;300(5627):1884-5.

[2] Simonsen L, Spreeuwenberg P, Lustig R, Taylor RJ, Fleming DM, Kroneman M, et al. Global mortality estimates for the 2009 influenza pandemic from the GLaMOR project: a modeling study. PLoS Medicine. 2013;10(11):e1001558.

[3] Centers for Disease Control and Prevention. Preliminary Estimated Flu Disease Burden 2024-2025 Flu Season. https://wwwcdcgov/flu-burden/php/data-vis/2024-2025html. January 27, 2025.

[4] Huerta R, Tsimring LS. Contact tracing and epidemics control in social networks. Physical Review E. 2002;66(5):056115.

[5] De Silva U, Warachit J, Waicharoen S, Chittaganpitch M. A preliminary analysis of the epidemiology of influenza A (H1N1) v virus infection in Thailand from early outbreak data, June-July 2009. Eurosurveillance. 2009;14(31).

[6] Ma J. Estimating epidemic exponential growth rate and basic reproduction number. Infectious Disease Modelling. 2020;5:129-41.

[7] de Silva E, Ferguson NM, Fraser C. Inferring pandemic growth rates from sequence data. Journal of The Royal Society Interface. 2012;9(73):1797-808.

[8] Kobayashi H. Stochastic Modeling of an Infectious Disease, Part I: Understand the Negative Binomial Distribution and Predict an Epidemic More Reliably. arXiv preprint arXiv:200601586. 2020.

[9] Kermack WO, McKendrick AG. A contribution to the mathematical theory of epidemics. Proceedings of the Royal Society of London Series A, Containing papers of a mathematical and physical character. 1927;115(772):700-21.

[10] Kermack WO, McKendrick AG. Contributions to the mathematical theory of epidemics. II.—The problem of endemicity. Proceedings of the Royal Society of London Series A, containing papers of a mathematical and physical character. 1932;138(834):55-83.

[11] Kermack WO, McKendrick AG. Contributions to the mathematical theory of epidemics. III.—Further studies of the problem of endemicity. Proceedings of the Royal Society of London Series A, Containing papers of a mathematical and physical character. 1933;141(843):94-122.

[12] Anderson RM, May RM. Population biology of infectious diseases: Part I. Nature. 1979;280(5721):361-7.

[13] May RM, Anderson RM. Population biology of infectious diseases: Part II. Nature. 1979;280(5722):455-61.

[14] Aron JL, Schwartz IB. Seasonality and period-doubling bifurcations in an epidemic model. Journal of Theoretical Biology. 1984;110(4):665-79.

[15] Hethcote HW. The mathematics of infectious diseases. SIAM Review. 2000;42(4):599-653.

[16] Guo H, Li MY. Impacts of migration and immigration on disease transmission dynamics in heterogeneous populations. Discrete Contin Dyn Syst Ser B. 2012;17(7):2413-30.

[17] Yang C, Yang Y, Li Y. Assessing vaccination priorities for different ages and age-specific vaccination strategies of COVID-19 using an SEIR modelling approach. Plos One. 2021;16(12):e0261236.

[18] López L, Rodo X. A modified SEIR model to predict the COVID-19 outbreak in Spain and Italy: simulating control scenarios and multi-scale epidemics. Results in Physics. 2021;21:103746.

[19] Sanjuán R, Domingo-Calap P. Mechanisms of viral mutation. Cellular and Molecular Life Sciences. 2016;73:4433-48.

[20] Otto SP, MacPherson A, Colijn C. Endemic does not mean constant as SARS-CoV-2 continues to evolve. Evolution. 2024;78(6):1092-108.

[21] Gani R, Leach S. Transmission potential of smallpox in contemporary populations. Nature. 2001;414(6865):748-51.

[22] Hernández-Orallo E, Manzoni P, Calafate CT, Cano JC. Evaluating how smartphone contact tracing technology can reduce the spread of infectious diseases: The case of COVID-19. Ieee Access. 2020;8:99083-97.

[23] Lipsitch M, Cohen T, Cooper B, Robins JM, Ma S, James L, et al. Transmission dynamics and control of severe acute respiratory syndrome. Science. 2003;300(5627):1966-70.

[24] Wu J, Tang B, Bragazzi NL, Nah K, McCarthy Z. Quantifying the role of social distancing, personal protection and case detection in mitigating COVID-19 outbreak in Ontario, Canada. Journal of Mathematics in Industry. 2020;10(1):1-12.

[25] Odagaki T. New compartment model for COVID-19. Scientific Reports. 2023;13(1):5409.

[26] Bansal S, Read J, Pourbohloul B, Meyers LA. The dynamic nature of contact networks in infectious disease epidemiology. Journal of Biological Dynamics. 2010;4(5):478-89.

[27] Lindquist J, Ma J, van den Driessche P, Willeboordse FH. Effective degree network disease models. Journal of Mathematical Biology. 2011;62:143-64.

[28] Stehlé J, Voirin N, Barrat A, Cattuto C, Colizza V, Isella L, et al. Simulation of an SEIR infectious disease model on the dynamic contact network of conference attendees. BMC Medicine. 2011;9:1-15.

[29] Kiss IZ, Miller JC, Simon PL, et al. Mathematics of epidemics on networks. Cham: Springer. 2017;598(2017):31.

[30] Moore C, Newman ME. Epidemics and percolation in small-world networks. Physical Review E. 2000;61(5):5678.

[31] Pastor-Satorras R, Vespignani A. Epidemic spreading in scale-free networks. Physical Review Letters. 2001;86(14):3200.

[32] Newman ME. Spread of epidemic disease on networks. Physical Review E. 2002;66(1):016128.

[33] Boguná M, Pastor-Satorras R, Vespignani A. Absence of epidemic threshold in scale-free networks with degree correlations. Physical Review Letters. 2003;90(2):028701.

[34] Keeling MJ. The effects of local spatial structure on epidemiological invasions. Proceedings of the Royal Society of London Series B: Biological Sciences. 1999;266(1421):859-67.

[35] Volz E. SIR dynamics in random networks with heterogeneous connectivity. Journal of Mathematical Biology. 2008;56:293-310.

[36] Miller JC. A note on a paper by Erik Volz: SIR dynamics in random networks. Journal of Mathematical Biology. 2011;62(3):349-58.

[37] Rand DA. Correlation equations and pair approximations for spatial ecologies. In: Advanced ecological theory: principles and applications. Oxford: Blackwell Science; 1999. p. 100-42.

[38] Hellewell J, Abbott S, Gimma A, Bosse NI, Jarvis CI, Russell TW, et al. Feasibility of controlling COVID-19 outbreaks by isolation of cases and contacts. The Lancet Global Health. 2020;8(4):e488-96.

[39] Aldrich J. RA Fisher and the making of maximum likelihood 1912-1922. Statistical Science. 1997;12(3):162-76.

[40] Valderrama-Bahamóndez GI, Fröhlich H. MCMC techniques for parameter estimation of ODE based models in systems biology. Frontiers in Applied Mathematics and Statistics. 2019;5:55.

[41] Brauer F, Castillo-Chavez C, Feng Z, et al. Mathematical models in epidemiology. vol. 32. Springer; 2019.

[42] Bednarski S, Cowen LL, Ma J, Philippsen T, van den Driessche P, Wang M. A contact tracing SIR model for randomly mixed populations. Journal of Biological Dynamics. 2022;16(1):859-79.

[43] Swanson KC, Altare C, Wesseh CS, Nyenswah T, Ahmed T, Eyal N, et al. Contact tracing performance during the Ebola epidemic in Liberia, 2014-2015. PLoS Neglected Tropical Diseases. 2018;12(9):e0006762.

[44] Kwok KO, Tang A, Wei VW, Park WH, Yeoh EK, Riley S. Epidemic models of contact tracing: systematic review of transmission studies of severe acute respiratory syndrome and middle east respiratory syndrome. Computational and Structural Biotechnology Journal. 2019;17:186-94.

[45] Kretzschmar ME, Rozhnova G, Van Boven M. Isolation and contact tracing can tip the scale to containment of COVID-19 in populations with social distancing. Frontiers in Physics. 2021;8:677.

[46] Fraser C, Riley S, Anderson RM, Ferguson NM. Factors that make an infectious disease outbreak controllable. Proceedings of the National Academy of Sciences. 2004;101(16):6146-51.

[47] Johansson MA, Quandelacy TM, Kada S, Prasad PV, Steele M, Brooks JT, et al. SARS-CoV-2 transmission from people without COVID-19 symptoms. JAMA Network Open. 2021;4(1):e2035057-7.

[48] Nussbaumer-Streit B, Mayr V, Dobrescu AI, Chapman A, Persad E, Klerings I, et al. Quarantine alone or in combination with other public health measures to control COVID-19: a rapid review. Cochrane Database of Systematic Reviews. 2020;4:CD013574.

[49] Zayed RA, Omran D, Zayed AA. COVID-19 clinical and laboratory diagnosis overview. Journal of the Egyptian Public Health Association. 2021;96:1-5.

[50] Centers for Disease Control and Prevention (CDC). CDC Diagnostic Tests for COVID-19. https://wwwcdcgov/coronavirus/2019-ncov/lab/testinghtml. August, 2021.

[51] Tsang TK, Wu P, Lin Y, Lau EH, Leung GM, Cowling BJ. Effect of changing case definitions for COVID-19 on the epidemic curve and transmission parameters in mainland China: a modelling study. The Lancet Public Health. 2020;5(5):e289-96.

[52] World Health Organization (WHO). Coronavirus disease 2019 (COVID-19) - Situation Report -73. https://appswhoint/iris/bitstream/handle/10665/331686/nCoVsitrep02Apr2020-engpdf?sequence=1isAllowed=y. April, 2020.

[53] Fontanet A, Autran B, Lina B, Kieny MP, Karim SSA, Sridhar D. SARS-CoV-2 variants and ending the COVID-19 pandemic. The Lancet. 2021;397(10278):952-4.

[54] Otto SP, Day T, Arino J, Colijn C, Dushoff J, Li M, et al. The origins and potential future of SARS-CoV-2 variants of concern in the evolving COVID-19 pandemic. Current Biology. 2021;31(14):R918-29.

[55] Canadian Broadcasting Corporation (CBC). B.C.'s contact tracing and testing at maximum capacity, health officials say | CBC News. https://wwwcbcca/news/canada/british-columbia/covid-briefing-dec24-16297668. December, 2021.

[56] Overton CE, Stage HB, Ahmad S, Curran-Sebastian J, Dark P, Das R, et al. Using statistics and mathematical modelling to understand infectious disease outbreaks: COVID-19 as an example. Infectious Disease Modelling. 2020;5:409-41.

[57] Gumel AB, Iboi EA, Ngonghala CN, Elbasha EH. A primer on using mathematics to understand COVID-19 dynamics: Modeling, analysis and simulations. Infectious Disease Modelling. 2021;6:148-68.

[58] Brauer F. Compartmental models in epidemiology. Mathematical Epidemiology. 2008:19-79.

[59] Lunz D, Batt G, Ruess J. To quarantine, or not to quarantine: A theoretical framework for disease control via contact tracing. Epidemics. 2021;34:100428.

[60] Sturniolo S, Waites W, Colbourn T, Manheim D, Panovska-Griffiths J. Testing, tracing and isolation in compartmental models. PLoS Computational Biology. 2021;17(3):e1008633.

[61] Wearing HJ, Rohani P, Keeling MJ. Appropriate models for the management of infectious diseases. PLoS Medicine. 2005;2(7):e174.

[62] Nåsell I. The quasi-stationary distribution of the closed endemic SIS model. Advances in Applied Probability. 1996;28(3):895-932.

[63] Lambert A. A mathematical assessment of the efficiency of quarantining and contact tracing in curbing the COVID-19 epidemic. Mathematical Modelling of Natural Phenomena. 2021;16:53.

[64] Green DM, Kiss IZ. Large-scale properties of clustered networks: Implications for disease dynamics. Journal of Biological Dynamics. 2010;4(5):431-45.

[65] Miller JC. Percolation and epidemics in random clustered networks. Physical Review E. 2009;80(2):020901.

[66] Ames GM, George DB, Hampson CP, Kanarek AR, McBee CD, Lockwood DR, et al. Using network properties to predict disease dynamics on human contact networks. Proceedings of the Royal Society B: Biological Sciences. 2011;278(1724):3544-50.

[67] Haw DJ, Pung R, Read JM, Riley S. Strong spatial embedding of social networks generates nonstandard epidemic dynamics independent of degree distribution and clustering. Proceedings of the National Academy of Sciences. 2020;117(38):23636-42.

[68] Keeling M, Rand D. Spatial correlations and local fluctuations in host-parasite models. Springer; 2001.

[69] Tunc I, Shkarayev MS, Shaw LB. Epidemics in adaptive social networks with temporary link deactivation. Journal of Statistical Physics. 2013;151(1):355-66.

[70] Shkarayev MS, Tunc I, Shaw LB. Epidemics with temporary link deactivation in scale-free networks. Journal of Physics A: Mathematical and Theoretical. 2014;47(45):455006.

[71] Wang M, Ma J, van den Driessche P, Cowen LL. Estimating the Effect of Contact Tracing During the Early Stage of an Epidemic. Infectious Disease Modelling. 2025;In Press.

[72] Donnelly CA, Ghani AC, Leung GM, Hedley AJ, Fraser C, Riley S, et al. Epidemiological determinants of spread of causal agent of severe acute respiratory syndrome in Hong Kong. The Lancet. 2003;361(9371):1761-6.

[73] Gardner BJ, Kilpatrick AM. Contact tracing efficiency, transmission heterogeneity, and accelerating COVID-19 epidemics. PLOS Computational Biology. 2021;17(6):e1009122.

[74] Linden M, Dehning J, Mohr SB, Mohring J, Meyer-Hermann M, Pigeot I, et al. Case numbers beyond contact tracing capacity are endangering the containment of COVID-19. Deutsches Ärzteblatt International. 2020;117(46):790.

[75] Roda WC, Varughese MB, Han D, Li MY. Why is it difficult to accurately predict the COVID-19 epidemic? Infectious Disease Modelling. 2020;5:271-81.

[76] Tupper P, Otto SP, Colijn C. Fundamental limitations of contact tracing for COVID-19. Facets. 2021;6(1):1993-2001.

[77] Canadian Institute for Health Information. Canadian COVID-19 Intervention Timeline. https://wwwcihica/en/canadian-covid-19-intervention-timeline. Accessed 13 October 2022.

[78] Casey M, Griffin J, McAloon CG, Byrne AW, Madden JM, Mc Evoy D, et al. Estimating pre-symptomatic transmission of COVID-19: a secondary analysis using published data. MedRxiv. 2020:2020-05.

[79] Li H, Gu M. Robust estimation of SARS-CoV-2 epidemic in US counties. Scientific Reports. 2021;11(1):11841.

[80] Zou L, Ruan F, Huang M, Liang L, Huang H, Hong Z, et al. SARS-CoV-2 viral load in upper respiratory specimens of infected patients. New England Journal of Medicine. 2020;382(12):1177-9.

[81] Lovell-Read FA, Funk S, Obolski U, Donnelly CA, Thompson RN. Interventions targeting non-symptomatic cases can be important to prevent local outbreaks: SARS-CoV-2 as a case study. Journal of The Royal Society Interface. 2021;18(178):20201014.

[82] Ge J, He D, Lin Z, Zhu H, Zhuang Z. Four-tier response system and spatial propagation of COVID-19 in China by a network model. Mathematical Biosciences. 2020;330:108484.

[83] Demongeot J, Magal P. Data-Driven Mathematical Modeling Approaches for COVID-19: a survey. arXiv preprint arXiv:230917087. 2023.

[84] Ministry of Health. Public health management of cases and contacts of COVID-19 in Ontario. https://wwwcorhealthontarioca/PH-Mgmt-COVID-19-Version-60-Sharedpdf. March 25, 2020.

[85] Public Health Ontario. COVID-19 Contact Tracing Initiative: A significant achievement in an extraordinary time. https://wwwpublichealthontarioca/en/About/News/2021/COVID-19-Contact-Tracing-Initiative. September 3, 2021.

[86] Government of Canada. Confirmed positive cases of COVID-19 in Ontario. https://opencanadaca/data/en/dataset/f4112442-bdc8-45d2-be3c-12efae72fb27. Accessed 22 November 2023.

[87] Van Kerkhove MD, Bento AI, Mills HL, Ferguson NM, Donnelly CA. A review of epidemiological parameters from Ebola outbreaks to inform early public health decision-making. Scientific Data. 2015;2(1):1-10.

[88] Read JM, Bridgen JR, Cummings DA, Ho A, Jewell CP. Novel coronavirus 2019-nCoV (COVID-19): early estimation of epidemiological parameters and epidemic size estimates. Philosophical Transactions of the Royal Society B. 2021;376(1829):20200265.

[89] Carcione JM, Santos JE, Bagaini C, Ba J. A simulation of a COVID-19 epidemic based on a deterministic SEIR model. Frontiers in Public Health. 2020;8:230.

[90] Minayev P, Ferguson N. Improving the realism of deterministic multi-strain models: implications for modelling influenza A. Journal of The Royal Society Interface. 2009;6(35):509-18.

[91] Zuur AF, Ieno EN, Smith GM. Analysing ecological data. vol. 680. Springer; 2007.

[92] Lloyd-Smith JO, Schreiber SJ, Kopp PE, Getz WM. Superspreading and the effect of individual variation on disease emergence. Nature. 2005;438(7066):355-9.

[93] Mutiso F, Pearce JL, Benjamin-Neelon SE, Mueller NT, Li H, Neelon B. Bayesian negative binomial regression with spatially varying dispersion: Modeling COVID-19 incidence in Georgia. Spatial Statistics. 2022;52:100703.

[94] O'Hara R, Kotze J. Do not log-transform count data. Nature Precedings. 2010;1(2):118-22.

[95] Warton DI. Many zeros does not mean zero inflation: comparing the goodness-of-fit of parametric models to multivariate abundance data. Environmetrics. 2005;16(3):275-89.

[96] Warton DI, Foster SD, De'ath G, Stoklosa J, Dunstan PK. Model-based thinking for community ecology. Plant Ecology. 2015;216:669-82.

[97] Lloyd-Smith JO. Maximum likelihood estimation of the negative binomial dispersion parameter for highly overdispersed data, with applications to infectious diseases. PloS One. 2007;2(2):e180.

[98] Bi Q, Wu Y, Mei S, Ye C, Zou X, Zhang Z, et al. Epidemiology and Transmission of COVID-19 in Shenzhen China: Analysis of 391 cases and 1,286 of their close contacts. Medrxiv. 2020:2020-03.

[99] Endo A, Abbott S, Kucharski AJ, Funk S, et al. Estimating the overdispersion in COVID-19 transmission using outbreak sizes outside China. Wellcome Open Research. 2020;5.

[100] Laxminarayan R, Wahl B, Dudala SR, Gopal K, Mohan B C, Neelima S, et al. Epidemiology and transmission dynamics of COVID-19 in two Indian states. Science. 2020;370(6517):691-7.

[101] Gómez-Déniz E, Sarabia JM, Calderín-Ojeda E. Univariate and multivariate versions of the negative binomial-inverse Gaussian distributions with applications. Insurance: Mathematics and Economics. 2008;42(1):39-49.

[102] Zamani H, Ismail N. Negative binomial-Lindley distribution and its application. Journal of Mathematics and Statistics. 2010;6(1):4-9.

[103] Bartlett M. Some evolutionary stochastic processes. Journal of the Royal Statistical Society Series B (Methodological). 1949;11(2):211-29.

[104] Bailey NT. The elements of stochastic processes with applications to the natural sciences. vol. 25. John Wiley & Sons; 1991.

[105] Kobayashi H. Stochastic modeling of an infectious disease part II: Simulation experiments and verification of the analysis. arXiv preprint arXiv:210111394. 2021.

[106] Tritch W, Allen LJ. Duration of a minor epidemic. Infectious Disease Modelling. 2018;3:60-73.

[107] Grimmett G, Stirzaker D. Probability and random processes. Oxford University Press; 2020.

[108] Ge Y, Martinez L, Sun S, Chen Z, Zhang F, Li F, et al. COVID-19 transmission dynamics among close contacts of index patients with COVID-19: a population-based cohort study in Zhejiang Province, China. JAMA Internal Medicine. 2021;181(10):1343-50.

[109] Rong X, Yang L, Chu H, Fan M. Effect of delay in diagnosis on transmission of COVID-19. Math Biosci Eng. 2020;17(3):2725-40.

[110] Li Q, Guan X, Wu P, Wang X, Zhou L, Tong Y, et al. Early transmission dynamics in Wuhan, China, of novel coronavirus–infected pneumonia. New England journal of medicine. 2020;382(13):1199-207.

[111] Gardner W, Mulvey EP, Shaw EC. Regression analyses of counts and rates: Poisson, overdispersed Poisson, and negative binomial models. Psychological bulletin. 1995;118(3):392.

[112] Coly S, Yao AF, Abrial D, Charras-Garrido M. Distributions to model overdispersed count data. Journal de la Société Française de Statistique. 2016;157(2):39-63.

[113] Ross S. A First Course in Probability. 7th ed. Pearson Prentice Hall; 2006.

[114] Casella G, Berger R. Statistical inference. CRC Press; 2024.

[115] Anderson DF, Kurtz TG. Continuous time Markov chain models for chemical reaction networks. In: Design and analysis of biomolecular circuits: engineering approaches to systems and synthetic biology. Springer; 2011. p. 3-42.

[116] Andersson H, Britton T. Stochastic epidemic models and their statistical analysis. vol. 151. New York: Springer Science & Business Media; 2012.

[117] Brémaud P. Point process calculus in time and space. Springer Cham doi. 2020;10:978-3.

[118] Rogers LCG, Williams D. Diffusions, Markov processes, and martingales: Itô calculus. vol. 2. Cambridge: Cambridge University Press; 2000.

[119] Dynkin E. Kolmogorov and the theory of Markov processes. The Annals of Probability. 1989;17(3):822-32.

[120] Roberts M, Heesterbeek J. Model-consistent estimation of the basic reproduction number from the incidence of an emerging infection. Journal of Mathematical Biology. 2007;55(5):803-16.

[121] Chowell G, Shim E, Brauer F, Diaz-Dueñas P, Hyman J, Castillo-Chavez C. Modelling the transmission dynamics of acute haemorrhagic conjunctivitis: application to the 2003 outbreak in Mexico. Statistics in medicine. 2006;25(11):1840-57.

[122] Mills CE, Robins JM, Lipsitch M. Transmissibility of 1918 pandemic influenza. Nature. 2004;432(7019):904-6.

[123] Elliott P, Haw D, Wang H, Eales O, Walters CE, Ainslie KE, et al. Exponential growth, high prevalence of SARS-CoV-2, and vaccine effectiveness associated with the Delta variant. Science. 2021;374(6574):eabl9551.

[124] Chowell G, Ammon C, Hengartner NW, Hyman J. Transmission dynamics of the great influenza pandemic of 1918 in Geneva, Switzerland: Assessing the effects of hypothetical interventions. Journal of theoretical biology. 2006;241(2):193-204.

[125] Ma J, Dushoff J, Bolker BM, Earn DJ. Estimating initial epidemic growth rates. Bulletin of mathematical biology. 2014;76(1):245-60.

[126] Björck Å. Least squares methods. Handbook of numerical analysis. 1990;1:465-652.

[127] Myung IJ. Tutorial on maximum likelihood estimation. Journal of Mathematical Psychology. 2003;47(1):90-100.

[128] Bolker B. Ecological models and data in R. vol. 396. Princeton University Press; 2008.

[129] Cauchemez S, Carrat F, Viboud C, Valleron AJ, Boëlle P. A Bayesian MCMC approach to study transmission of influenza: application to household longitudinal data. Statistics in medicine. 2004;23(22):3469-87.

[130] Vynnycky E, Trindall A, Mangtani P. Estimates of the reproduction numbers of Spanish influenza using morbidity data. International Journal of Epidemiology. 2007;36(4):881-9.

[131] Chowell G, Fenimore PW, Castillo-Garsow MA, Castillo-Chavez C. SARS outbreaks in Ontario, Hong Kong and Singapore: the role of diagnosis and isolation as a control mechanism. Journal of theoretical biology. 2003;224(1):1-8.

[132] Hutchinson MK, Holtman MC. Analysis of count data using poisson regression. Research in Nursing & Health. 2005;28(5):408-18.

[133] Coxe S, West SG, Aiken LS. The analysis of count data: A gentle introduction to Poisson regression and its alternatives. Journal of Personality Assessment. 2009;91(2):121-36.

[134] Huang A, Kim A. Bayesian Conway–Maxwell–Poisson regression models for overdispersed and underdispersed counts. Communications in Statistics-Theory and Methods. 2021;50(13):3094-105.

[135] Mor B, Garhwal S, Kumar A. A systematic review of hidden Markov models and their applications. Archives of computational methods in engineering. 2021;28:1429-48.

[136] Fort A, Mugnaini M, Vignoli V. Hidden Markov Models approach used for life parameters estimations. Reliability Engineering & System Safety. 2015;136:85-91.

[137] Le Strat Y, Carrat F. Monitoring epidemiologic surveillance data using hidden Markov models. Statistics in medicine. 1999;18(24):3463-78.

[138] Cooper B, Lipsitch M. The analysis of hospital infection data using hidden Markov models. Biostatistics. 2004;5(2):223-37.

[139] Green PJ, Richardson S. Hidden Markov models and disease mapping. Journal of the American statistical association. 2002;97(460):1055-70.

[140] van den Driessche P, Watmough J. Reproduction numbers and sub-threshold endemic equilibria for compartmental models of disease transmission. Mathematical Biosciences. 2002;180(1-2):29-48.

[141] Billingsley P. Probability and measure. John Wiley & Sons; 2017.